MATHEMATICAL MODELING IN SYSTEMS MEDICINE: NEW PARADIGMS FOR GLUCOSE CONTROL IN CRITICAL CARE

by

Ari Pritchard-Bell

B.S. Chemical Engineering, University of California Santa Barbara, 2011

Submitted to the Graduate Faculty of
the Swanson School of Engineering in partial fulfillment
of the requirements for the degree of

Doctor of Philosophy

University of Pittsburgh

2016

UNIVERSITY OF PITTSBURGH

SWANSON SCHOOL OF ENGINEERING

This dissertation was presented

by

Ari Pritchard-Bell

It was defended on

January 25th, 2016

and approved by

Robert S. Parker, Ph.D., Professor, Department of Chemical and Petroleum Engineering

Gilles Clermont, Ph.D., Professor, Department of Critical Care Medicine

Ipsita Banerjee, Ph.D., Assistant Professor, Department of Chemical and Petroleum Engineering

Zhi-Hong Mao, Ph.D., Associate Professor, Department of Electrical and Computer Engineering

Dissertation Advisors: Robert S. Parker, Ph.D., Professor, Department of Chemical and Petroleum Engineering,

Gilles Clermont, Ph.D., Professor, Department of Critical Care Medicine

MATHEMATICAL MODELING IN SYSTEMS MEDICINE: NEW PARADIGMS FOR GLUCOSE CONTROL IN CRITICAL CARE

Ari Pritchard-Bell, PhD

University of Pittsburgh, 2016

Stress hyperglycemia occurs frequently in critical care patients and many of the harmful repercussions may be mitigated by maintaining glucose within a "healthy" zone. While the exact range of the zone varies, glucose below 80 mg/dl or above 130 mg/dl increases risk of mortality. Zone glucose control (ZGC) is accomplished primarily using insulin administration to reduce hyperglycemia. Alternatively, we propose also allowing glucose administration to be used to raise blood glucose and avoid hypoglycemia.

While there have been attempts to create improved paradigms for treatment of stress hyperglycemia, inconsistencies in glycemic control protocols as well as variation in outcomes for different ICU subpopulations has contributed to the mixed success of glucose control in critical care and subsequent disagreement regarding treatment protocols. Therefore, a more accurate, personalized treatment that is tailored to an individual may significantly improve patient outcome. The most promising method to achieve better control using a personalized strategy is through the use of a model-based decision support system (DSS), wherein a mathematical patient model is coupled with a controller and user interface that provides for semi-automatic control under the supervision of a clinician.

Much of the error and subsequent failure to control blood glucose comes from the failure to resolve inter- and intrapatient variations in glucose dynamics following insulin administration. The observed variation arises from the many biologically pathways that affect insulin signaling for patients in the ICU. Mathematical modeling of the biological pathways of stress hyperglycemia can improve understanding and treatment.

Trauma and infection lead to the development of systemic insulin resistance and elevated blood glucose levels associated with stress hyperglycemia. We develop mathematical models of the biological signaling pathways driving fluctuations in insulin sensitivity and resistance. Key metabolic mediators from the inflammatory response and counterregulatory response are mathematically represented acting on insulin-mediated effects causing increases or decreases in blood glucose concentration. Data from published human studies are used to calibrate a composite model of glucose and insulin dynamics augmented with biomarkers relevant to critical care. The resulting mathematical description of the underlying mechanisms of insulin resistance could be used in a model-based decision support system to estimate patient-specific metabolic status and provide more accurate insulin treatment and glucose control for critical care patients.

TABLE OF CONTENTS

LIST OF TABLES

LIST OF FIGURES

PREFACE

There are a number of people that have influenced my path through academia. It makes writing this section difficult, as I try to include everyone who has not only stimulated my scientific curiosity, but also provided me with support critical to my success in graduate school. In addition to those mentioned below, I am grateful for the inspiring and talented teachers I have throughout my education.

First, I would like to thank my family. My wife, Natania, for trekking across the country to be my supporting partner in the frigid Pittsburgh tundra (summer is great). For giving me the perfect balance of comforting support and critical reminders to get-it-done. My mom, for influencing my eternal curiosity for nature and medicine - from the flora and fauna of the California coast, to the microbiota within the human body. My dad, for encouraging my excitement in computers, logic, and buckets of water on conveyor belts. My sister, for providing the right amount of existential discussions to keep me in academia for this long. And to all of my family, for giving me way too much encouragement for all my ranting on random (mostly) scientific topics.

Going through graduate school has been a transformative process for me. Research has been one of the most challenging as well as rewarding experiences of my life. The process has been a combination of self-discipline, self-doubt, optimism, pessimism, and passion. I would like to thank my advisor, Bob, for sharing his unrelenting passion and optimism for research. Though not something explicitly taught, this infectious mindset will follow me throughout my future endeavors. I would also like to thank my co-advisor, Gilles, who taught me to make things relevant and gave me a clinical perspective for thinking with purpose and application.

Finally, I would like to express my gratitude to my labmates and colleagues who had to deal with me on a daily basis. Tim, for always being willing to lend his help and expertise.

Thang, for the insightful guidance he provided early in my graduate career. Li Ang, Matt, Shibin, and Christy for their help and patience for whatever random questions, technical or otherwise, I asked them.

ACKNOWLEDGMENT

My graduate research was supported by the National Institute of Diabetes, Digestive and Kidney Disease (NIDDK) of the National Institutes of Health under award number R21-DK-92813. Additionally, this work was supported by the U.S. Department of Education Graduate Assistance in Areas of National Need (GAANN) award number P200A120195. This work was supported partially by the Research Experiences for Undergraduates (REU) Program of the National Science Foundation under Award Number EEC-1156899.

1.0 INTRODUCTION

Critical illness is often concomitant with metabolic dysregulation. The most common manifestation of metabolic dysregulation in the intensive care unit (ICU) is elevated levels of blood glucose, also known as stress hyperglycemia [1, 2]. Severity and duration of stress hyperglycemia are directly correlated to mortality and morbidity in the ICU [3, 4]. Data from the High-Density Intensive Care (HIDENIC) database, collected from the University of Pittsburgh Medical Center (UPMC), was compiled in Figure 1 and demonstrates a clear advantage of maintaining glucose within a zone of 110 to 130 mg/dl. This association persisted after adjustment for a large number of known and potential confounders. Mortality increases for average glucose values of greater than 130 mg/dl and rapidly increases for values decreasing below 80 mg/dl. Therefore, we propose a lower bound to the zone 110 mg/dl to provide a safety margin to protect against hypoglycemia. Additional studies show hypoglycemia [5, 6] and overall glycemic variability [7, 8] correlate with worsened outcomes for patients in critical care. Our hypothesis, from retrospective observational studies [3, 9, 10, 11], is that there exists a normoglycemic range of blood glucose values that, if maintained, results in decreased mortality and morbidity in the ICU. Therapeutic intervention (e.g., the administration of the anabolic hormone insulin, glucose, or the catabolic hormone glucagon) is essential to mitigate the harmful repercussions of dysglycemia. A plausible solution to maintain the aforementioned ideal range is through the implementation of zone glucose control (ZGC). The primary challenge in implementing ZGC in critical care revolves around identifying metabolic variability. Unlike the ambulatory diabetic, insulin sensitivity can fluctuate rapidly within an individual resulting in dynamics that are difficult to predict. Additionally, changing critical care conditions such as surgeries [12], inflammation [13], and drug administration [14] may

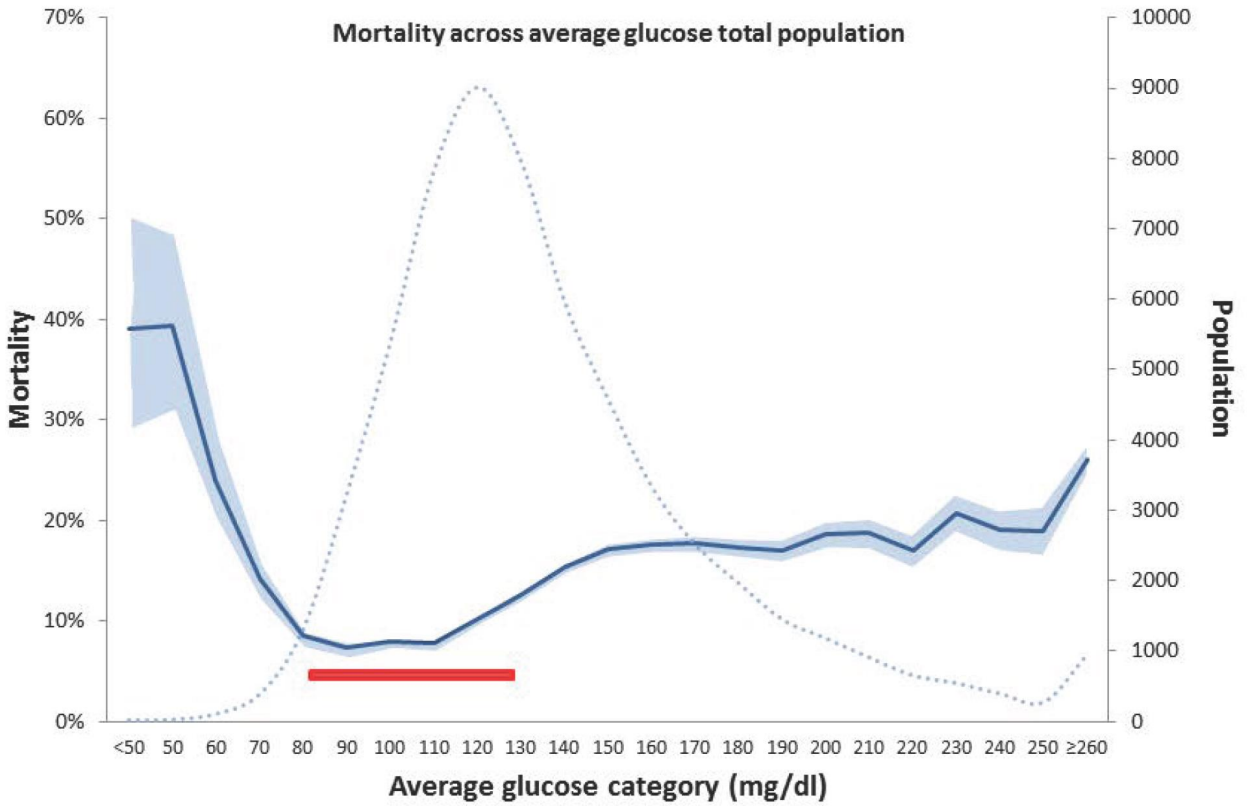

Figure 1: Mortality percentage vs. average glucose in HIDENIC (High-Density Intensive Care) study database. Mortality minimum for normal glycemic range seen between 80 and 130 mg/dl. Mortality gradually increases for values rising above 130 mg/dl, and steeply rises for values falling below 80 mg/dl.

further confound attempts for glucose control. To gain better insight, and ultimately better dynamic predictions, we focus on the biological mechanisms governing human metabolism.

Human metabolism is a robust process through which the body adapts substrate utilization based on relative availability of macronutrients such as proteins, carbohydrates, and fat. In addition to substrate availability, metabolic processes are heavily influenced by changes in immune system and hormonal fluctuations [15]. Metabolism has evolved to allow survival under extreme conditions such as starvation, injury, and many other changes in our environment. Though we are able to adapt quickly and effectively, there can be long-term

consequences that become apparent after immediate danger has subsided. For example, the physiological response to infection or trauma is to maintain energy substrate supply (e.g., blood glucose) and avoid catastrophic system failure caused by hypoglycemia. Hyperglycemic detriments accrued from the naturally aggressive avoidance of hypoglycemia are evolutionarily tolerated because they cause health problems which, unlike immediate hypoglycemic system failure, develop over the course of days and months and are beyond the scope of imminent survival [16]. The resulting asymmetry of endogenous blood glucose control mechanisms cause pathologies coinciding with moderate to extreme inflammation that induces a prolonged state of hyperglycemia. The consequences of an over active endogenous response to physiological stress must be mediated to avoid the long-term damaging effects of persistent activation. This cascade is triggered by severe trauma and must be critically addressed in the same manner as short-term risk.

1.1 GLYCEMIC CONTROL IN CRITICAL CARE

In 2001 a prospective randomized controlled trial was performed on over 1,500 patients in the Leuven ICU showing that tight glycemic control (TGC), through administration of insulin, reduced mortality from 8% to 4.6% [17]. This landmark study generated new paradigms for insulin therapy in the critical care population [18]. In a similar study [19] on 800 critically ill patients, TGC reduced mortality 29.3% and overall length of stay (LOS) by 10.8%, with no significant changes in hypoglycemia. Treating stress hyperglycemia through insulin administration exhibited decreased mortality as expected from the retrospective literature showing hyperglycemia correlating to mortality [20].

Despite the literature and prospective studies supporting TGC, several follow-up studies to the 2001 Leuven study showed limited benefit: morbidity and not mortality reduction in the case of the Leuven follow-up study in 2006 [21], or no change in outcome whatsoever as seen in both Glucontrol [22] and CREATE-ECLA [23]. The waning motivation for controlling stress hyperglycemia was further exacerbated in 2009 when a multicenter prospective study (NICE-SUGAR) [24] of over 6,000 patients showed an increase in mortality in the

group receiving intensive insulin treatment. Retrospective analysis of the NICE-SUGAR study [25] indicated that improved outcomes from glycemic control are overwhelmed by the increased risk of hypoglycemia and the accompanying increase in mortality associated with hypoglycemia [5, 6]. As a result, current guidelines allow for hyperglycemia so as to appropriately promote safety set well beyond an optimal zone.

Analysis of the literature reveals inconsistencies in glycemic control protocols [26], as well as variation in TGC outcomes for different ICU subpopulations [27, 28, 29]. Due to the mixed success of TGC, there is significant disagreement regarding treatment protocols using insulin [30, 31]. Methods for TGC require further investigation of the biological mechanisms of stress hyperglycemia. Mathematically describing the underlying biological mechanisms leading to stress hyperglycemia could allow for increasingly accurate, patient-specific insulin treatment protocols (*i.e.*, personalized medicine). Increasing biological resolution and subsequent accuracy of mathematical models is a critical component for good control [32]. However, to maintain control relevance, the model must be identifiable in a clinical setting. Therefore, models of both biological and clinical scope must be explored and evaluated in the context of human treatment in critical care.

Blood glucose in critical care can be maintained within a target zone via either glucose (to increase) or insulin (to decrease) infusion. Two critical components of ZGC, regardless of how low and tight this zone is, must be addressed to overcome the challenges and biases observed in clinical trials of ZGC in critically ill patients: (i) standardization of treatment [26, 30, 31] and (ii) characterization of the biologically driven variations among critical care cohorts [27, 28, 29]. A model-based decision support system (DSS), similar to those deployed for type 1 diabetes [33, 34, 35, 36], could address both needs. A closed-loop system with clinical oversight provides an algorithmic standardization between patients, while an accurate mechanistic model provides predictions grounded in the underlying biology that can result in a more robust, patient-specific ZGC. There have been encouraging studies investigating the use of a DSS in critical care [37, 38]. Therefore, to balance biological understanding with control relevance, we create a decision support system with semi-automated control architecture that allows for ZGC consistency across many different ICUs, potentially reducing variability in treatment implementation.

1.2 ETIOLOGY OF INSULIN RESISTANCE

Major trauma or infection triggers a hyper-catabolic state, providing the necessary substrate for damaged or infected tissue [39] to recover. The most effective anabolic hormone capable of counteracting hyper-catabolism is insulin, but it must be administered with care so as to avoid hypoglycemia. Precise insulin treatment is particularly challenging in the ICU due to irregular fluctuations in insulin sensitivity, which can manifest concomitantly in a variety of tissues, resulting in unexpected blood glucose fluctuations. Therefore, a crucial step for successful glycemic control is to identify patient-specific insulin sensitivity dynamics and make accurate predictions using mathematical models.

The primary challenge in modeling and understanding insulin sensitivity is that, while there are many biological pathways involved in elevated glucose levels [40, 41], the governing mechanism through which the pathological state of stress hyperglycemia progresses and persists remains convoluted. Low frequency blood glucose data are the primary measurements available. Therefore, to build a useful model, we must analyze the contributing factors (e.g., stress hormones, cytokines, etc.) and be able to describe their interactions not only with insulin sensitivity but any synergistic or overlapping mechanisms they may invoke to create changes in blood glucose. A comprehensive model would allow blood sample measurements of various species to depict a systems-level prediction of how a patient will respond to insulin treatment. Such a system could estimate an individual patient's underlying metabolic state, via simulation and collection of key measurements, to allow for real-time personalized treatment.

1.3 CELLULAR MECHANISMS OF INSULIN RESISTANCE

Due to the multiple potential drivers of insulin resistance present in circulation at any given time, we expect there to be multiple phenotypes of stress hyperglycemia. This phenotype behavior would be expected between patients but also perhaps in the same patient who is recovering from a particular trauma and returning to health. These mechanistic changes

over time are informed by additional measurements that may be available in the clinic. Cortisol has been shown to be the most correlated marker to insulin resistance following cardiac surgery [15], though metabolically active components such as TNF, IL6, leptin, and adiponectin are also present. Initial contributions we focus on are the effect of TNF, inducing glucose uptake and cortisol, the latter of which inhibits insulin signaling and increases hepatic glucose output. Relative tissue contributions to stress hyperglycemia are a way to begin to decouple the many components and mechanism altering glucose metabolism.

1.3.1 Insulin Resistance and Inflammation

Insulin resistance develops in numerous pathological conditions: metabolic syndrome [16], type-2 diabetes mellitus (T2DM), and following trauma or infection [42]. In all the above cases, the common factor is inflammation, in which signaling proteins are released to counteract the anabolic effects of insulin. Specifically, mechanisms for T2DM insulin resistance have been investigated [43] and there is some mechanistic overlap with the inflammatory pathways activated in critical care [44]. While species of interest from T2DM such as TNF, IL1β, and many other cytokines [45] play an active role in regulating insulin resistance and metabolism, the degree to which these species interact with the additional milieu of trauma-related species found in the critical care population remains to be determined.

The challenge in elucidating the underlying mechanism of stress hyperglycemia is determining how pathways such as inflammation and anti-inflammation affect insulin resistance. Insulin resistance is a general term for a variety of pathological conditions in which insulin signaling becomes impaired [46]. Insulin is one of the most potent anabolic hormones found in the human body and it plays a central role in globally signaling tissues to stop releasing nutrients into the blood and to start storing them locally. Therefore, desensitization of the insulin signal blocks the anabolic effects of insulin and is the fundamental reason why insulin is the downstream signaling target of so many different biological processes that require increased available nutrients in the blood. While insulin is an effective global messenger inducing system-wide anabolism, selective inhibition of the insulin signal in specific tissues allows for an extra layer of control over where nutrients are directed [47]. For example,

selective insulin resistance in the muscle would allow adequate glucose for the CNS while allowing the liver to maintain glycogen reserves as a result of working insulin signaling. Such downstream trafficking allows tissue-specific insulin signaling mediation to act as a robust mechanism for orchestrating metabolism. This is particularly important due to the fact that each tissue plays a specific role in metabolic regulation.

1.3.2 Glucose Transporters Govern Tissue Specificity

The key tissue types in metabolic actuation and control are: pancreas, liver, muscle, adipose, and the central nervous system (CNS: brain, erythrocytes, etc.). Glucose transport is facilitated within each tissue differently depending on which types of glucose transporters (GLUT) are present in that tissue. The GLUT transporters are a family of transmembrane proteins that allow glucose to move from the extracellular space to the cytosol. In the CNS, glucose is transported via GLUT1 and GLUT3, passive glucose transporters that are independent of insulin and allow glucose flux into cells to be driven by diffusion [47]. In muscle and adipose tissues, the insulin-sensitive GLUT4 is the primary glucose transporter and is constantly being exocytosed in response to insulin and endocytosed in the absence of insulin. The liver and pancreas utilize GLUT2, an insulin-independent glucose transporter with a very high saturation limit, allowing glucose to flow quasi-linearly into these tissues in order to sense blood glucose with high precision.

Combined, GLUT transporters play a critical role in defining tissue-specific actuation of glucose metabolism. For example, elevated glucose is sensed in the liver and pancreas via GLUT2, and insulin is released from the pancreas while the liver begins storing excess glucose as glycogen. GLUT4 is subsequently translocated to the membrane of adipose and muscle cells receiving an insulin signal, lowering blood glucose levels by trafficking glucose out of the bloodstream. Keeping blood glucose levels in the correct range is critical at the cellular level so as to provide consistent diffusive flux to the CNS via GLUT1 and GLUT3 and to avoid overloading the GLUT2 sensing mechanism in the pancreas and liver. Inflammation, or other biological pathways signaling increased nutrient requirements, induce insulin resistance primarily by decreasing GLUT4 translocation [43] and thus decrease uptake of blood glucose

by adipose and muscle tissues in anticipation of increased demand by the CNS and immune system. Similarly, a disrupted insulin signal in the liver leads to increased forkhead box protein O1 (FOXO1) and increased glucose production via gluconeogenesis [48].

1.3.3 Inhibition of Insulin Receptor Substrate

GLUT4 translocation is the primary glucose transporter that responds to insulin signaling. Early in the insulin signaling pathway is a critical node, insulin receptor substrate 1 (IRS-1), which can become serine and/or threonine phosphorylated [49] (see Figure 2) preventing it from propagating the insulin signal via tyrosine phosphorylation. Serine phosphorylation of IRS-1 plays a central role in insulin resistance [50, 51, 52], though it is not independently responsible [53]. Antagonists of early insulin signaling are the primary drivers of insulin resistance but are numerous and may overlap in mechanism. A common characteristic of conditions leading to insulin resistance is the activation of the inflammatory response [16, 44]. It follows that this is the probable initiating mechanism in critical care due to the frequent occurrence of inflammation as a result of surgery, trauma, etc. [54]. Serine kinases such as c-Jun N-terminal kinases (JNK) are responsible for serine phosphorylation and subsequent inhibition of IRS-1 as well as propagating the inflammatory cascade. This cascade ultimately leads to transcription of the cytokine interleukin-6 (IL-6), whose activation induces suppressor of cytokine 3 (SOCS3) in adipose [55] and muscle [56] cells. SOCS3 has been shown to activate ubiquitin-dependent IRS-1 degradation [57, 58] leading to reduced insulin signaling. Many sources attribute stress hyperglycemia to these two mechanisms based on correlation with deactivation of the critical IRS-1 node [59]. However, there remains open debate regarding the underlying cellular and tissue mechanisms causing (not correlating to) the response. A previously published study [42] found the cytokine interleukin 6 (IL-6) to be directly correlated to insulin resistance as quantified via hyperinsulinemic euglycemic clamp [60] following elective surgery. Therefore, IL-6 has been a proposed driver of insulin resistance, a mechanism corroborated by multiple animal and cellular studies [48, 55, 56, 59, 61, 62, 63, 64, 65] showing a mechanism of insulin resistance via (i) IL-6 activating suppressor of cytokines III (SOCS-3) via the JAK-STAT pathway; and (ii) SOCS-3 inhibiting insulin receptor substrate

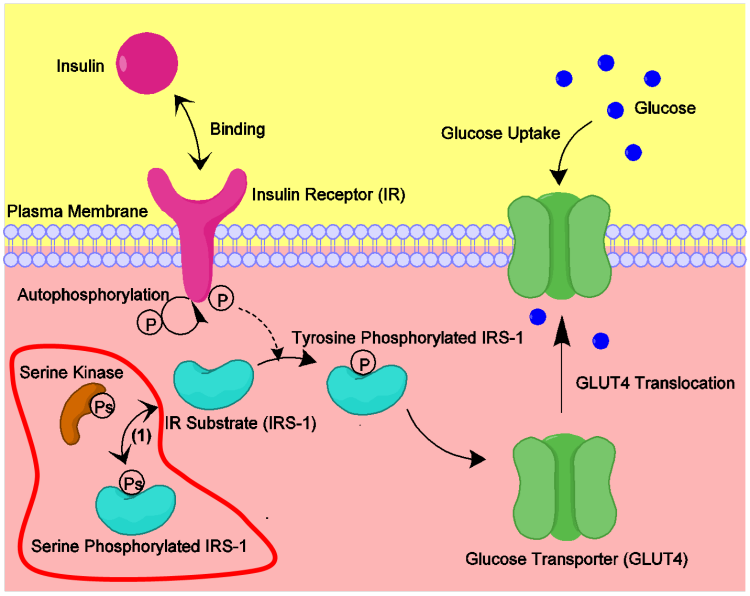

Figure 2: Insulin binding results in receptor autophosphorylation and subsequent tyrosine phosphorylation of insulin receptor substrate (IRS-1). The cascade leading to GLUT4 translocation / glucose uptake is disrupted by serine phosphorylation of IRS-1 (outlined in red).

1 (IRS-1) through ubiquitin-mediated degradation [57]. However, when IL-6 and insulin are infused into healthy human subjects [66, 67], glucose uptake is higher than when compared to insulin alone, reflecting a paradoxical increase in insulin sensitivity, possibly caused by AMPK up-regulation in response to IL-6 [68], despite elevated SOCS-3 levels [66]. Similarly, TNF is implicated as a driver of insulin resistance [69, 70], via NF-κB and c-Jun N-terminal kinase (JNK) leading to serine phosphorylation (and deactivation) of IRS-1 [48, 52]. However, a human study looking at local effects of TNF infusion [71] found an increase in glucose uptake following TNF infusion in humans. Both IL-6 and TNF drive endogenous release of the hormone cortisol [69, 70, 72], which has been found to inhibit insulin-mediated glucose uptake in humans [15, 73, 74]. Additionally, in a study of humans with low cortisol and growth hormone [75], TNF infusion did not trigger the metabolic response found in

the control group. Therefore we propose cortisol (and growth hormone) as the explanatory mechanism for the contradictory cytokine effects.

1.3.4 Published Mechanisms of Insulin Resistance

In this section, many of the mechanistic components identified in humans have been compiled to evaluate their relative contributions to stress hyperglycemia. While these components are metabolically active when identified, further analysis is required to determine if they play an important role in describing metabolic fluctuations in critical care. The metabolically active components listed in Table 1 contain mostly *in vivo* human studies. Previously published reviews [45, 48, 76] use studies including *in vitro* and *in vivo* data to inform mechanism provide a basis understanding mechanisms in the ICU. Any component from Table 1 whose role in human metabolism remains unclear for humans in critical care is a candidate for further mechanistic discovery.

1.3.5 Identifying Human Mechanisms

Figure 3 shows a simplified insulin signaling cascade highlighting key pathway differences in the three primary insulin-responsive tissues: liver, adipose, and muscle. Stress response molecules (left box) act via epinephrine inhibiting the production of insulin [80], cortisol, epinephrine, and growth hormone inhibiting insulin in all tissues, and all three hormones in addition to glucagon activating gluconeogenesis [74, 78, 79, 80, 81, 82]. The innate immune response (right box) shows the synergy of adiponectin citeleh08,piy13,hil12, IL-6 [66], and IL-10 [76, 83] to enhance insulin sensitivity. TNF has shown a mixed role, in [84], infusion of TNF decreased insulin sensitivity in the muscle and not the liver [84]. However, local metabolic measurement studies following infusion show that TNF enhances insulin sensitivity in muscle [71] during a human infusion. Therefore, TNF can be considered to increase glucose uptake. Additionally, IGFBP-1 is associated with liver specific insulin resistance [70] and serves as a marker of critical care outcome [85]. Cortisol plays a central role in causing insulin resistance in critical care. It has been correlated as a predictor of insulin resistance in humans [15, 86] and human studies show cortisol to both increase endogenous glucose

Table 1: Components involved in metabolic regulation having either a positive (+), negative (-) effect on stress hyperglycemia. Source is shown as either human or mixed. A mixed source entry represents a combination of *in vitro* and *in vivo* studies used to corroborate mechanism.

Component	Stress Hyperglycemia	Source(s)
ACTH	+	Human [77]
Adiponectin	-	Mixed [45]
Cortisol	+	Human [73, 74]
CRH	+	Human [77]
Epinephrine	+	Human [78]
Glucagon	+	Human [79]
IGFBP-1	+	Human [70]
IL-1	+	Mixed [76]
IL-10	-	Mixed [76]
IL-6	-	Human [66]
JNK	+	Mixed [48]
NF-κb	+	Mixed [48]
TNF-α	-	Human [71]
Vistafin	-	Mixed [76]

production [73, 74, 87] and increase insulin resistance [73, 74, 88]. Cortisol release is triggered by a number of different cytokines and could be the mechanism of action through which these cytokines correlate to insulin resistance [67, 69, 89]. The observed correlations between cytokines and insulin resistance could be explained by cortisol activation, while the direct mechanistic role of the cytokines act to increase insulin sensitivity in humans [66, 71].

TNF is a cytokine strongly associated with the inflammatory cascade and insulin resistance in humans [69, 70, 84, 90]. However, in many of the human studies, cortisol is

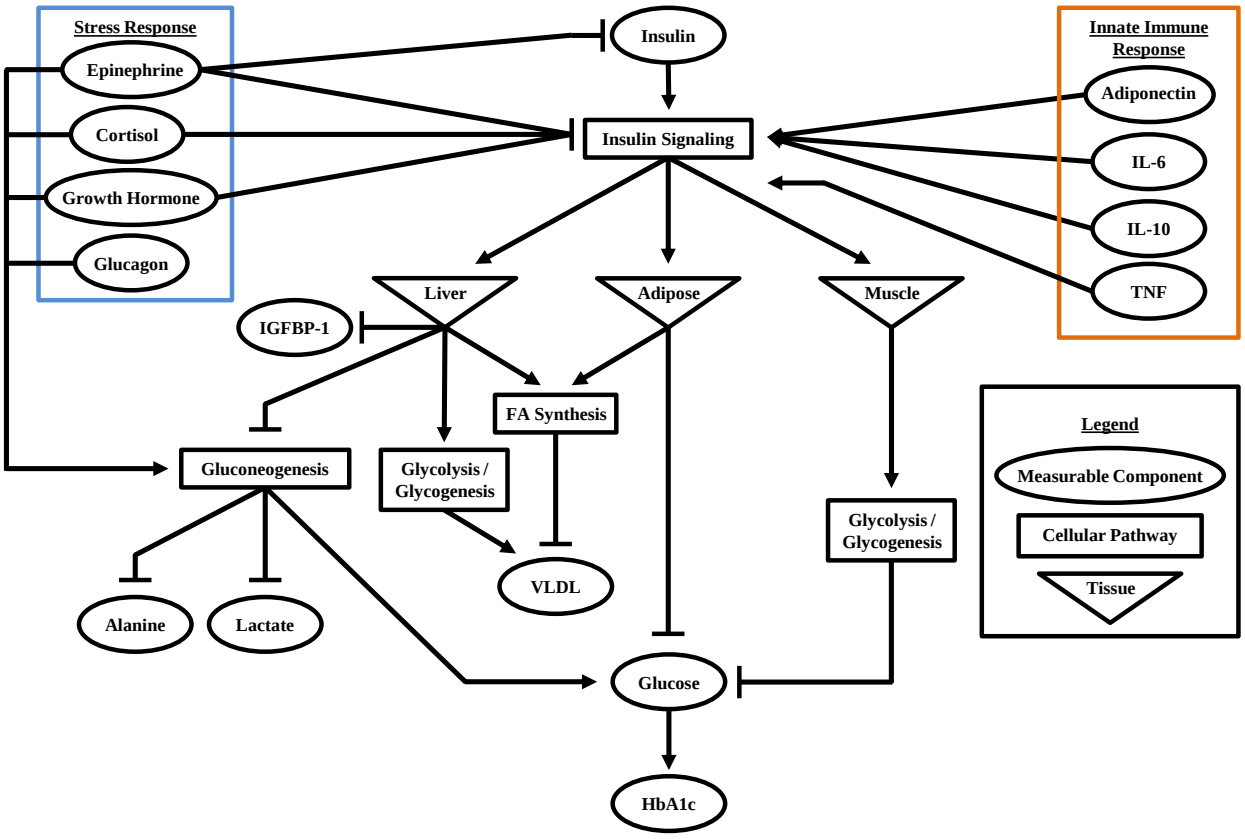

Figure 3: Insulin is released by the pancreas and signals to other tissue types (liver, muscle, and adipose) via plasma circulation. Simplified tissue specific processes are activated via insulin (boxes). Components of interest are shown on either side (ovals) belonging to stress response hormones (left) and the innate immune response (right). Cortisol, epinephrine, and growth hormone act on insulin signaling in all tissues, while all three hormones in addition to glucagon act to promote gluconeogenesis and glycogenolysis. Epinephrine additionally suppresses insulin release, lowering the total insulin available. Adiponectin, IL-6, and IL-10 are generally associated with increased insulin sensitivity while TNF acts locally in muscle to promote insulin-mediated glucose uptake.

either correlated with TNF [15] or significantly elevated following TNF infusion [69, 70, 84]. Cortisol is released via the hypothalamic-pituitary-adrenal (HPA) axis. In a comparison study done in humans [75] TNF was infused, comparing the metabolic response of patients

with hypopituitary function to healthy controls. The study [75] showed cortisol and growth hormone release were necessary to facilitate the metabolic changes driven by TNF infusion. Furthermore, local glucose uptake measurements in humans during TNF infusion show an enhancement in insulin sensitivity [71] indicating TNF as an activator of glucose uptake.

Similar to TNF, studies investigating the effects of IL-6 on insulin sensitivity are contradictory [68]. Correlation analysis [15, 42] shows that IL-6 is one of the best predictors of insulin resistance in critical care patients, second only to cortisol [15]. A study of patients undergoing varying degrees of elective surgery found a "linear relationship between the reduction in relative insulin sensitivity and the concomitant plasma levels of IL-6" [42]. Taken together, these studies [15, 42] begin to describe IL-6 as a mechanistic link to insulin resistance. However, three different human studies found that IL-6 infusion (3-4 hours) either increased insulin-mediated glucose uptake [66], increased rate of glucose appearance [67], or had no effect on glucose appearance or disposal [89]. While cortisol was not reported in [66], the steady-state IL-6 concentration averaged 195 pg/ml, which falls between the two different levels 143 and 319 pg/ml reached during the low and high IL-6 infusions in [89]. Importantly, the cortisol levels in [89] reached approximately 3 times basal levels following both high and low levels of IL-6 infusion. In [67], IL-6 levels reached an average of 594 pg/ml resulting in an approximate 2.5 fold increase in cortisol concentrations. In two separate studies [73, 74], glucose production and insulin resistance were significantly increased when cortisol increased by approximately 1.5 fold [74] or approximately 2.5 fold [73], respectively. Taken together, these human studies [15, 42, 66, 67, 73, 74, 89] suggest two potential mechanisms that balance glucose metabolism. The cytokines TNF [71] and IL-6 [66] increase glucose uptake while simultaneously causing the endogenous release of cortisol. Subsequently, cortisol [73, 74] induces glucose production and insulin resistance. These interactions have been summarized in Figure 4. Incidents of hypoglycemia in critical care are common [5] and have been shown to increase patient mortality risk with even one episode [6]. A follow-up study of the NICE-SUGAR [24] trial found that 45% of the critical care population had moderate hypoglycemia (41-70 mg/dl). The study [25] also found "the adjusted hazard ratios for death among patients with moderate [hypoglycemia was] 1.41." An insulin infusion study [91] shows that a dropping glucose concentration at about 75 mg/dl elicits the counterregulatory response.

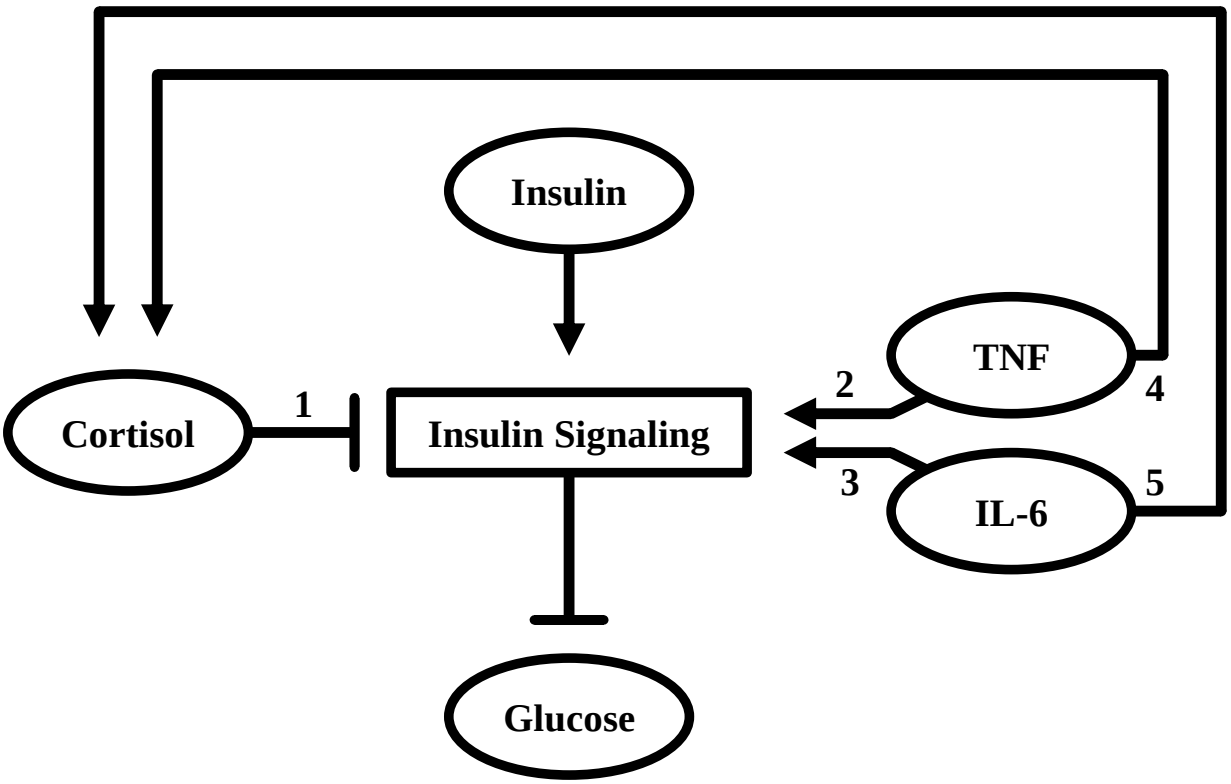

Figure 4: Diagram of key molecules driving changes to glucose metabolism. Cytokines TNF and IL-6 correlate with insulin resistance [15, 42, 67], however, the mechanism of action could be through cortisol activation. (1) Cortisol levels of 1.5 fold [74] and 2.5 fold [73] normal levels cause significant increases in glucose production and insulin resistance. (2) TNF [71] and (3) IL-6 [66] infusions in humans cause increases in glucose uptake. (4) TNF [69, 70, 84] and (5) IL-6 [66, 67, 89] infusions in humans also cause increases in cortisol resulting in metabolically active concentrations seen in [73, 74].

The counterregulatory response consists of the release of glucagon [79], epinpehrine [78], cortisol [74], and growth hormone [82]. Taken together, these studies [5, 6, 25, 74, 78, 79, 82, 91] describe counterregulation as a possible mechanism for glucose-related complications and increased mortality in critical care.

1.4 THESIS OVERVIEW

Chapter one is an overview of stress hyperglycemia and the motivation for glucose control in critical care. The chapter describes the mechanisms leading to stress hyperglycemia and how modeling specific biological pathways could help understand the disease and improve patient outcomes. Certain metabolically active components are investigated to better understand mechanisms and correlations observed in critical care patients. This results in identifying a small number of key biological markers that describe the primary components of stress hyperglycemia.

Chapter two describes the construction of a mathematical model of acute inflammatory effects on glucose metabolism. Lipopolysaccharide (LPS) as an acute inflammatory activator is used to develop the combination of metabolic effects following infection. There are consistent changes to glucose metabolism following the introduction of LPS, where glucose uptake increases and is followed by a period of insulin resistance. The interactions include LPS, TNF as a glucose uptake activator, and cortisol causing insulin resistance. These components represent the core components leading to metabolic changes and shed some light onto the mechanisms of stress hyperglycemia in humans.

Chapter three describes the construction of a mathematical model of the counterregulatory response and how it affects glucose metabolism. Counterregulation occurs as a natural response to low blood glucose concentration, a problem that occurs frequently in critical care. The dynamic changes and mechanistic components causing changes to blood glucose dynamics are examined and modeled. A series of early studies[91] elucidate the four individual components: glucagon, epinephrine, cortisol, and growth hormone. Each of these four components are modeled to form a mechanism of action starting from low glucose, leading to activated hepatic glucose output and systemic insulin resistance.

Chapter four describes the construction of a mathematical model of plasma insulin appearance following a subcutaneous insulin infusion or bolus. This model is motivated by the need for a simple structure that can account for multiple types of insulin (fast-acting release and regular release). The final model contains three parameters to describe plasma

insulin appearance following insulin infusion or bolus. Only one parameter varies between fast-acting insulin and regular insulin.

Chapter five describes the construction of a virtual patient simulator and how it can be used for controller tuning and testing. A nonlinear control algorithm is developed and the performance is evaluated using *in silico* methods to compare to the current clinical standard of care. This chapter also details the ways in which additional dynamic models can be added to form a more realistic biological response. Finally, chapter six is a summary of the work within this thesis, followed by possible extensions of this work providing the basis for additional research studies.

2.0 MODELING GLUCOSE DYNAMICS FOLLOWING AN ACUTE INFLAMMATORY CHALLENGE

2.1 INTRODUCTION

A mathematical model capable of capturing and predicting the biological drivers of stress hyperglycemia can help identify the underlying metabolic dynamics. Ideally, each molecular component contributing to stress hyperglycemia would be built into a systems-level mathematical model to then analyze whether the whole system is equal to, greater, or less than the sum of each part. In practice, however, we develop mechanistic approximations that capture primary pathway effects in light of often infeasible cellular resolution. Herein, we develop a mass-action-based mathematical model to characterize the key regulators of stress hyperglycemia and how they contribute to dynamic metabolic variability and the observed inter- and intra-patient variations in critical care.

2.1.1 Tissue-Specific Modeling of Stress Hyperglycemia

We can understand stress hyperglycemia as a glucose mass balance and explicitly identify the tissue-specific sources and sinks of glucose in the body. Elevated blood glucose levels are primarily caused by the following three mechanisms: (i) uninhibited endogenous glucose production by the liver, (ii) inhibited insulin-mediated glucose uptake and storage as glycogen in primarily muscle and adipose tissue, or (iii) suppressed insulin secretion by the pancreas. While there is some debate as to which process dominates in critical care, there are a number of tissue-specific mechanisms to be elucidated by isolating these three processes.

This material is to be submitted to PLOS Computational Biology

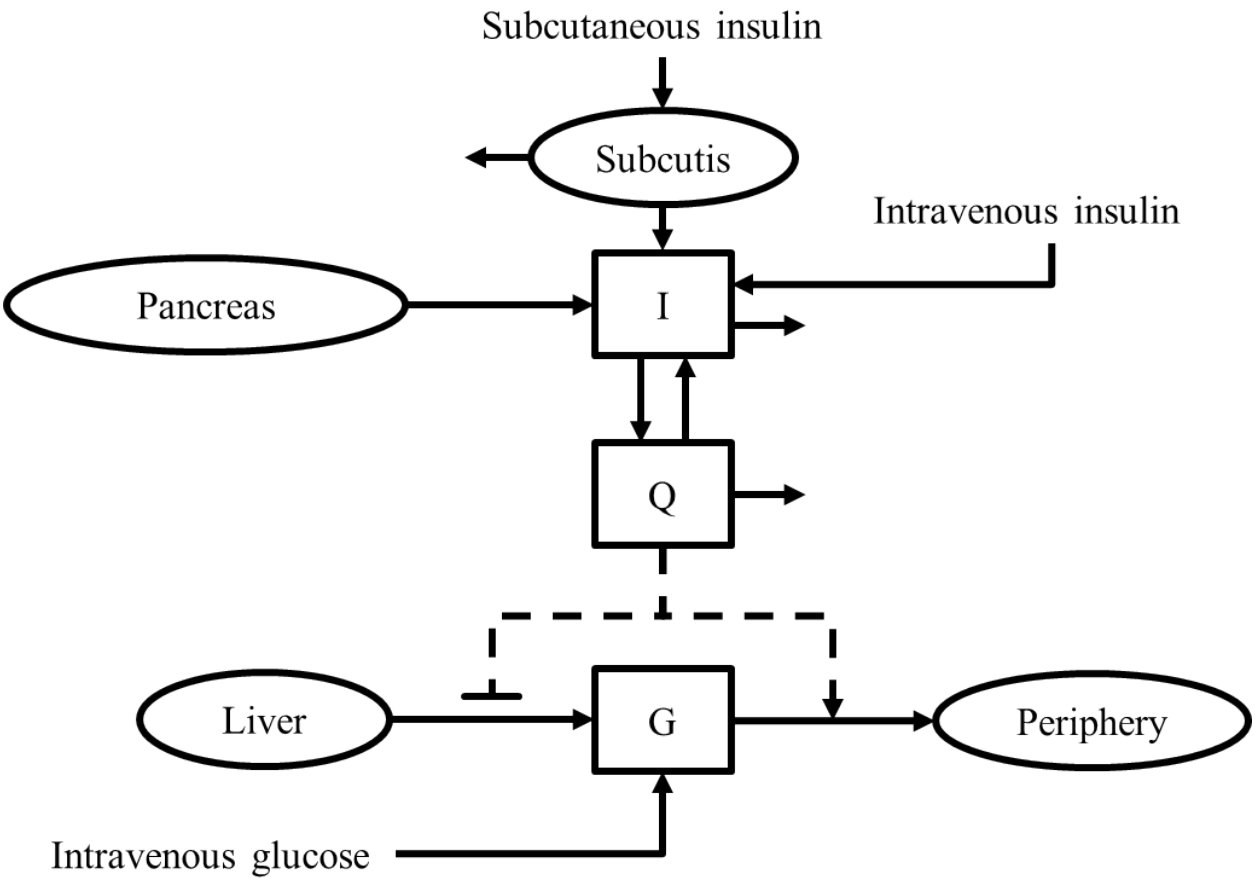

Figure 5: Composite model structure showing insulin and glucose plasma concentrations (squares), along with exogenous and endogenous sources of glucose and insulin.

2.1.2 Insulin Signaling

Endogenous glucose production and insulin-mediated glucose uptake in peripheral tissue are both governed by insulin signaling. Therefore, we build a mechanistic mathematical model of stress hyperglycemia with the insulin signaling cascade. This cascade, depicted in Figure 2, describes the pathway starting from insulin binding to surface receptors, to the translocation of glucose transporters (GLUT4) to the cell membrane, resulting in increased glucose uptake. This process takes place primarily in adipose and muscle tissues, causing glucose uptake into

the target cells. Similarly, the insulin signaling pathway leads to the down-regulation of glucose production via gluconeogenesis and glycogenolysis in the liver.

A previously published mathematical model of the insulin binding pathway [92] is used as a starting point for developing a multiscale, tissue-specific model of the development of insulin resistance leading to stress hyperglycemia. The 22-state ordinary differential equation (ODE) model was originally constructed by measuring insulin-sensitive cells in response to insulin exposure. This creates a number of numerical problems when combining the model with the original organism-level model of glucose and insulin dynamics. First, when the model is exposed to prolonged insulin input, there is a failure in mass-balance closure leading to a drift in insulin-mediated activation. This is addressed by fitting a two-state, nonlinear simplified model to the original model [92] using a series of insulin challenges, as shown in Figure 6. The simplified insulin signaling model is combined with the overall model of glucose and insulin dynamics where the insulin effect state, $Q(t)$, in Figure 5 is replaced with the cell-level model as shown in Figure 7. Plasma concentration of insulin is fed as input to the cell model and GLUT4 translocation output from the cell model is scaled to represent the insulin effect lowering glucose. The combined model is used to fit insulin sensitivity recovery in patients following surgery [93]. The study [93] measured insulin resistance and the cytokine IL-6, and claims IL-6 is responsible for causing insulin resistance. The results of this model fit are not shown due to the overall inaccuracy of this assumption. As previously discussed, IL-6 infusion in humans [66] fails to cause the proposed insulin resistance and thus required a more rigorous analysis of the underlying biology. While the proposed mechanism in [93] does not appear to govern human metabolism, this paper provides an important biological link between the immune system and glucose metabolism. The resolution of measurements in [93] is on the order of days, while in the previous sections, we have shown this mechanism to take place more rapidly, on the order of hours. Therefore, it is likely that the IL-6/insulin resistance relationship forms from the following sequence: inflammatory mechanisms increase IL-6 concentrations, which subsequently increases cortisol levels, leading to insulin resistance. The missing component in [93] is cortisol, which could describe the observed correlation between IL-6 and insulin resistance.

2.1.3 Modeling the Hypothalamic-Pituitary-Adrenal Axis

Cortisol is a key element to model the overlap between the innate immune response and the stress response. It is a stress response hormone responsible for insulin resistance, activated by the inflammatory cytokine response. When modeling cortisol, the primary challenge is representing the endogenous diurnal variations in the Hypothalamic-Pituitary-Adrenal (HPA) axis. The cyclical activation of the HPA axis has been studied and modeled using various waveforms. For example in [94] six different mathematical functions were compared while fitting the diurnal variations in cortisol serum measurements. A cosine driving function is used in our own preliminary work. However, the parameters of such a cycle are impractical to identify in real-time for critical care patients. There are also a number of factors affecting the baseline cycles, including nervous [95] and immune [95, 96] system interactions, creating an unidentifiable situation in critical care [96].

In order to study the effects of IL-6 activating cortisol release, a baseline release model is fit using the control study [67] described as follows. First, cortisol is modeled using an auto-inhibition term:

$$\frac{X_{COR}(t)}{dt} = \frac{U_b(t) + U_I(t)}{X_{COR}(t)/k_3 + 1} - k_d X_{COR}(t) \tag{2.1}$$

Here k_d is the clearance coefficient of cortisol found in the literature [97]. Cortisol release comes from two sources: baseline $U_b(t)$, and IL-6 triggered, $U_I(t)$. Auto-inhibition is represented by the denominator of the first term in Equation (2.1), where k_3 is the normalization concentration of cortisol. IL-6 activates cortisol release $U_I(t)$ as follows:

$$U_I(t) = \frac{k_1 X_{IL6}(t)}{X_{IL6}(t) + k_2} \tag{2.2}$$

Here IL-6 activation of cortisol is represented as a saturating Michaelis-Menten function with maximum rate k_1 and concentration of half-maximal activation k_2. The plasma concentration of IL-6, X_{IL6}, is used as input to the model, activating cortisol release, $U_I(t)$. The results of fitting a human IL-6 infusion study [67] are shown in Figure 8. At each measurement, a baseline cortisol release value $U_b(t)$ is fit to match the baseline plasma cortisol. The same baseline profile, $U_b(t)$, is then simulated when fitting the effects of IL-6 infusion to remove

the confounding effects of changing baseline cortisol. The model is calibrated using nonlinear least-squares regression. $U_b(t)$ varies for the control case at each measurement time point to capture the baseline cortisol release profile shown in Figure 8. The error between model predictions and data at each time point was weighted by the inverse of the standard deviation of the data at that point in time as in Equation (2.12). $U_b(t)$ at each measurement. The baseline release found from the control is used along with the IL-6 infusion to capture IL-6 only activation of cortisol. Results of the fit are shown in Figure 8.

The 95% confidence intervals of the estimated parameters are computed by using *nlparci* in MATLAB (©2015, The Mathworks, Natick, MA). The resulting parameter values and confidence intervals are shown in Table 2. After model calibration using a human infusion study of IL-6 [67], the model was used to predict two different LPS challenges in humans [72]. The hypothesis tested was that the cortisol response observed following LPS infusion is primarily governed by the interaction of IL-6 activating cortisol release. Thus, our model previously calibrated in Figure 8 was first fit to baseline cortisol dynamics to extract the time-varying baseline release $U_b(t)$ as shown in Figure 9. Once baseline release was extracted from the control case, the model of IL-6 driven cortisol release is validated by simulating IL-6 driven effects using the model calibrated previously in Figure 9. The IL-6 trajectories following both low and high dose LPS boluses are used to drive the previously calibrated model as shown in Figure 10. The results shown in Figure 10 validate our model and hypothesis, which describes IL-6 as the primary connection driving the stress response hormone cortisol from the innate immune activation of IL-6. This model provides a groundwork for linking the two processes present in critical care that interact to contribute to significant changes in glucose metabolism. The final model (section 2.2.1) describing LPS and glucose metabolism incorporates this effect using TNF in place of IL-6 as driving cortisol. This simplification was necessary due to data constraints and the fact that the dynamics between TNF and IL-6 following an LPS challenge are similar [72]. The similar dynamics between TNF and IL-6 combined with the fact that TNF activates IL-6 makes the relative contribution of each component unidentifiable without specific experimental data. Additionally, auto-inhibition of cortisol was removed once the full network was developed,

due to the fact that the inhibitory effect of cortisol on the innate immune response (TNF) had the same effect since TNF was used as the driver of cortisol.

The previously described work ultimately leads to a simplified approach where key elements of each major pathway are incorporated into a simplified model described in section 2.2.1. Interleukin 6 (IL-6) is a key innate immune marker responsible for driving cortisol, a primary stress hormone inducing hepatic and peripheral insulin resistance; paradoxically, IL-6 directly increases glucose uptake via AMPK [68]. Our final model describes this dual activation/inhibition of stress hyperglycemia with TNF (combining TNF and IL-6) driving cortisol and simultaneously increasing glucose uptake. Each arrow shown in Figure 12 represents a vital constituent of stress hyperglycemia. Corresponding human infusion data from literature accompanies each arrow which is a prerequisite for our models to represent *in vivo* human responses.

2.2 MATERIALS AND METHODS

2.2.1 Model Development and Assumptions

We model cytokine and hormone driven metabolic changes following infusion of lipopolysaccharide (LPS) in humans. LPS triggers an inflammatory response characterized by the cytokines TNF and IL-6, followed by an anti-inflammatory counterregulatory response primarily acting through cortisol, and growth hormone, and including release of gluconeogenesis activator glucagon. A parsimonious mathematical model represents inflammatory cytokine effects as TNF and the anti-inflammatory effects as a single cortisol state. The network of interactions shown in Figure 11 was developed using data from human studies only [13, 67, 70, 72, 73], in an effort to avoid the inconsistencies and confounders observed between mouse models and humans [42, 66, 68, 98]. These studies are used to develop the activation/inhibition relationships between TNF [71], cortisol [15, 72, 74], and insulin [13]. Figure 11 is represented mathematically by the system of coupled ordinary differential equations (ODEs) shown in Equations (2.3) to (2.11). Pharmacokinetics of injected LPS [99]

are modeled with Equation (2.3). Equations (2.3) to (2.7) describe the relationships between LPS, TNF, and cortisol. A previously published, clinically validated mathematical model [100], shown in Equations (2.8) to (2.11), describes glucose and insulin dynamics.

$$\frac{dX_{LPS}(t)}{dt} = -\frac{X_{LPS}(t)}{1.0+\alpha_{ld}X_{LPS}(t)}, \quad X_{LPS}(0) = \frac{U_{LPS}}{V_{LPS}} \tag{2.3}$$

$$\frac{dX_{LPS2}(t)}{dt} = k_{lf}(X_{LPS}(t) - X_{LPS2}(t)) \tag{2.4}$$

$$\frac{dX_{TNF}(t)}{dt} = k_{lt}\left(1 - \frac{X_{COR}(t)}{X_{COR}(t)+K_{Mct}}\right)X_{LPS2}(t-\psi_{ldt}) + U_{TNF} - k_{td}X_{TNF}(t) \tag{2.5}$$

$$\frac{dX_{COR}(t)}{dt} = \frac{k_{tc}X_{TNF}(t)}{X_{TNF}(t)+K_{Mtc}} - k_{cd}X_{COR}(t) \tag{2.6}$$

$$\frac{dX_{COR2}(t)}{dt} = k_{cf}(X_{COR}(t) - X_{COR2}(t)) \tag{2.7}$$

$$\frac{dQ(t)}{dt} = n_I(I(t) - Q(t)) - n_C\frac{Q(t)}{1+\alpha_G Q(t)} \tag{2.8}$$

$$\frac{dI(t)}{dt} = -n_K I(t) - \frac{n_L I(t)}{1+\alpha_I I(t)} - n_I(I(t) - Q(t)) + \frac{U_{ex}(t)}{V_I} + (1-x_L)\frac{U_{en}}{V_I} \tag{2.9}$$

$$\frac{dG(t)}{dt} = -p_G G(t) - X_{IMGD}(t) + \frac{P + EGP_b - CNS}{V_G} \tag{2.10}$$

$$X_{IMGD}(t) = S_I\frac{Q(t)}{1+\alpha_G Q(t)}G(t) + k_{tg}X_{TNF}^2(t)G(t) - k_{c2g}X_{COR2}(t-\psi_{cdg}) \tag{2.11}$$

The states $X_{LPS}(t)$ and $X_{LPS2}(t)$ represent the effective LPS in the system and the active pathways driven by LPS, respectively. A time delay, ψ_{ltd}, is added between the lagged LPS signal, $X_{LPS2}(t)$ and TNF activation to capture the time necessary for biological processing of the LPS signal (*i.e.,* cell signaling, transcription, and translation). Changes in cytokine and hormone concentrations, $X_{TNF}(t)$ and $X_{COR}(t)$, respectively, represent the change from baseline concentrations of TNF and cortisol. The parameter U_{TNF} represents the TNF infusion from [70] scaled by the TNF volume of distribution. Equations (2.8) to (2.10) come from [100], with Equation (2.11) modified to include cytokine and cortisol concentration effects, as appended to the original formulation. The states $I(t)$ and $G(t)$ are the plasma concentrations of insulin and glucose, respectively. The intermediate insulin state, $Q(t)$, represents the remote insulin that drives the insulin-dependent term in the glucose balance, $X_{IMGD}(t)$, and accounts for both insulin suppression of endogenous glucose

production (EGP) as well as insulin-mediated glucose uptake (IMGU), referred to collectively as insulin-mediated glucose dynamics (IMGD; Equation (2.11)). $X_{IMGD}(t)$, herein modified to represent both IMGU and EGP. Equation (2.11) captures the changes in insulin effect induced by inflammatory cytokines (increased sensitivity) and hormones (decreased sensitivity), as seen in humans [15, 66, 71, 73]. This is represented by the state X_{TNF} and is squared to capture the sharp dynamic increase in IMGD activation. Cortisol inhibits $X_{IMGD}(t)$ through a filtered state X_{COR2} which has a time delay of ψ_{cdg} which accounts for the aforementioned signaling time. The cortisol effect is lagged through a filter in addition to the delay to account for the signal dispersal that appears in the glucose inhibition dynamics.

2.2.2 Human *in vivo* Data for Model Calibration

Data from three different studies [13, 70, 99] were digitized using WebPlotDigitizer [101] and used to fit the parameters of the model (Equations (2.3) to (2.11)). Human *in vivo* data was explicitly used so that the final model represents clinically-relevant patient-level dynamics. Three studies were used together to capture varying levels of inflammatory response, as well as capture multiple components and interactions not measured simultaneously within a single dataset. Figure 12 shows the interactive species measured in each respective dataset. The three datasets consist of two different LPS challenges [13, 99] and a continuous infusion of TNF [70]. Data from [99], an LPS type EC-5 injection of 2 $\frac{ng}{kg}$, were used to fit parameters describing LPS dynamics and LPS activation of endogenous TNF release. Data from [70], a continuous 1 $\frac{\mu g}{hr\ m^2}$ infusion of recombinant human TNF, were used to capture TNF dynamics and TNF effects on endogenous cortisol release. Plasma TNF appearance following infusion is constrained to reach 99% of steady-state concentration a minimum of 30 minutes after infusion. This constraint is based on TNF infusion data from [102]. Data from [13], an LPS type EC-6 injection of 20 $\frac{U}{kg}$, were used to fit parameters describing LPS-induced endogenous TNF release, TNF-induced cortisol production, and the inhibition of TNF by cortisol. Since the two types of LPS vary between [13] and [99], a scaling factor (k_{LPS}) is used to estimate the EC-5 equivalent (from [99]) of the EC-6 LPS used in [13]. The dataset from [13] is also used to calibrate the insulin and glucose dynamics resulting from the insulin infusion

and LPS injection. During the study, a hyperinsulinemic euglycemic clamp with an insulin infusion of 80 $mU/m^2/min$ was performed over a period of 10 hours, during which either an LPS challenge was administered after the first 2 hours of the clamp, or no LPS was administered in the control case. The cytokine TNF and the hormone cortisol were sampled every hour from blood. Blood glucose was held approximately constant at 90 mg/dl using a continuous glucose infusion; therefore, the amount of glucose infused as a function of time represents the IMGU in addition to the insulin-driven suppression of EGP, as represented in Equation (2.11).

2.2.3 Parameter Identification

Model calibration is performed in two stages. First, baseline insulin and glucose dynamics (Equations (2.8) to (2.11)) were calibrated with glucose and insulin measurements following a hyperinsulinemic euglycemic clamp [13] using nonlinear regression. During the calibration, regularization was used to maintain model parameters close to the originally published parameters from [100]. The recalibrated baseline parameters were then used in the second fitting stage, where the model captures the additional effects of TNF and cortisol on glucose uptake. During the second fitting stage, parameters from Equation (2.3) to (2.7) and Equation (2.11) are simultaneously fit using Markov chain Monte Carlo (MCMC) optimization to the three datasets [13, 70, 99], as previously described and shown in Figure 12.

2.2.3.1 Stage I: Nonlinear Regression with Regularization Parameter estimation in stage I was performed using least-squares nonlinear regression, *lsqnonlin*, implemented in MATLAB (©2015, The Mathworks, Natick, MA). The residual error between model predictions and data at each time point is weighted by the inverse of the sample standard deviation of the data at that point in time as follows:

$$\min_{\underline{\theta}} \sum_{i=1}^{N} \left[\frac{y_j(t_i) - y(t_i, \underline{\theta})}{\sigma_{ij}} \right]^2 \tag{2.12}$$

Here, $y_j(t_i)$ is the measured data at time t_i during experiment j, which has a standard deviation of σ_{ij}. The model prediction is given by $y(t_i, \theta_1, \ldots, \theta_M)$, which depends on θ_m,

$m \in [1, M]$, the model parameters. N is the number of data points, and M is the total number of model parameters being calibrated. The log transformed regularization penalizes parameter deviations from the previously published model [100]. Shown in Equation (2.13), the baseline parameters governing glucose and insulin dynamics were fit while minimizing the logarithm of fraction difference between the previously published studies' parameters. Such regularization penalizes large deviations from the published parameters and is asymmetric to more strongly penalize driving existing parameters to zero, a possible consequence of having data that is more sparse than the data used to build the original model [100].

$$\min_{\underline{\theta}} \left\{ \sum_{i=1}^{N} \left[\frac{y_i(t_i) - y(t_i, \underline{\theta})}{\sigma_i} \right]^2 + \Gamma \sum_{j=1}^{M} \left[\log_{10} \left(\frac{\theta_j}{\theta_j^*} \right) \right]^2 \right\} \tag{2.13}$$

Here the residual sum of squared error is supplemented with a penalty for parameter deviation from nominal parameters θ_j^* from [100]. The weighting parameter, Γ, is used to trade off the relative contributions of quality of fit, $\sum_{i=1}^{N} \left[\frac{y_i(t_i) - y(t_i, \underline{\theta})}{\sigma_i} \right]^2$ and parameter consistency with [100], $\sum_{j=1}^{M} \left[\log_{10}(\frac{\theta_j}{\theta_j^*}) \right]^2$.

2.2.3.2 Stage II: Markov chain Monte Carlo After the baseline insulin and glucose dynamics are fit in stage I, the parameter space is explored using a Markov chain Monte Carlo (MCMC) search with parallel tempering to provide posterior distributions for the model parameters, as in [103]. Relative parameter steps are sampled from a Gaussian distribution and accepted according to the probability $e^{(-\Delta J / T(k))}$. Parameter values swap with values found in neighboring temperature chains, $\underline{T}$, with probability $e^{(-\Delta J / \Delta T)}$. The vector $\underline{T}$ is the range of parallel temperatures $T(index) \in \{T(1) \dots T(k)\}$. Here $J(\underline{\theta})$ is the energy function defined as:

$$J(\underline{\theta}) = \sum_{d=1}^{D} \sum_{i=1}^{N_d} \left[\frac{y_i(t_i) - y(t_i, \underline{\theta})}{\sigma_i} \right]^2 \tag{2.14}$$

Equation (2.14) contains the sum of squared residual error and is proportional to the negative log-likelihood estimate. The measured data at time t_i are compared to the model with parameters θ_j, $j \in [1, M]$. N_d is the number of data points per dataset $d \in D$ and M is the total number of model parameters.

MCMC was run for a total of $1e06$ steps with a swap attempt every 25 steps. Parameter values are saved during each swap attempt, resulting in $4e04$ saved parameter sets. The integrated autocorrelation time as defined in [104] is calculated for each parameter. The maximum absolute integrated autocorrelation time among parameters is $3e-12$. The low integrated autocorrelation time indicates that the number of simulations during MCMC is sufficient to approximate the posterior parameter distributions.

2.3 RESULTS

2.3.1 Calibrating Baseline Glucose and Insulin Dynamics

For the first stage of model calibration, regularized nonlinear regression was used to fit baseline insulin pharmacokinetics and pharmacodynamics during an 80 $\frac{mU}{m^2\ min}$ insulin infusion [13]. Insulin-mediated glucose dynamics are calculated as in [13], where $M(t)$ is the percentage change in glucose uptake starting from 120 minutes after beginning an insulin infusion as shown in Equation 2.15.

$$M(t) \quad = \quad 100 \times \left(\frac{IMGD(t) - IMGD(120)}{IMGD(120)} \right) \tag{2.15}$$

The parameters in Equations (2.8) to (2.11) were fit to match $M(t)$, while simultaneously capturing baseline endogenous insulin (constant) as well as the insulin concentration, $I(t)$. The regularization coefficient, Γ from Equation (2.13), was determined by scanning over a range of Γ values from 0 to 2 in increments of 0.001. The maximum absolute slope of the derivative for each term occurred at $\Gamma = 0.74$, indicating a reasonable trade-off between fitting the current data set and proximity to the original parameter values. Values of the fitted parameters compared to nominal values are shown in Table 3.

2.3.2 LPS Pharmacokinetics and Pharmacodynamics

In the second fitting stage, three different datasets were used to calibrate model Equations (2.3) to (2.7) and Equation (2.11). Figure 14 shows the calibrated model capturing LPS pharmacokinetics, as well as the TNF response from [99] following a 2 $\frac{ng}{kg}$ LPS injection. The parameter V_{LPS} is found as the initial dose of 2 $\frac{ng}{kg}$ divided by the initial condition of the model simulation in Figure 14 (top). Nonlinear clearance from Equation (2.3) was necessary to capture the rapid elimination of plasma LPS seen in Figure 14. Much of the variability in TNF response occurs during the maximum, between 50 and 100 minutes following LPS administration, which is recapitulated in the model variability represented as red and beige confidence intervals in Figure 14 (bottom). Figure 15 shows the model compared to TNF and cortisol data from [70], where 1 $\frac{\mu g}{hr\ m^2}$ of recombinant human TNF is continuously infused into healthy human subjects. Simulated plasma TNF and cortisol concentrations shown in Figure 15 follow the data from [70]. Figure 16 shows the calibrated model capturing TNF and cortisol dynamics from [13] following a 20 $\frac{U}{kg}$ LPS injection. The conversion factor between EC-5 and EC-6 type LPS, k_{LPS}, was fit to capture the magnitude of TNF response seen in Figure 16 (top), where the largest variability in both the data and the model occurs during the peak TNF response following LPS administration. Cortisol dynamics driven by TNF are captured at two different magnitudes: (1) following a high LPS bolus, shown in Figure 16 (bottom), and (2) during a low TNF infusion, shown in Figure 15 (bottom). Agreement between simulations and the data show the model captures both the range and nonlinearity of the dynamic relationship between TNF and cortisol. Cortisol overestimation of the last data point is caused by the simultaneous fit of cortisol in 15 and additional long term measurements could elucidate which cortisol value is more accurate. Figure 17 shows the model capturing the effects of inflammation (TNF) and anti-inflammation (cortisol) on insulin-mediated glucose dynamics in Equation (2.15). The TNF and cortisol dependent terms in Equation (2.11) are fit to match data from [13] following a 2 $\frac{U}{kg}$ LPS injection given 120 minutes following the start of a continuous insulin infusion of 80 $\frac{mU}{min\ m^2}$. The large amount of model variability around 90 minutes following the insulin infusion is indicative of the effects of TNF (inflammation) on rapid increases in glucose uptake. The model captures

possible individual variations and highlights the time range during which we expect patient-specific variations to have the largest impact on blood glucose dynamics. The model can therefore inform potential time periods of higher risk based on these highly variable regions in time as seen in Figure 17. The decrease in glucose uptake beginning around 250 minutes after the start of insulin infusion shows the delayed effects of cortisol (anti-inflammation) causing insulin resistance.

2.4 DISCUSSION

We show that the interactions between the human innate immune system and the endocrine metabolic response can be modeled using a simplified structure relating key mechanistic drivers. Baseline insulin pharmacokinetics and pharmacodynamics are calibrated using data from a previously published LPS infusion study [13]; regularization was used to maintain the parameters of the physiologically-motivated model near their originally published values for critical care patients [100]. The complex activation and negative feedback between TNF, cortisol, and LPS is captured using an ordinary differential equation structure with parameters fit via Markov Chain Monte Carlo (MCMC) search to explore the parameter landscape across three different datasets [13, 70, 99]. The baseline and inflammatory challenge models combine to describe the contributions of the inflammatory response to insulin mediated glucose dynamics. The resulting model provides a mechanistically motivated description of key biomarkers driving transient changes to glucose metabolism following an acute inflammatory challenge.

The original model from literature [100] and the published insulin pharmacokinetic and pharmacodynamic data [13] show agreement with the literature-derived model parameters, to within small changes (Table 3). Such agreement indicates that the model effectively captures the combined effects of both insulin mediated glucose uptake (IMGU) and insulin suppression of endogenous glucose production (EGP) in a mathematically combined effect, collectively referred to herein as insulin mediated glucose dynamics ($IMGD(t)$, Equation (2.11)). The only free parameter fit during the baseline calibration is the parameter U_{en}, the endogenous

release of insulin. We chose to model U_{en} as a constant, instead of employing physiologically driven dynamics, due to the rapid increase in exogenous insulin that would marginalize the effect of changes in endogenous insulin release.

Correlation analysis is performed on the parameter distributions obtained from MCMC. The correlation coefficient (ρ) is calculated between each pair of parameters over the $4e04$ saved parameter values. The analysis excluded the regularized parameters previously published [100] resulting in analysis for the remaining 16 in table 4. Two pairs were found to be highly correlated with a $\rho \geq 0.95$. TNF degradation rate, k_{td}, is highly correlated with the scaled TNF infusion rate U_{TNF} ($\rho = 0.99$). Similarly, cortisol degradation k_{cd} and the magnitude of cortisol activation by TNF, k_{tc} is highly correlated ($\rho = 0.95$). These correlations indicate that a single parameter could be used in place of each correlated pair, with a corresponding constant scaling factor. This constant substitution would be useful for fitting patients in critical care because it reduces the total number of fitted parameters to capture the inflammation-driven metabolic model.

The simplified mass-action model captures the activation, propagation, and negative inhibition dynamics of LPS driving TNF and cortisol, which ultimately cause changes in insulin-mediated glucose dynamics. The scale and scope of the interactions within the model were chosen to emphasize observed human dynamics, thereby excluding some inconsistent findings from cell and animal studies to maintain applicability to human subjects.

The primary components of the model represent a simplified network combining multiple effects. The increased glucose uptake observed with both TNF [71] and IL-6 [66] infusions in humans are combined into the TNF state, because their relative contributions cannot be independently identified from the time series data in [13, 70, 99]. Similarly, the counter-insulin effects of cortisol, glucagon, and growth hormone are combined into the cortisol state due to the fact that, in many of the datasets used, there is a large amount of dynamic overlap between these species. These simplified primary components play a key role in regulating the effect of insulin on glucose dynamics and are the first step towards mathematically describing the complex interplay of inflammation, anti-inflammation, and metabolism on glucose-insulin dynamics. Additional experiments in, and measurements from, human subjects could help

resolve the individual contributions of these combined species of interest while simultaneously informing estimates of interpatient variability.

Stress hyperglycemia is induced mechanistically by inflammatory, anti-inflammatory, and metabolic signaling. The mathematical model we developed reconciles this complex dynamic relationship and provides temporal resolution to explain the observed insulin effects during acute inflammation. The overall model describes the core drivers of metabolic change during acute inflammation. Key measurements of these primary components in the two pathways could provide a metabolic fingerprint to be used to identify the degree of insulin resistance in a patient during acute inflammation. This type of fundamental metabolic knowledge can be used for treatment of stress hyperglycemia in critical care.

Our model is a first step towards understanding the dynamics of between inflammation and endocrine function. Mechanistic understanding through modeling can identify points of actuation within the interaction cascade. Though additional cytokines, hormones and signaling pathways require further experimental and modeling study (*e.g.*, IL-6, IL-10, epinephrine, growth hormone, glucagon), additional experiments will further improve the quality and resolution of both the model and clinical understanding of stress-induced hyperglycemia. This metabolic resolution could be used to differentiate treatment cohorts, as well as provide dynamic predictions of various outcome and risk trajectories. Furthermore, the establishment of additional points of actuation may also identify novel treatments to improve blood glucose control in critical care patients. Resolving the contributions leading to rapid blood glucose dynamics provides key insight for design of a decision support system for maintaining blood glucose control. Such a system could estimate an individual patient's underlying metabolic state, via simulation and collection key measurements, to allow for real-time personalized treatment.

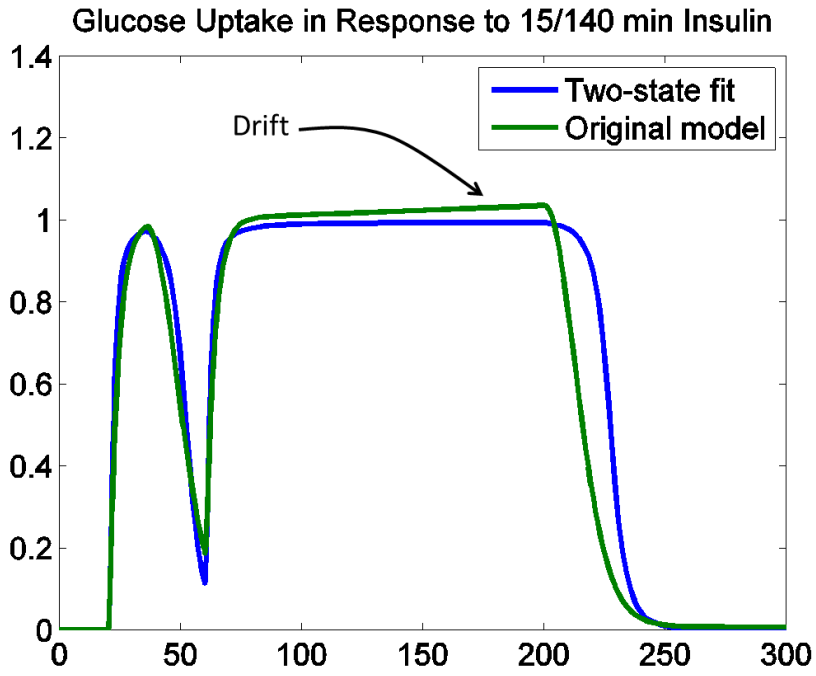

Figure 6: Simplified model (blue) fit to original model (green) following two different insulin challenges of 15 minutes, and 140 minutes. Drift becomes clear during the longer, 140 min insulin infusion.

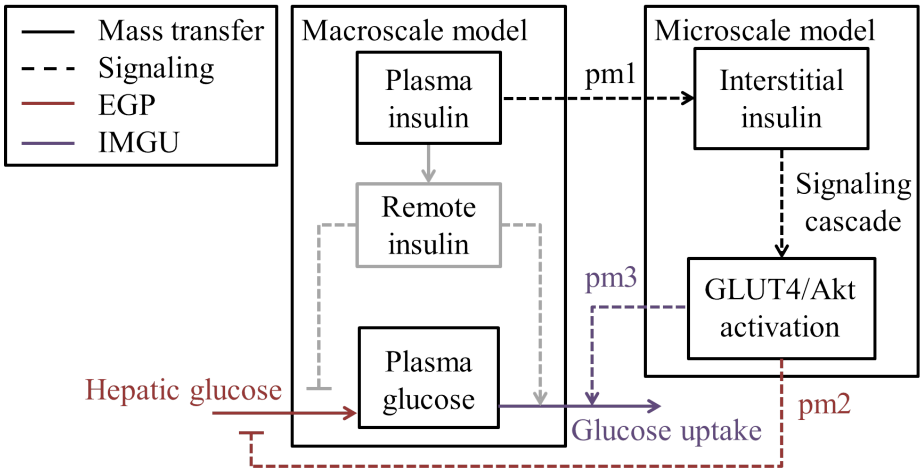

Figure 7: Multiscale model structure. Plasma insulin is scaled by parameter pm1 as fraction diffused. Cellular effects (right) are multiplied by the scaling factors pm2 (Endogenous glucose production: EGP) and pm3 (Insulin mediated glucose uptake: IMGU).

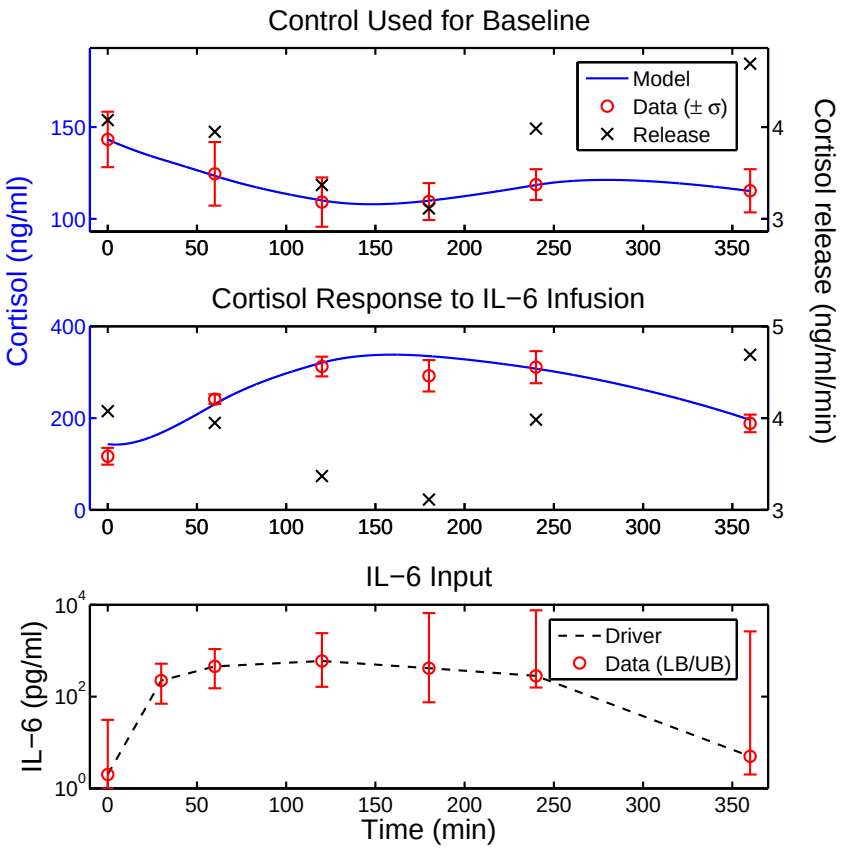

Figure 8: Baseline cortisol levels (top: red) used to fit basal cortisol release (top/middle: black) to match model baseline (top: blue) to data (top/middle: red). Resulting model fit (middle: blue) of plasma cortisol as a function of IL-6 infusion (bottom).

Table 2: Parameter set for IL-6 driving cortisol model.

Parameter	Value	CI(±)	Units
k_d	0.0105	fixed [97]	min^{-1}
k_1	169.4	35.6	ng pg^{-1} min^{-1}
k_2	2,059	391.2	pg ml^{-1}
k_3	27.9	< 0.0	ng ml^{-1}
$u_b(t)$	3.1-4.7	0.7	ng ml^{-1} min^{-1}

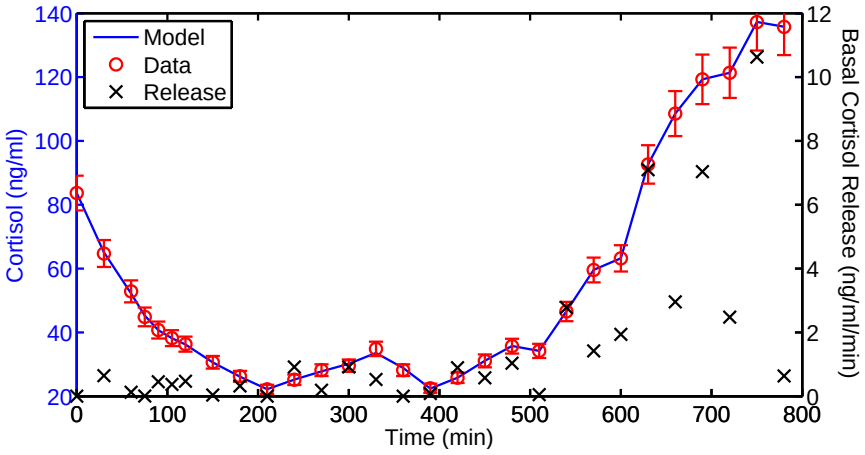

Figure 9: Cortisol baseline measured for prediction data set (n = 26) [72]. Model (blue) fit to control data (red) by adjusting baseline cortisol release (right: black).

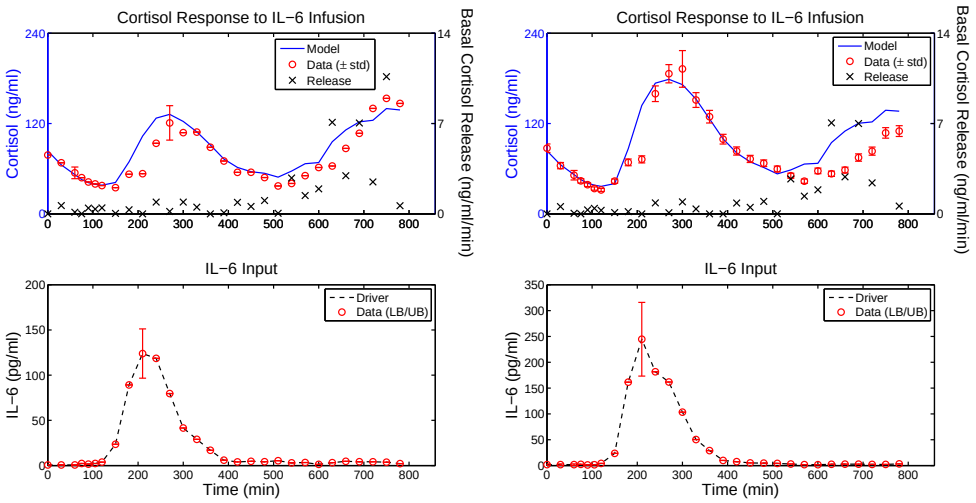

Figure 10: Low, 0.4 $\frac{ng}{kg}$ (n = 16), LPS infusion (left) and high, 0.8 $\frac{ng}{kg}$ (n = 12), LPS infusion (right) are predicted by model from previous dataset [67]. IL-6 (bottom) drives cortisol release. Baseline release used as underlying source for two different LPS dose levels.

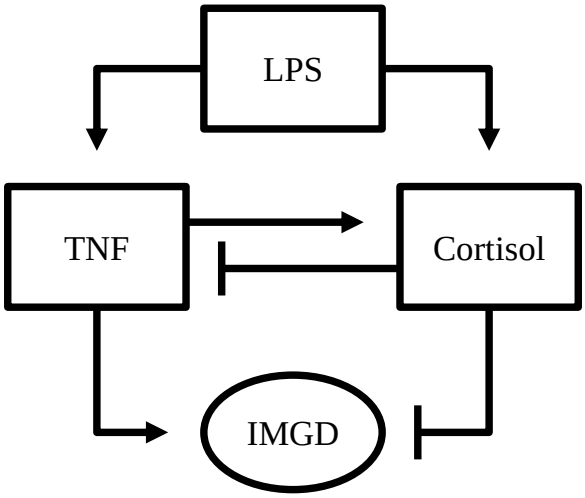

Figure 11: Crosstalk between the inflammatory response (represented by TNF, left) and the anti-inflammatory response (represented by cortisol, right). Both pathways lead to changes in insulin-mediated glucose dynamics (IMGD).

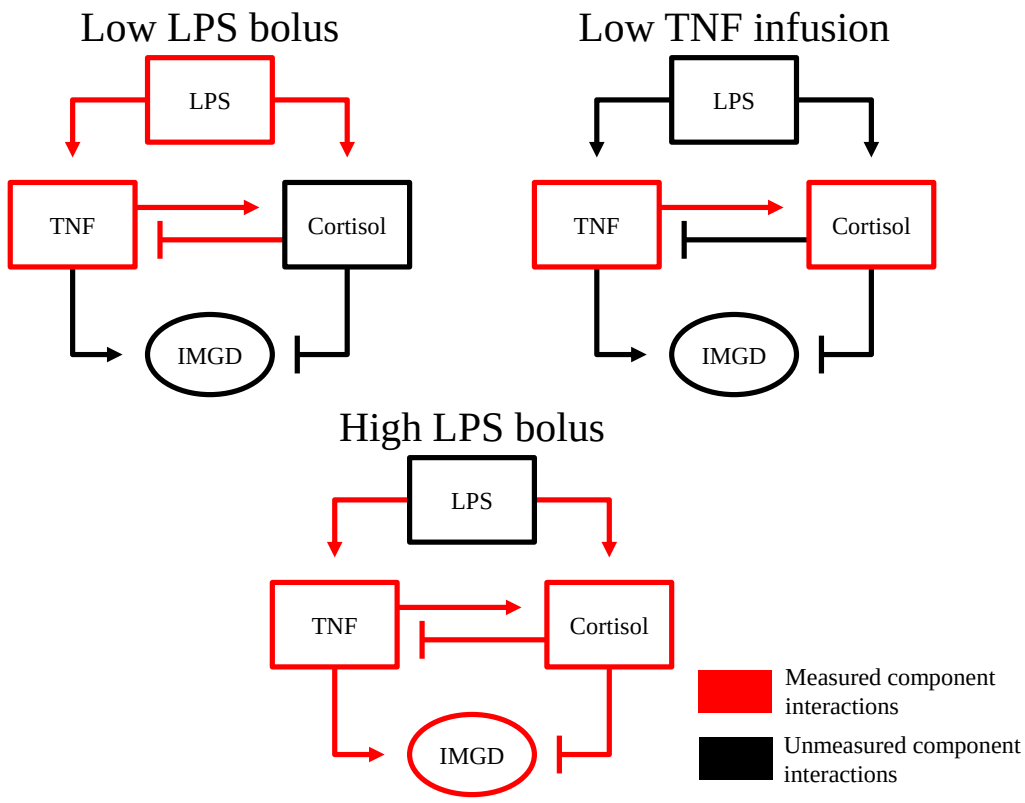

Figure 12: Measured components from the three different datasets used simultaneously in fitting the model (Equations (2.3) to (2.7) and Equation (2.11)). Top left: a low-dose LPS bolus [99] is delivered with plasma LPS and TNF measured. Top right: a continuous, low-dose intravenous infusion of TNF [70] with plasma TNF and cortisol measured. Bottom center: a high-dose LPS bolus [13] is delivered with plasma TNF, cortisol, insulin, and glucose measured.

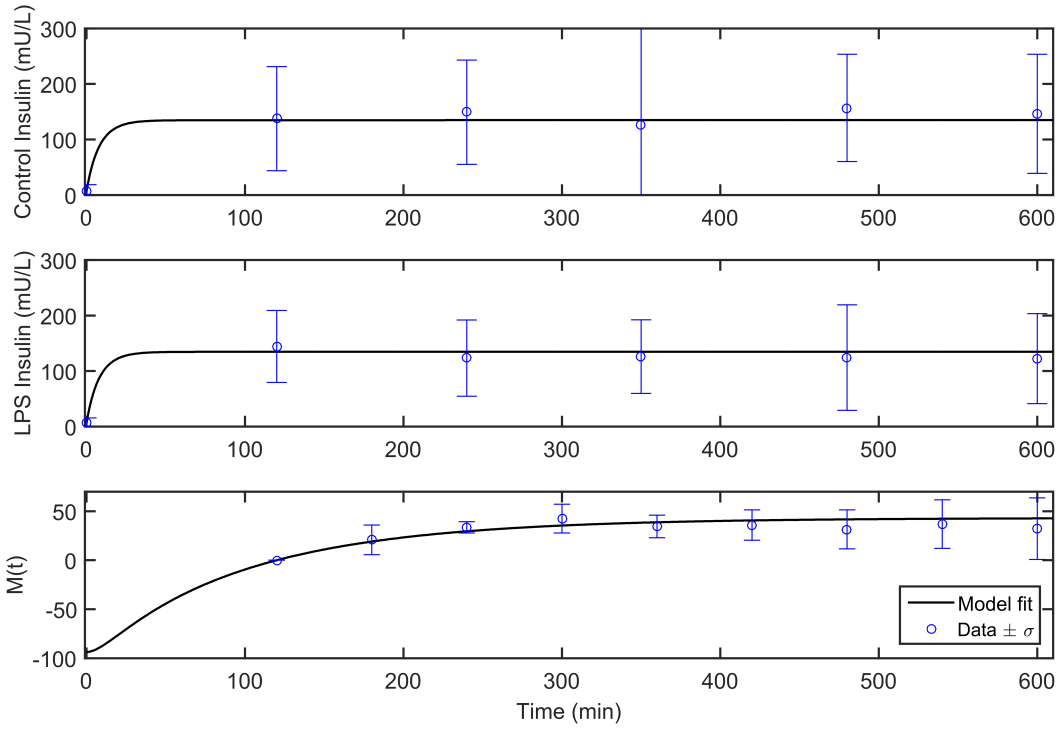

Figure 13: Model dynamics (black line) compared to data (blue, mean ± 1 standard deviation, from [13]) during a continuous insulin infusion. Insulin concentrations for control (top) and LPS challenge (middle) are fit in addition to insulin effect on glucose uptake (bottom). The parameters used to fit these data are regularized to account for the lack of dynamic resolution.

Table 3: **Stage I model parameters. Parameters without a value for Best were not adjusted from the original publication [100].**

Parameter	Units	Nominal [100]	Best	Ratio
a_G	$\frac{L}{mU}$	$1.54e-02$	$5.67e-03$	$3.68e-01$
n_I	min^{-1}	$3.00e-03$	$1.47e-03$	$4.91e-01$
n_C	min^{-1}	$3.00e-03$	$9.63e-03$	$3.21e+00$
n_K	min^{-1}	$5.42e-02$	$4.36e-02$	$8.05e-01$
n_L	min^{-1}	$1.58e-01$	$1.12e-01$	$7.07e-01$
a_I	$\frac{L}{mU}$	$1.70e-03$	$2.01e-03$	$1.18e+00$
V_I	L	$3.15e+00$	$4.76e+00$	$1.51e+00$
x_L	$none$	$6.70e-01$	$6.77e0-1$	$1.01e+00$
U_{en}	$\frac{mU}{min}$	–	$1.49e+01$	–
Γ	$none$	–	$7.41e-01$	–
p_G	min^{-1}	$6.00e-03$	–	–
SI	$\frac{L}{mU \cdot min}$	$3.00e-04$	–	–
P	$\frac{mg}{min}$	$0e+00$	–	–
EGP_b	$\frac{mg}{min}$	$2.09e+02$	–	–
CNS	$\frac{mg}{min}$	$5.40e+01$	–	–
V_G	dl	$1.33e+02$	–	–

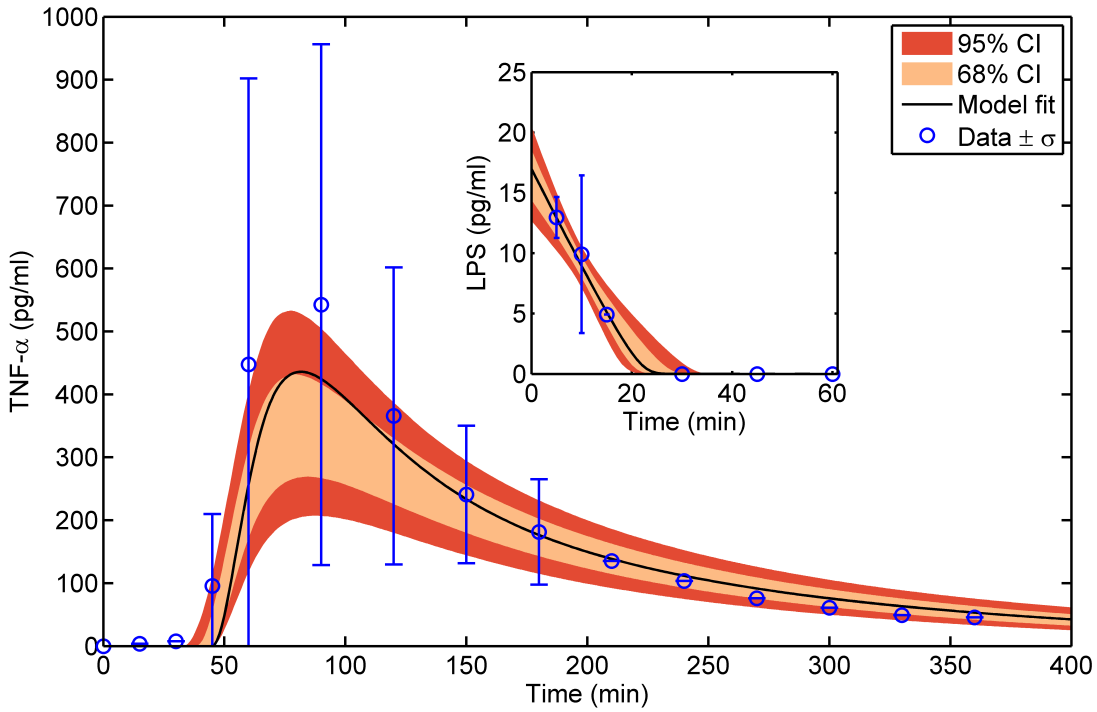

Figure 14: Model dynamics (black line) compared to data (mean: blue circles; error bars represent ± 1 standard deviation) for LPS (top) and TNF (bottom) from [99] following a 2 $\frac{ng}{kg}$ EC-5 LPS bolus injection at time=0. The shaded region denotes 68% (beige) and 95% (red) confidence in dynamic response using accepted parameter sets found via MCMC.

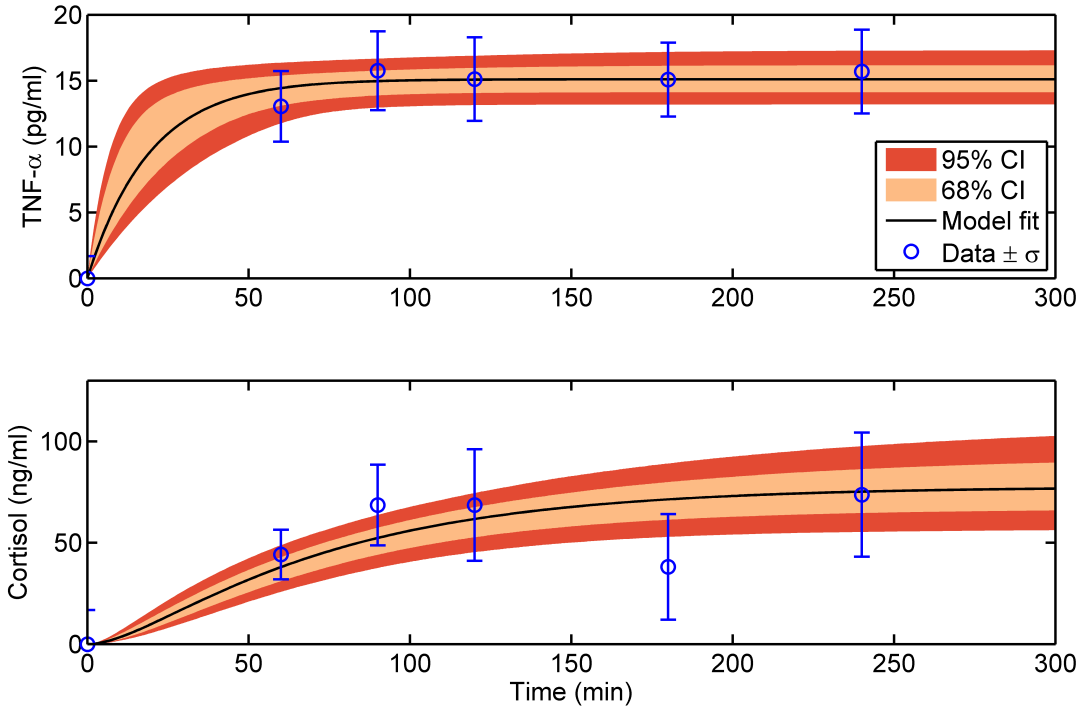

Figure 15: Model dynamics (black line) compared to data (mean: blue circles; error bars represent ± 1 standard deviation) for TNF (top) and cortisol (bottom) from [70] following a continuous TNF infusion. The shaded region denotes 68% (beige) and 95% (red) confidence in dynamic response using accepted parameter sets found via MCMC.

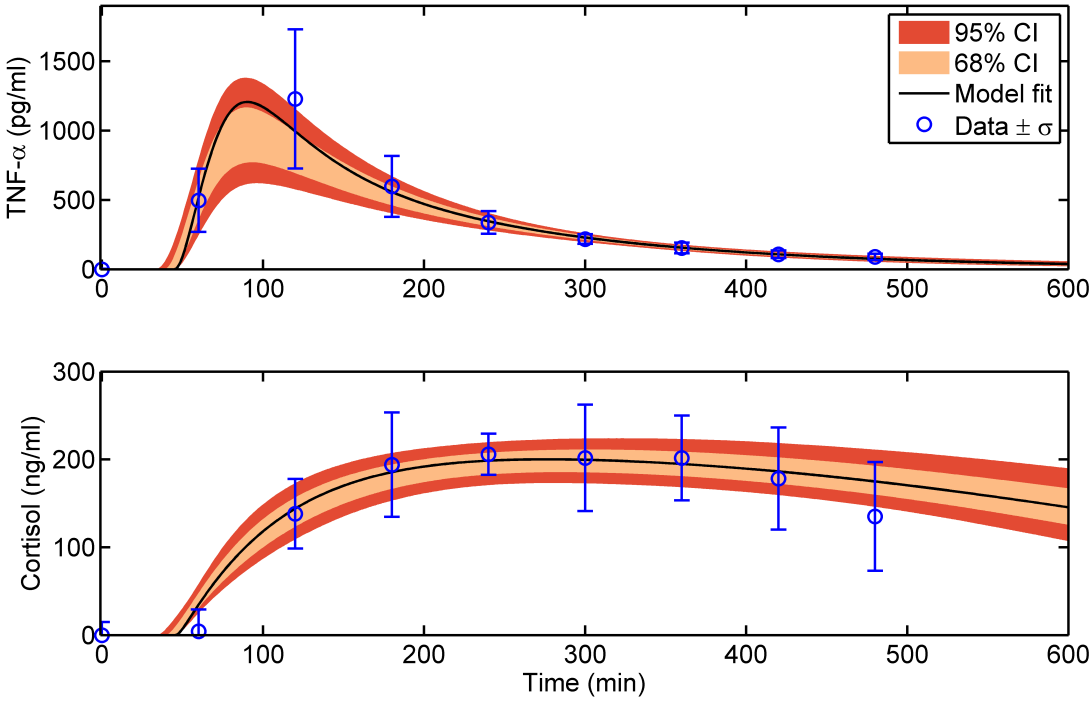

Figure 16: Model dynamics (black line) compared to data (mean: blue circles; error bars represent ± 1 standard deviation) for TNF (top) and cortisol (bottom) from [13] following an LPS bolus injection at time=0. The shaded region denotes 68% (beige) and 95% (red) confidence in dynamic response using accepted parameter sets found via MCMC.

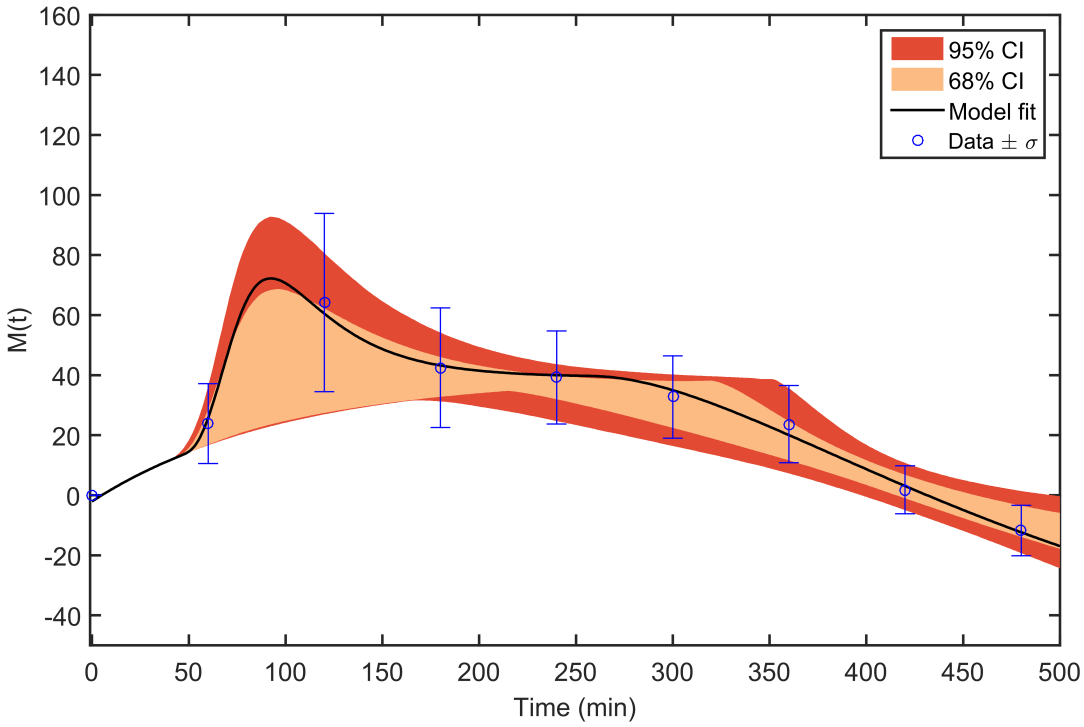

Figure 17: Model dynamics (black line) compared to data (mean: blue circles; error bars represent ± 1 standard deviation) for IMGD percent change described in Equation (2.15). Data from [13] following an LPS bolus injection at time=0 minutes during a continuous insulin infusion starting at time=-120 minutes. The shaded region denotes 68% (beige) and 95% (red) confidence in dynamic response using accepted parameter sets found via MCMC.

Table 4: **Stage II model parameters. Best model parameter values found with MCMC with minimum and maximum value of top 95% of accepted MCMC samples.**

Parameter (units)	Best	Min 95%	Max 95%
$V_{LPS}(\frac{L}{kg})$	$1.18e-01$	$8.26e-02$	$1.98e-01$
$\alpha_{ld}(\frac{mL}{pg})$	$1.16e+00$	$5.14e-01$	$3.29e+00$
$k_{lf}(min^{-1})$	$6.58e-03$	$2.88e-03$	$1.01e-02$
$K_{Mct}(\frac{ng}{mL})$	$8.69e+01$	$8.70e-02$	$8.69e+04$
$k_{lt}(min^{-1})$	$4.35e+01$	$5.04e+00$	$1.64e+04$
$\psi_{ldt}(min)$	$4.47e+01$	$1.70e+01$	$4.50e+01$
$U_{tnf}(\frac{pg}{min})$	$7.84e-01$	$2.55e-01$	$2.74e+00$
$k_{td}(min^{-1})$	$5.19e-02$	$1.41e-02$	$1.59e-01$
$k_{tc}(\frac{ng}{pg \cdot min})$	$3.43e+00$	$1.39e+00$	$8.21e+00$
$K_{Mtc}(\frac{pg}{mL})$	$2.78e+01$	$8.43e+00$	$7.56e+01$
$k_{cd}(min^{-1})$	$1.55e-02$	$5.12e-03$	$3.82e-02$
$k_{cf}(min^{-1})$	$3.24e-03$	$3.24e-06$	$3.24e+00$
$k_{c2g}(\frac{mL}{ng}\frac{mg}{dl \cdot min})$	$2.14e-03$	$5.44e-04$	$1.23e+00$
$\psi_{cdg}(min)$	$2.55e+02$	$2.55e-01$	$1.60e+05$
$k_{tg}(\frac{mL^2}{pg^2 \cdot min})$	$1.28e-09$	$1.28e-12$	$1.03e-08$
$k_{lps}(\frac{ngEC5}{UEC6})$	$1.82e-01$	$6.70e-02$	$5.43e-01$

3.0 MODELING THE COUNTERREGULATORY HORMONE RESPONSE FOLLOWING HYPOGLYCEMIA

3.1 INTRODUCTION

The endogenous response to hypoglycemia consists of the release of the counterregulatory hormones epinephrine, norepinephrine, glucagon, cortisol, and growth hormone, with the primary factors being glucagon and epinephrine [91, 105]. These hormones perform a number of endogenous functions that result in increased blood glucose concentration. The collective functions of the counterregulatory hormone response are to decrease glucose absorption into peripheral tissues by lowering insulin sensitivity and to trigger the release of endogenous glucose supply into the bloodstream from the liver. Most glucose control studies see non-trivial rates of insulin-induced hypoglycemia. As a result, there is a need to understand the endogenous response to such an event, as clinicians, or a model-based DSS, will be making glucose control decisions in the presence of this response.

3.2 MATERIALS AND METHODS

3.2.1 Model Development and Assumptions

In order to capture the endogenous counterregulatory response to hypoglycemia, we synthesize mass-action-based model extensions to a previously published mathematical model of glucose and insulin dynamics [100] that describe data from previously published clinical studies [74, 78, 79, 82]. The counterregulatory hormones resulting from exogenously induced

hypoglycemia lead to the onset of resistance to insulin-mediated glucose uptake (IMGU) and increased endogenous glucose production (EGP). The resulting network of modeled interactions is shown in Figure 18. Figure 18 is mathematically represented and fit simultaneously

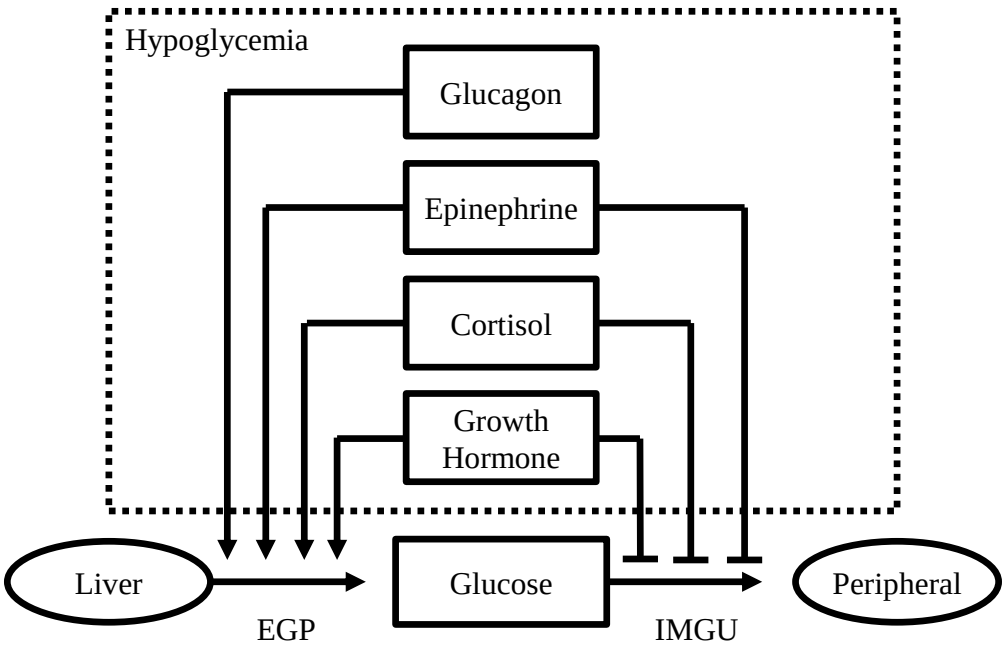

Figure 18: Counterregulatory response induced via hypoglycemia causes the release of four hormones: glucagon, epinephrine, cortisol, and growth hormone. All four hormones increase endogenous glucose production. Epinephrine, cortisol, and growth hormone decrease insulin-mediated glucose uptake.

to the data from [74, 78, 79, 82] as three different components: (i) **Hormone release** (Section 3.2.2.1), the decreasing glucose profile caused by insulin infusion is used to trigger the release of glucagon, epinephrine, cortisol, and growth hormone; (ii) **IMGU** (Section 3.2.2.2), the effect of epinephrine, cortisol, and growth hormone on insulin-mediated glucose uptake; and (iii) **EGP** (Section 3.2.2.2), the effect of glucagon, epinephrine, cortisol, and growth hormone on endogenous glucose production.

3.2.2 Human *in vivo* Data for Model Calibration

A previously published study [91] using the pancreatic-adrenocortical-pituitary (PAP) clamp, measures the counterregulatory hormones in response to an exogenously induced hypoglycemic event. The PAP clamp is used to mimic the endogenous counterregulatory response by infusing the primary hormones *exogenously* while suppressing their *endogenous* secretion, in such a way as to replicate the endogenous response. Once successful at mimicking the endogenous response, the researchers then withheld components one-by-one and measured the insulin and glucose response from withholding each independent species. The PAP clamp process introduced in [91] is illustrated in Figure 19. Data from four human studies [74, 78, 79, 82] were digitized using WebPlotDigitizer [101]. Each study was a separate published data set for each counterregulatory hormone being withheld during the PAP clamp. The individually published human studies represented adrenergic [78], glucagon [79], cortisol [74], and growth hormone [82] effects on glucose metabolism. The individual components were combined into the overall model constructed for the counterregulatory response.

3.2.2.1 Hormone Release Hormone release is modeled with a scaled activation and first-order degradation:

$$\frac{d\hat{C}_i(t)}{dt} = k_{ui}F_{release}(t) - k_{id}\hat{C}_i(t) \tag{3.1}$$

$$\tag{3.2}$$

The concentration of each hormone, subtracted from its baseline value, is given by $\hat{C}_i(t)$, where $i \in \{\text{glucagon, epinephrine, cortisol, growth hormone}\}$. For each hormone there is a corresponding activation gain, k_{ui}, as well as a first order elimination rate k_{id}. In Equation (3.1) the function $F_{release}$ is an activation function used to trigger the release of hormones. An easy function to trigger release is the Heaviside in Equation (3.3). However, it is more physiologically correct to incorporate glucose-driven effects, which also allows the driving function to turn off. As a result, the Heaviside function is ultimately replaced by

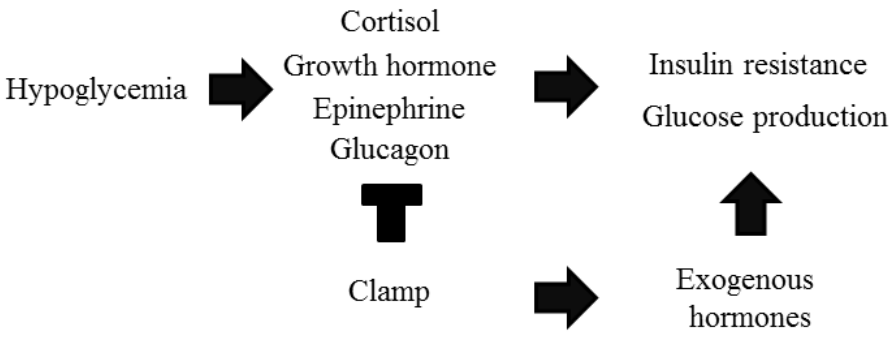

Figure 19: PAP clamp as described in [91]. Hypoglycemia is first induced via continuous subcutaneous insulin infusion (top left). Hypoglycemia leads to the counterregulatory hormone release. During the clamp, the endogenous counterregulatory hormones are first suppressed (bottom left), then reinfused exogenously to match endogenous effects on glucose (right). Individual exogenous hormones withheld to quantify relative contribution to glucose rate.

Equation (3.4).

$$F_{release}(t) = \begin{cases} 0 & t < \psi_{release} \\ 1 & t \geq \psi_{release} \end{cases} \tag{3.3}$$

Here the Heaviside step function has a time delay $\psi_{i,release}$ for the release of each counterregulatory hormone i. This Heaviside function approximation was made based on the dynamics of the blood glucose driving function. The data shown in Figure 20, from [78], following subcutaneous insulin infusion results in an approximately linear decrease in blood glucose that can be estimated as a linear integrator that crosses a threshold at $t = \psi_{release}$ resulting in the counterregulatory hormone release. The Heaviside release function only applies during a constant insulin infusion and only under the same glucose trajectory. Therefore, Equation (3.4) is used following the initial model structure development phase.

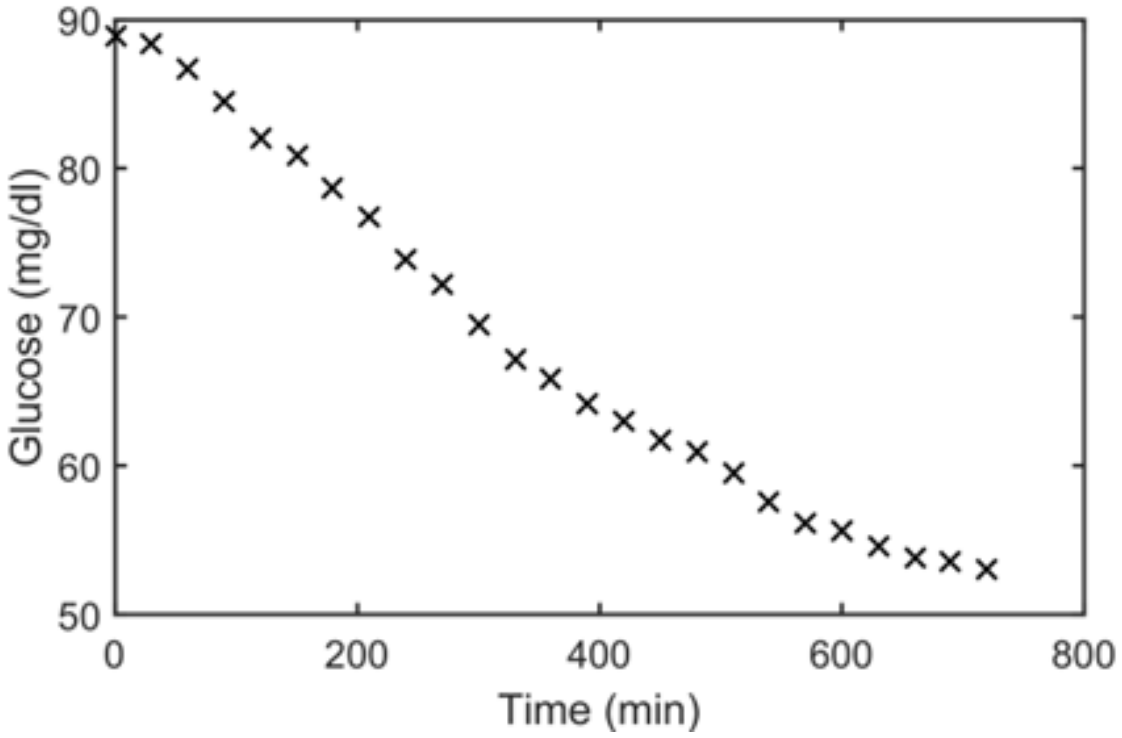

Figure 20: Data digitized from [78]. Blood glucose measurements following a 12 hour continuous subcutaneous insulin infusion of 15 $\frac{mU}{m^2\ min}$.

The initial Heaviside release function from Equation (3.3) is used to develop the model structure for hormone induced changes to IMGU and EGP described in sections 3.2.2.2. Subsequent modifications are made to the release function $F_{release}$ to incorporate the blood glucose values from [78]. In the updated formulation a sigmoid function is used to model the functionality between declining blood glucose and counterregulatory hormone release. The model formulation of hormone release as a function of blood glucose is:

$$F_{release}(G(t)) = 1 - \frac{1}{1 + e^{-k_{i,mg}G(t)+k_{gb}}} \tag{3.4}$$

The sigmoid is a function of blood glucose concentration $G(t)$ and is parameterized by the glucose scaling factor $k_{i,mg}$ for each hormone i and offset k_{gb} which is the same across all hormones. The functionality described in Equation (3.4) is preferred to Equation (3.3) because it is a continuous function of blood glucose concentration, $G(t)$. As $G(t)$ decreases, the exponential term $e^{-k_{i,mg}G(t)+k_{gb}}$ grows proportionally to $k_{i,mg}$, causing $F_{release}(G(t))$ to approach one. When $G(t)$ reaches the value of the ratio $\frac{k_{gb}}{k_{i,mg}}$ the exponential term becomes one and $F_{release}(G(t))$ is equal to $\frac{1}{2}$, or half of the maximal hormone release. This functionality is chosen over a Michaelis-Menten formulation due to the rapid dynamics it can produce without parameterizing (and identifying) higher-order exponents such as with a Hill function.

3.2.2.2 EGP and IMGU Endogenous glucose production (EGP) and insulin-mediated glucose uptake (IMGU) are modeled using a key assumption that the effects of each counterregulatory hormone are additive. Under this assumption, the glucose balance and insulin-mediated glucose dynamics (IMGD) from [100], previously introduced in Equations (2.10) and (2.11), are modified as follows:

$$\frac{dG(t)}{dt} = -p_G G(t) - X_{IMGD}(t) + \frac{P + EGP_b - CNS}{V_G} \tag{3.5}$$

$$X_{IMGD}(t) = S_I \frac{Q(t)}{1 + \alpha_G Q(t)} G(t) - F_{IMGU} - F_{EGP} \tag{3.6}$$

The algebraically defined $X_{IMGD}(t)$ describes the lumped effects of both decreased IMGU (F_{IMGU}) and increased EGP (F_{EGP}). The IMGU term, F_{IMGU} is negative as it represents

a resistance to insulin-mediated glucose uptake. Similarly, the EGP term, F_{EGP}, is negative because it acts to increase blood glucose concentration $G(t)$.

By assuming that each counterregulatory hormone contribution is additive, we fit the difference when the challenge experiment (hormone suppressed) is subtracted from the control (hormone present). By doing, so Equation (3.6) becomes:

$$\Delta X_{i,IMGD}(t) = -\Delta F_{i,IMGU} - \Delta F_{i,EGP} \tag{3.7}$$

Here the Δ indicates the difference between the experiment with the hormone i and without. The first term from Equation (3.6), $\left(S_I \frac{Q(t)}{1+\alpha_G Q(t)} G(t)\right)$ does not appear in Equation (3.7) because all of the time-varying components ($Q(t)$ and $G(t)$) are the same in the control and challenge cases, resulting in a cancellation. The resulting terms $\Delta F_{i,IMGU}$ and $\Delta F_{i,EGP}$ are then calculated by transforming the published experiments [74, 78, 79, 82]: subtracting the challenge from the control. Note that in keeping with convention to the publications [74, 78, 79, 82] that the control case is when hormone i is present and the challenge case is when the effect of hormone i is suppressed. Using this convention $\Delta F_{i,IMGU}$ and $\Delta F_{i,EGP}$ represent the contribution of the suppressed hormone.

The PAP clamp reproduces the endogenous counterregulatory response. In the control case, all four hormones (glucagon, epinephrine, cortisol, and growth hormone) are infused, activating the full response in glucose dynamics. In each challenge data, an individual hormone is not infused, thereby quantifying the changes in glucose dynamics when that hormone is not present. Taking the difference between control data and challenge data yields the relative contributions to EGP and IMGU of the individual hormone suppressed for that specific challenge. EGP driven by glucagon and epinephrine are both modeled using a filtered feedback term to achieve an overshoot response seen in the data [78, 79].

$$\frac{dR_i(t)}{dt} = \frac{k_{ir}\hat{C}_i(t)}{k_{mi}\hat{C}_i(t) + k_{ri}R_{i3}(t) + 1} - k_{rid}R_i(t) \tag{3.8}$$

$$\frac{dR_{i2}(t)}{dt} = k_{irf}(R_i(t) + R_{i2}(t)) \tag{3.9}$$

$$\frac{dR_{i3}(t)}{dt} = k_{irf}(R_{i2}(t) + R_{i3}(t)) \tag{3.10}$$

Here the state $R_i(t)$ represents the effect of component i, glucagon or epinephrine, on the EGP data, $\Delta F_{i,EGP}$ from Equation (3.7). The effect is driven by the change in hormone from baseline, $\hat{C}_i(t)$. The two states $R_{i2}(t)$ and $R_{i3}(t)$ with the filter coefficient k_{irf} represent the lagged auto-inhibition of component i, with the relative magnitude of auto-suppression parameterized by k_{ri} versus k_{mi} in the denominator of Equation (3.8).

Changes in EGP caused by cortisol and growth hormone are less dynamically complex and are modeled using a first order filter:

$$\frac{dR_i(t)}{dt} = k_{irf}(\hat{C}_i(t) - R_i(t)) \tag{3.11}$$

The state $R_i(t)$ is the contribution of component i, cortisol or growth hormone, on changes to EGP, $\Delta F_{i,EGP}$. The change from baseline of the released hormone, $\hat{C}_i(t)$, is lagged with a filter coefficient k_{irf}, and $R_i(t)$ is compared to the data describing $\Delta F_{i,EGP}$.

Modeling the dynamics of IMGU caused by counterregulatory hormones epinephrine, cortisol, and growth hormone is achieved using three consecutive lagged filter states.

$$\frac{dQ_{i1}(t)}{dt} = k_{iqf}(\hat{C}_i(t) + Q_{i1}(t)) \tag{3.12}$$

$$\frac{dQ_{i2}(t)}{dt} = k_{iqf}(Q_{i1}(t) + Q_{i2}(t)) \tag{3.13}$$

$$\frac{dQ_i(t)}{dt} = k_{iq}Q_{i2}(t) + k_{iqd}Q_i(t) \tag{3.14}$$

Here, the state $Q_i(t)$ is the contribution of component $i \in$ {epinephrine, cortisol, or growth hormone} on IMGU, $\Delta F_{i,IMGU}$. The change from baseline of the released hormone, $\hat{C}_i(t)$, is lagged with a filter coefficient k_iqf, and $Q_i(t)$ is compared to the data describing $\Delta F_{i,IMGU}$. The counterregulatory hormone glucagon does affect IMGU.

The models for hormone effects on IMGU and EGP are integrated with the overall model of insulin and glucose dynamics [100]. The simplification described in Equation (3.7) is useful for identifying the model structures in Equations (3.8) to (3.14). However, integration with the overall glucose homeostasis model [100] becomes more complex, as baseline EGP and IMGU model terms must be calibrated. Specifically, the first term in Equation (3.6): $\left(S_I \frac{Q(t)}{1+\alpha_G Q(t)} G(t)\right)$ must be modified to describe EGP functionality for baseline insulin as as well as changes from baseline following the counterregulatory response. Similarly, the original

homeostasis model does not contain an EGP functionality, so one is constructed which is activated by counterregulatory hormones and inhibited by insulin. The model equations describing the dynamics of insulin and glucose following a subcutaneous insulin infusion are given by:

$$\frac{dQ_{SC}(t)}{dt} = U_{sc}(t) - k_1 Q_{SC}(t) \tag{3.15}$$

$$\frac{dQ_{1a}(t)}{dt} = k_1 Q_{SC}(t) - (k_v + k_{a1}) Q_{1a}(t) \tag{3.16}$$

$$\frac{dQ_2(t)}{dt} = k_{a1} Q_{1a}(t) - k_{a1} Q_2(t) \tag{3.17}$$

$$\frac{dI(t)}{dt} = -n_K I(t) - \frac{n_L I(t)}{1 + \alpha_I I(t)} - n_I (I(t) - Q(t)) \tag{3.18}$$

$$+ \frac{U_{ex} + k_{a1} Q_2(t)}{V_I} + (1 - x_L) \frac{U_{en}}{V_I} \tag{3.19}$$

$$\frac{dQ(t)}{dt} = n_I (I(t) - Q(t)) - n_C \frac{Q(t)}{1 + \alpha_G Q(t)} \tag{3.20}$$

$$\frac{dG(t)}{dt} = -p_G G(t) + X_{IMGD}(t) \tag{3.21}$$

$$X_{IMGD}(t) = S_I \frac{Q(t)}{1 + \alpha_G Q(t) + \sum_i \alpha_i Q_i(t)} G(t) - \frac{C_{egp}}{1 + \beta_i R_I^4(t)} - \sum_j \eta_j R_j(t) \tag{3.22}$$

$$\frac{dR_I(t)}{dt} = k_{ifr} (I(t) - R_I(t)) \tag{3.23}$$

Here the subcutaneously infused insulin, $U_{SC}(t)$, passes through two filter states, $Q_{1a}(t)$ and $Q_2(t)$ (rate constant, k_{a1}), before reaching the plasma insulin compartment, $I(t)$. The subcutaneous insulin infusion model is developed in Chapter 4. Remote insulin, $Q(t)$, increases IMGU through the first term in Equation (3.22). The algebraic state, $IMGD(t)$, is modified with the term $\sum_i \alpha_i Q_i(t)$ representing the additive IMGU inhibitory effects of counterregulatory hormones $i \in \{$epinephrine, cortisol, growth hormone$\}$. The second term in Equation (3.22) is an endogenous glucose production term accounting for insulin-mediated effects. The constant C_{egp} is the maximum glucose production when no insulin is present. The filtered insulin state, $R_I(t)$, acts to suppress EGP in the presence of insulin. The final term describes insulin-independent EGP activation by the counterregulatory hormones with the term $\sum_j \eta_j R_j(t)$ for, $j \in \{$glucagon, epinephrine, cortisol, growth hormone$\}$. The final counterregulatory response model is given by combining the dynamics of the counterregulatory states with the modified model of glucose and insulin dynamics. The dynamics

of the counterregulatory states, $Q_i(t)$ and $R_j(t)$, are given by the previous Equations (3.8) to (3.14). These Equations are coupled with Equations (3.15) to (3.23) to form the final set of model equations.

3.2.3 Parameter Identification

Figure 18 is represented mathematically by the system of coupled ODEs shown in Equations (3.1) to (3.14). Initial calibration of the model is performed using least-squares nonlinear regression as described in Section 2.2.3.1. However, unlike in Section 2.2.3.1, no parameter regularization is used because prior parameter information is unknown. Final calibration of model parameters is achieved using the MCMC technique as described previously in Section 2.2.3.2. The overall model consists of the three different measurements following a continuous subcutaneous insulin infusion: hormone release, EGP, and IMGU. The datasets [74, 78, 79, 82] are fit to simultaneously calibrate the model.

3.3 RESULTS

3.3.1 Preliminary Counterregulatory Model

Initial counterregulatory hormone release is modeled using a Heaviside function described in Equation (3.3) with release delayed until $t = \psi_{i,release}$ for hormone i. In this model, the data is fit simultaneously using least-squares nonlinear regression described in Section 2.2.3.1. The hormone release profiles represent a first-order step response starting at each individual hormone delay parameter $\psi_{i,release}$. The resulting calibrated model is shown in Figure 21. Preliminary results for IMGU and EGP dynamics are modeled using the transformation in Equation (3.7), where the individual hormone suppression is subtracted from the full counterregulatory response. These results rely on the assumption that the counterregulatory effects on IMGU and EGP are additive, and are not integrated into the overall model of glucose and insulin homeostasis described in Equations (3.15) to (3.23). Instead, the results match the difference between control and challenge data and capture hormone induced changes

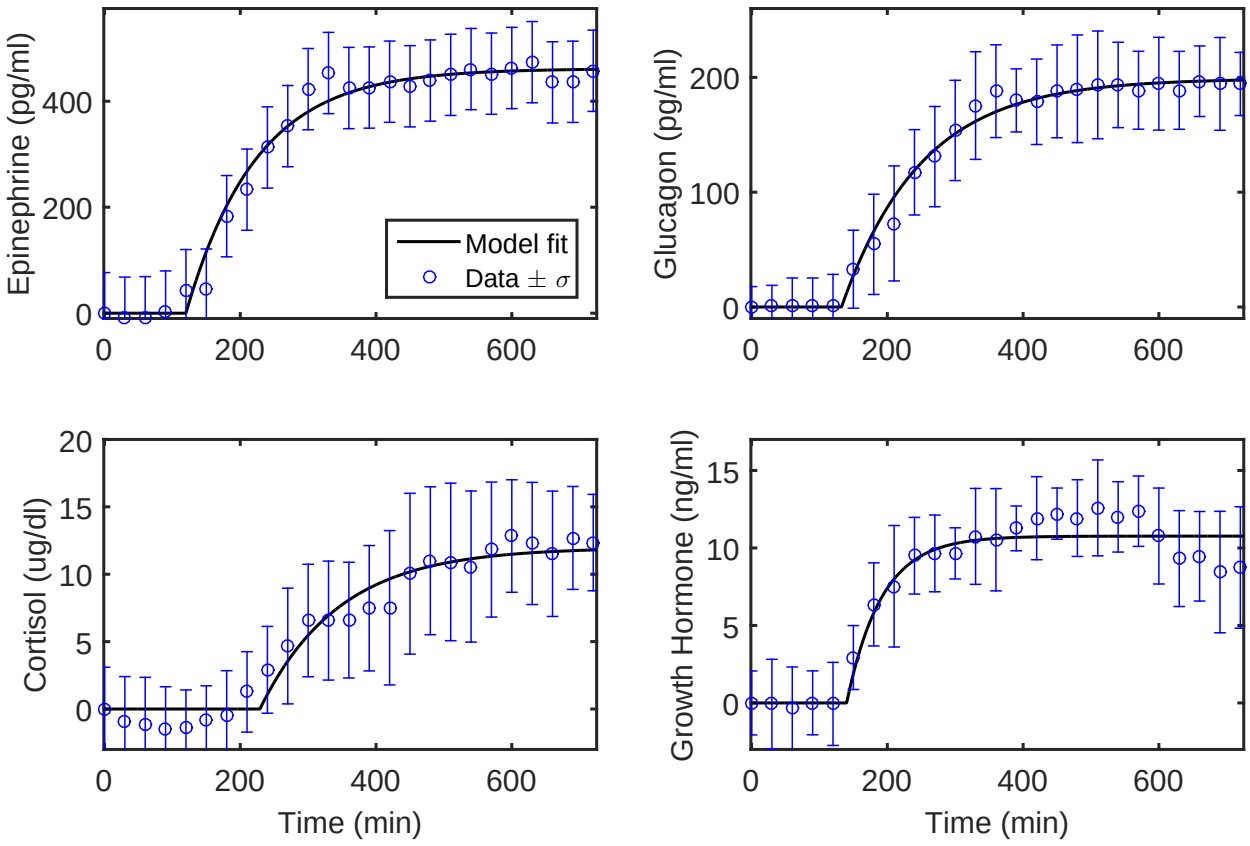

Figure 21: Heaviside hormone release model dynamics (black line) compared to data (blue, mean ± 1 standard deviation). Counterregulatory hormone data for epinpehrine [78], glucagon [79], cortisol [74], and growth hormone [82] during a continuous subcutaneous insulin infusion.

to IMGU and EGP. The counterregulatory ΔEGP and $\Delta IMGU$ responses shown in Figure 23 and 22 are transformed back into EGP $(mg/kg/min)$ and $IMGU$ $(mg/kg/min)$ by subtracting the modeled response from the data in the control cases [74, 78, 79, 82]. The resulting EGP and IMGU responses are shown in Figure 25 and Figure 24, respectively. Figure 26 shows the counterregulatory effect of EGP added to the glucose and insulin dynamic model. This can be used to simulate different possible scenarios depending on whether or not a given counterregulatory hormone is being suppressed. From Figure 26, there are large differences in patient safety when comparing a patient with or without a counterregu-

latory response. There could be significant differences in patients with abnormal HPA axis function, for example, a patient receiving steroids in critical care.

3.3.2 Final Counterregulatory Model

The final counterregulatory model captures three different processes: hormone release, IMGU, and EGP. Hormone release is shown in Figure 27. Figure 28 shows the full counterregulatory effect on IMGU (no suppression), as well as when each of the three IMGU-suppressing hormones is absent. Epinephrine, cortisol, and growth hormone all act with varying magnitude to reduce IMGU after an initial rise. The initial rise in IMGU can be attributed to the corresponding early increases in EGP (i.e., higher glucose concentration leads to increased disposal).

The final model for hormone release given by Equations (3.1) and (3.4) replaces the delay parameters $\psi_{i,release}$ with the parameters k_{gb} and $k_{i,mg}$. Thus, this model increases the total number of parameters by one, while providing a continuous function of blood glucose concentration. The final model shown in Figure 27 is calibrated using MCMC described in Section 2.2.3.2. Variability in the data exceeds the model confidence intervals due to the constrained model structure. If individual patient data is available and additional model variation is required, the parameter k_{gb} could be fit for each hormone. However, the model captures the mean data points well using a single value of k_{gb}. Each of the four counterregulatory hormones contribute to an increase in EGP, which counteracts the suppression of EGP by insulin. Figure 29 shows the counterregulatory hormone-induced increase of EGP following early suppression by subcutaneous insulin infusion. The full EGP response represents the additive effects of each counterregulatory hormone. The magnitude of each individual hormone effect is identified using the individual suppression datasets. Figure 30 shows the individual counterregulatory effects on EGP when each hormone is individually suppressed. The model captures the dynamics of glucagon, however, the overall magnitude of effect is under predicted by the model. Similarly, the peak response of EGP induced by cortisol is under predicted by the model. The error capturing magnitude in both of these responses is

caused by the data variable for those measurements, resulting in a lower calibration weight compared across all the other measured data.

3.4 DISCUSSION

The counterregulatory model describes the dynamics of the hormones epinephrine, glucagon, cortisol, and growth hormone when activated by low levels of blood glucose (parameterized by k_{gb} and $k_{i,mg}$) and the subsequent changes to metabolic insulin sensitivity and endogenous glucose production that result. This model provides mechanistic insight into the way multiple hormones react to counter hypoglycemia. The *in silico* results indicate that the components may be modeled as additive effects, and that the two hormones glucagon and epinephrine collectively contribute to approximately 76.4% of the overall peak EGP response to hypoglycemia.

The model captures hormone release triggered by glucose concentration which subsequently leads to changes in glucose production and uptake. The production and uptake rates could then be incorporated into the dynamic glucose concentration balance (right-hand-side of Equation 3.21). Incorporating rate feedback into the glucose balance remains difficult due to the error in measurement of the fitted rate data compared to the sensitivity of glucose concentration on the rates. This type of feedback in the model may require additional EGP and IMGU rate data to reduce some of the variability. However, this would allow for more robust simulations of glucose homeostasis dynamics.

A major assumption in the model is that the individual components are considered additive. The overall ability of the model to capture the data both of individual components (Figures 28 and 30) and the overall EGP effect (Figure 29) supports the claim that this approximation holds. However, a human infusion study [14] claims "the combined infusion of epinephrine, glucagon, and cortisol produces a greater than additive hyperglycemic response in normal humans," seeming to contradict the proposed model assumption. This could be due to the missing growth-hormone effect that our model accounts for, however, it could also be due to the fact that our model captures hormone effect through removal. This contradiction

could make the model over predict the effects of isolated epinephrine, glucagon, or cortisol infusions.

The mechanisms of the counterregulatory pathway described by this model further resolve the metabolic state of a critical care patient following hypoglycemia and quantify the individual roles of the contributing hormones within the counterregulatory response. Such information may be used to inform measurements of specific species and further identify the individual roles of the counterregulatory hormones, ultimately leading to more effective and safer control of blood glucose.

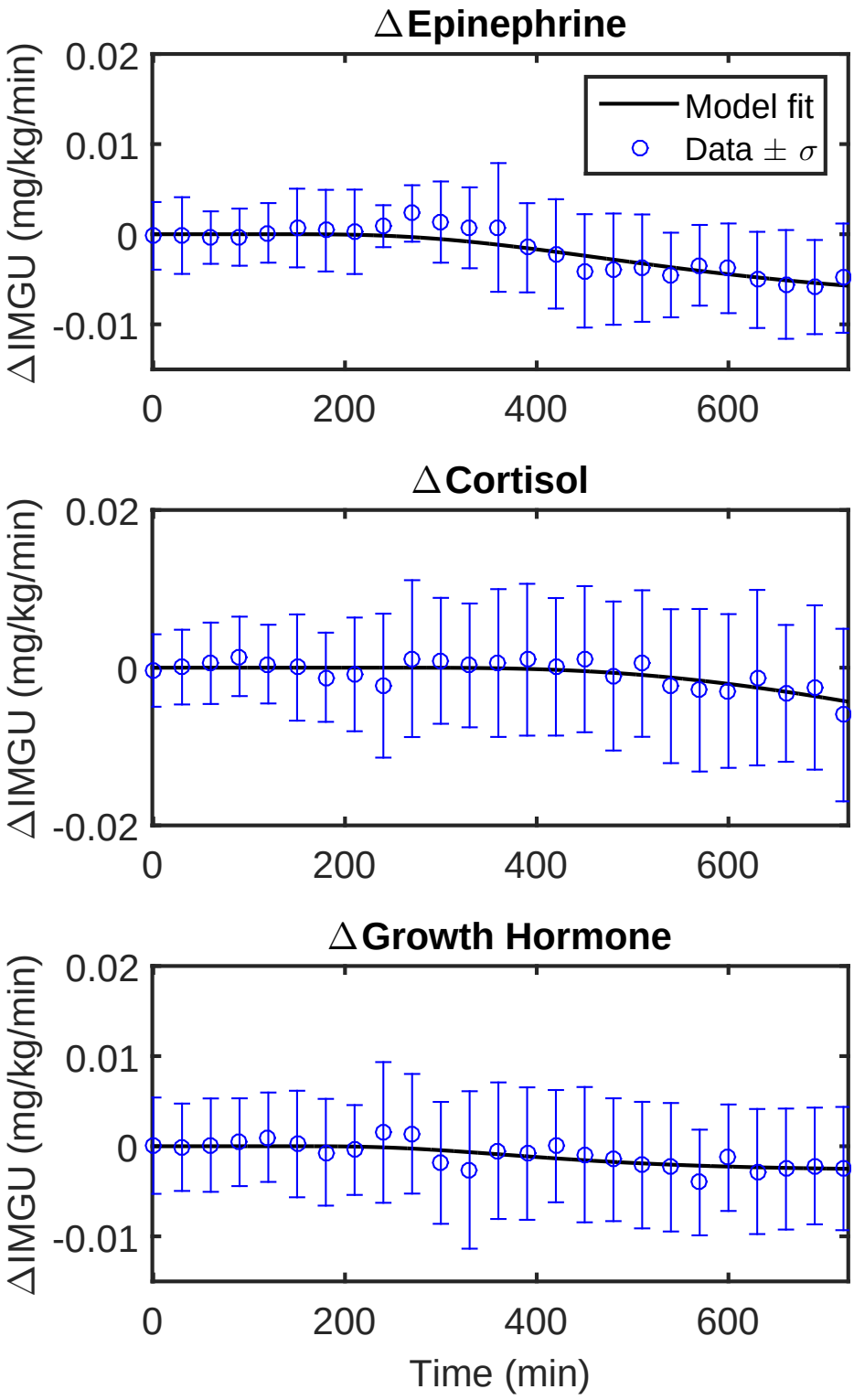

Figure 22: Preliminary counterregulatory IMGU model dynamics (black line) compared to transformed data (blue, mean ± 1 standard deviation). Counterregulatory hormone data for epinpehrine [78], cortisol [74], and growth hormone [82] is transformed by subtracting the challenge (without hormone) from the control (with hormone).

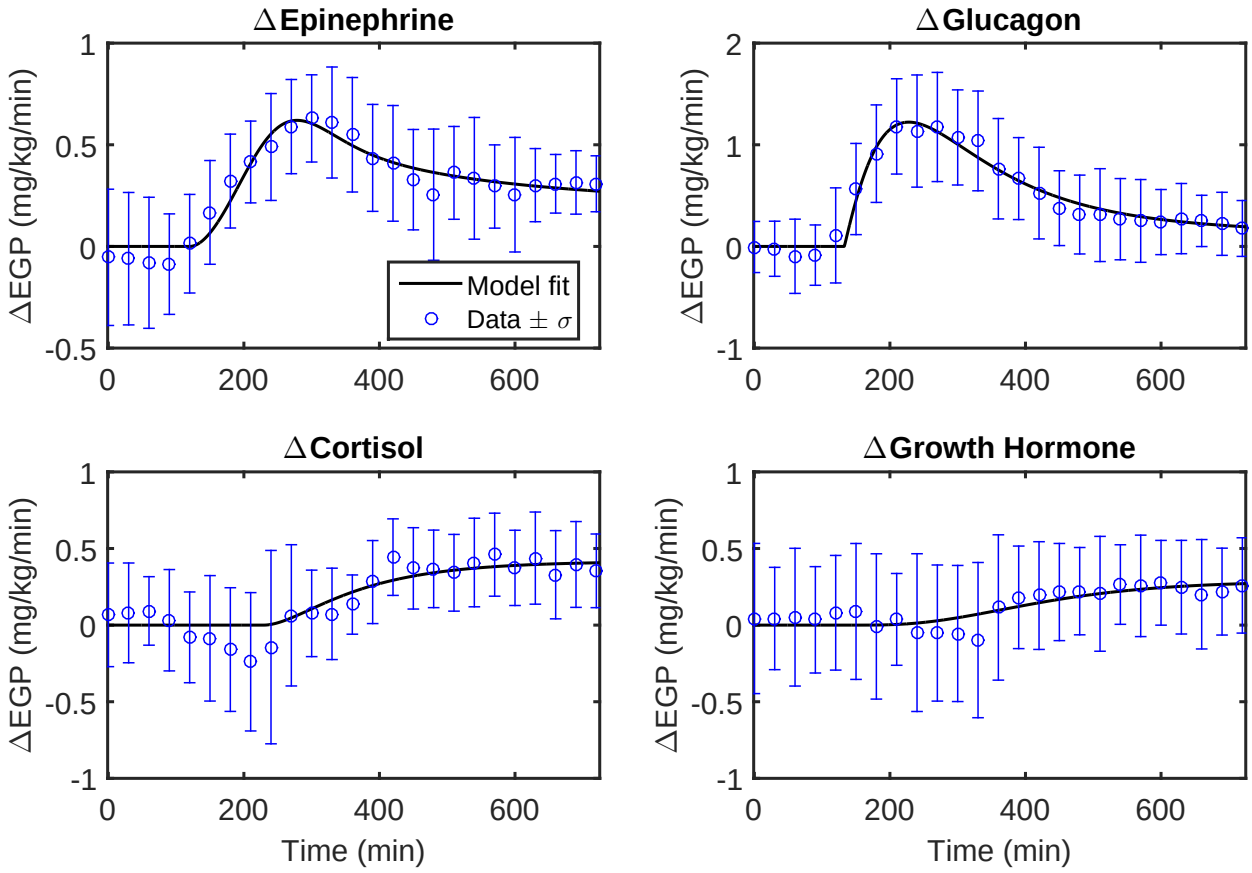

Figure 23: Preliminary counterregulatory EGP model dynamics (black line) compared to data (blue, mean ± 1 standard deviation). Counterregulatory hormone data for epinpehrine [78], glucagon [79], cortisol [74], and growth hormone [82] is transformed by subtracting the challenge (without hormone) from the control (with hormone).

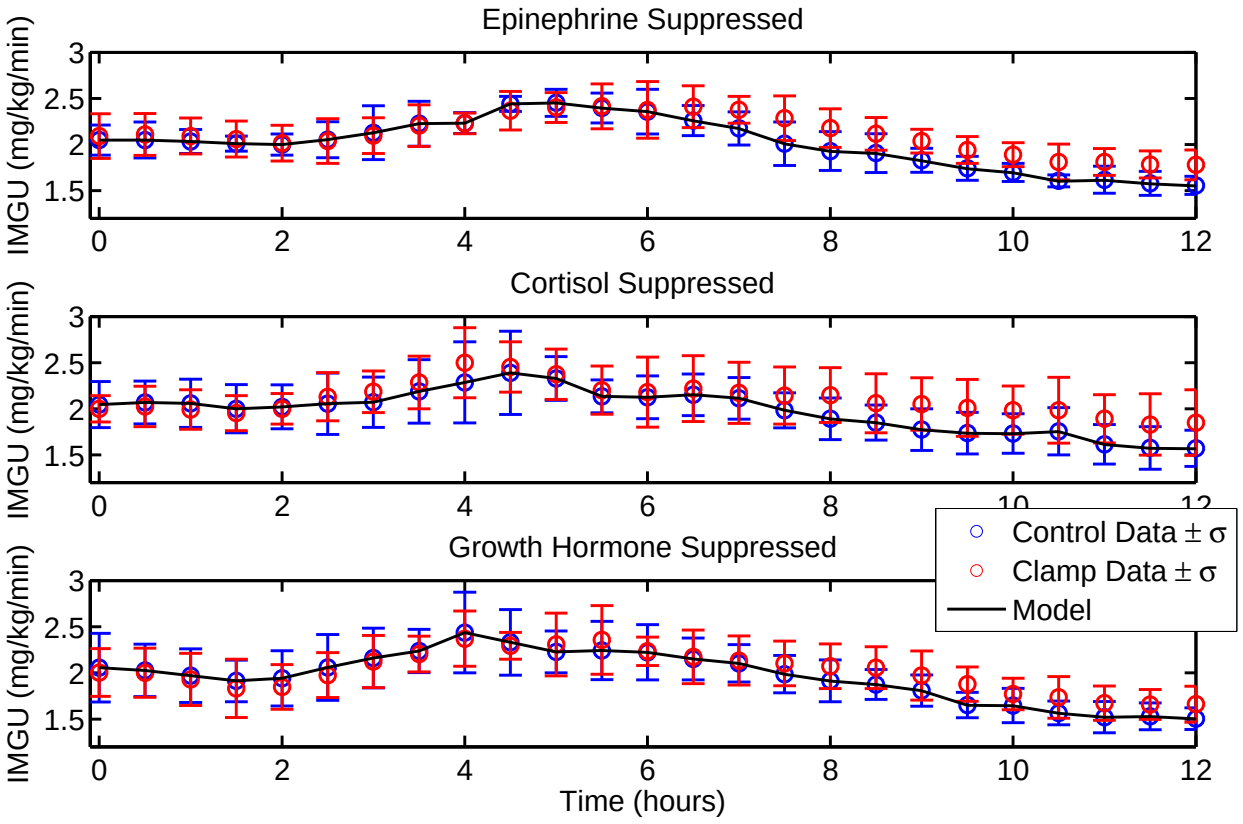

Figure 24: Preliminary counterregulatory IMGU model dynamics (black line) compared to challenge data (red, mean ± 1 standard deviation) shown with control data (blue, mean ± 1 standard deviation). Counterregulatory hormone model is transformed back into the challenge (hormone suppressed) IMGU rate by subtracting the model trajectory (individual hormone effect) from control data (hormones present) for epinpehrine [78], cortisol [74], and growth hormone [82]

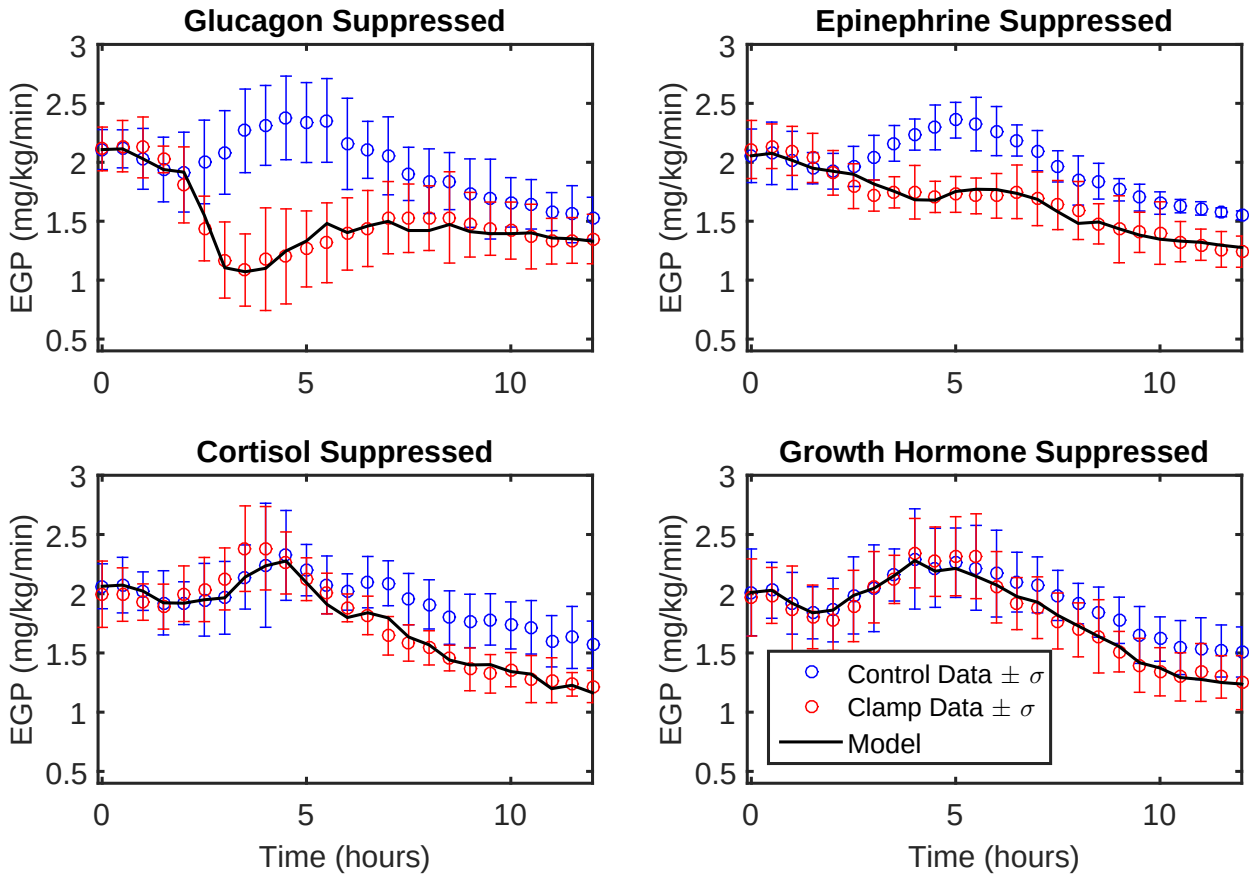

Figure 25: Preliminary counterregulatory EGP model dynamics (black line) compared to challenge data (red, mean ± 1 standard deviation) shown with control data (blue, mean ± 1 standard deviation). Counterregulatory hormone model is transformed back into the challenge (hormone suppressed) EGP rate by subtracting the model trajectory (individual hormone effect) from control data (hormones present) for epinpehrine [78], glucagon [79], cortisol [74], and growth hormone [82]

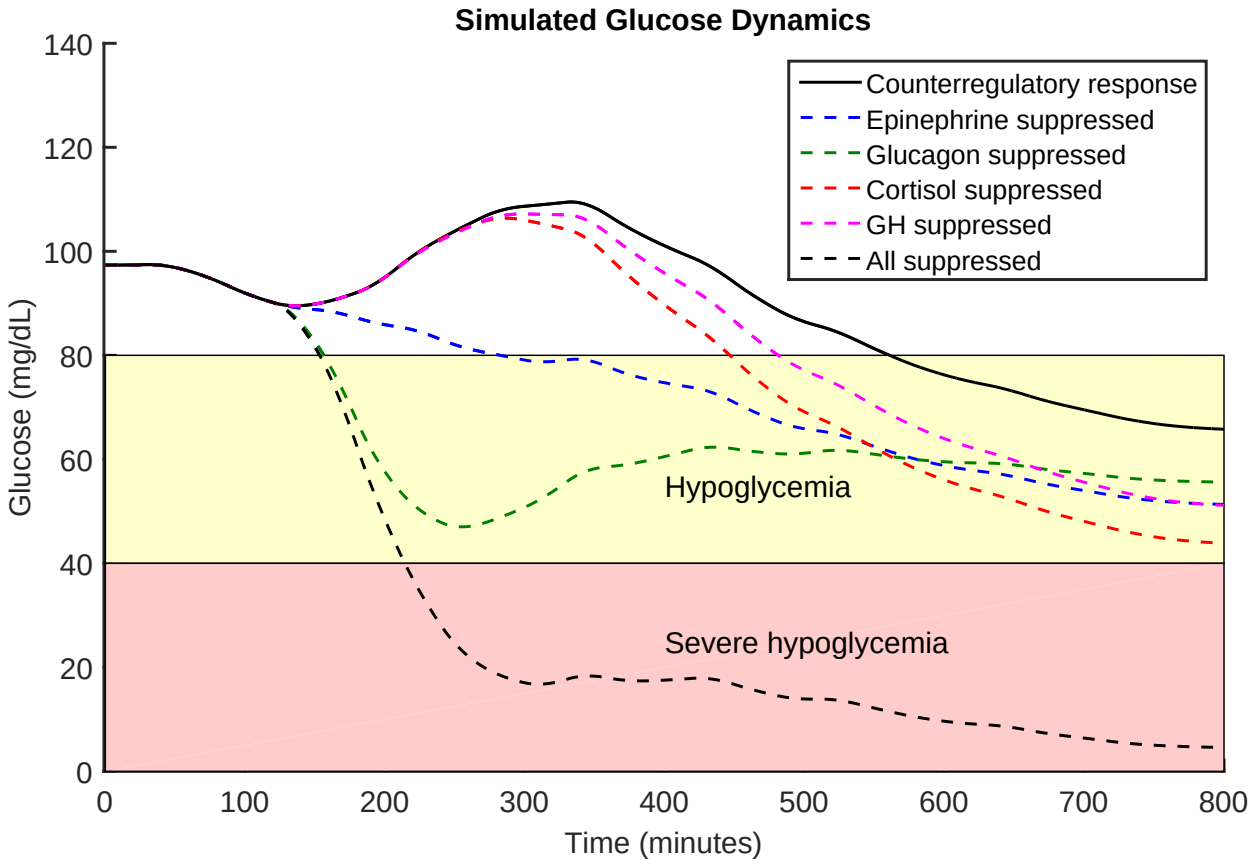

Figure 26: Simulated counterregulatory glucose dynamics (solid black line) following a subcutaneous insulin infusion starting a $t = 0$. The counterregulatory response occurs when $t = \psi_{i,release}$ for each i hormone. The missing contribution of each hormone is simulated to show the relative effects (dashed). Regions of hypoglycemia (yellow) and severe hypoglycemia (red) are highlighted. All four hormones suppressed (black dashed line) shows the largest drop in blood glucose followed by glucagon suppressed (green dashed line), epinephrine suppressed (blue dashed line), cortisol suppressed (red dashed line), and growth hormone suppressed (magenta dashed line).

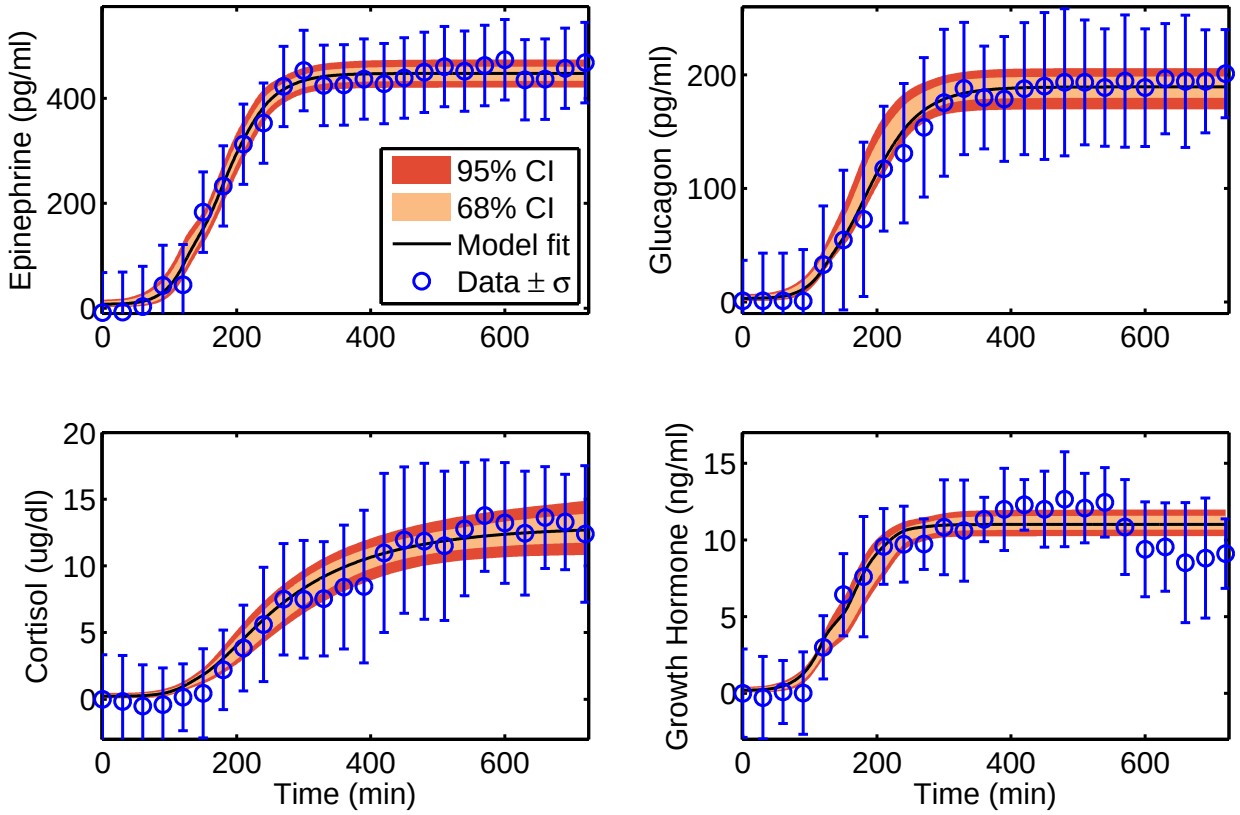

Figure 27: Final hormone release model dynamics (black line) compared to data (blue, mean $\pm$ 1 standard deviation). Counterregulatory hormone data for epinpehrine [78], glucagon [79], cortisol [74], and growth hormone [82] during a continuous subcutaneous insulin infusion. The shaded region denotes 68% (beige) and 95% (red) confidence in dynamic response using accepted parameter sets found via MCMC.

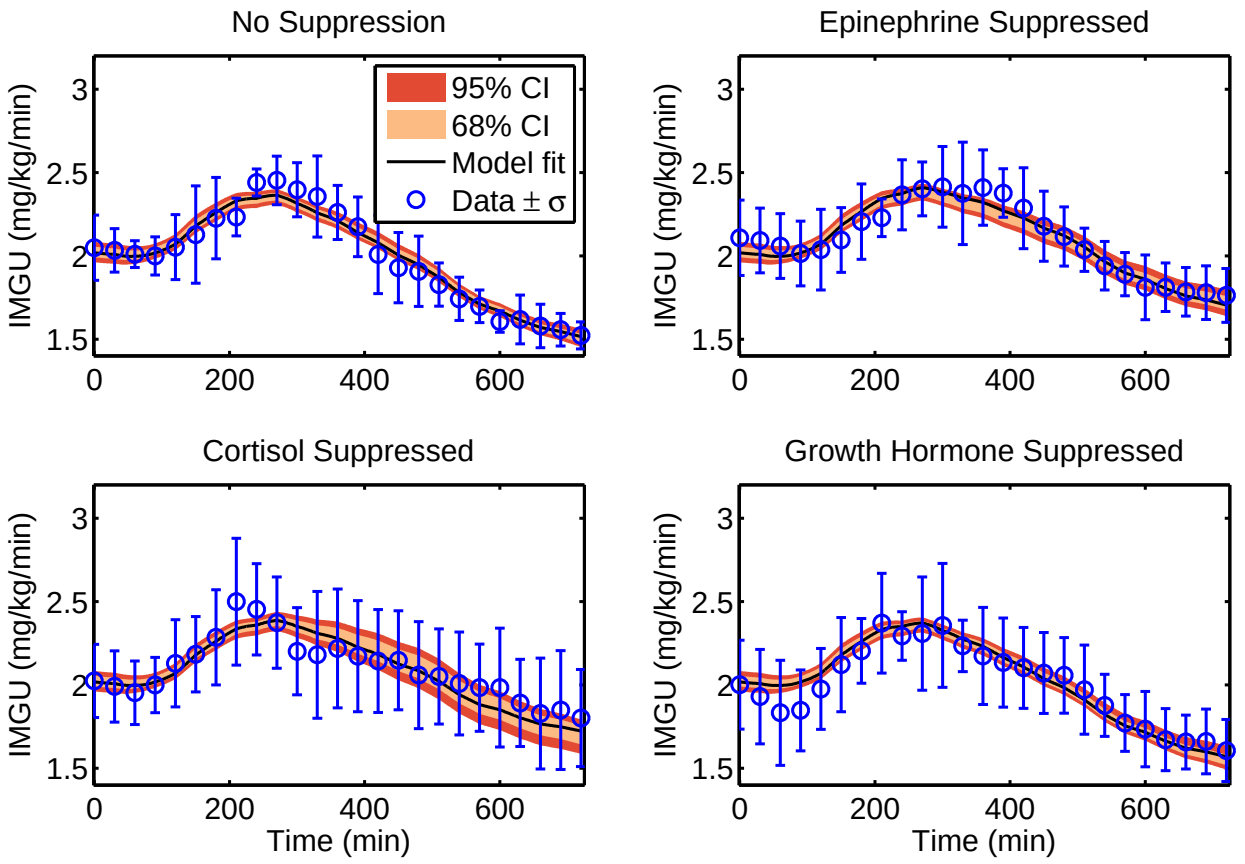

Figure 28: Final counterregulatory IMGU model dynamics (black line) compared to data (blue, mean $\pm$ 1 standard deviation). Counterregulatory hormone data for epinpehrine [78], cortisol [74], and growth hormone [82] during a continuous subcutaneous insulin infusion. The shaded region denotes 68% (beige) and 95% (red) confidence in dynamic response using accepted parameter sets found via MCMC.

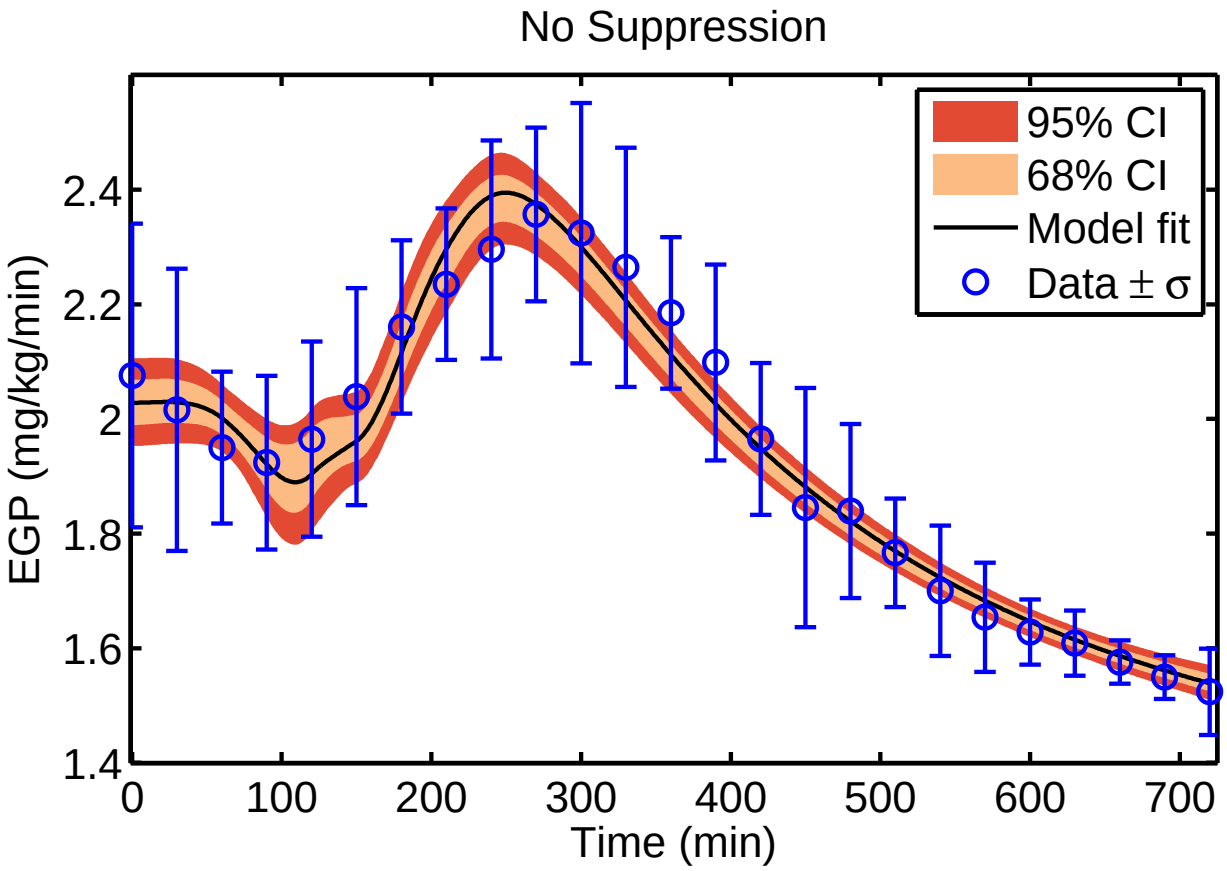

Figure 29: Final counterregulatory EGP model dynamics (black line) compared to data (blue, mean ± 1 standard deviation). Counterregulatory hormone data from [78] when all four hormones are active during a continuous subcutaneous insulin infusion. The shaded region denotes 68% (beige) and 95% (red) confidence in dynamic response using accepted parameter sets found via MCMC.

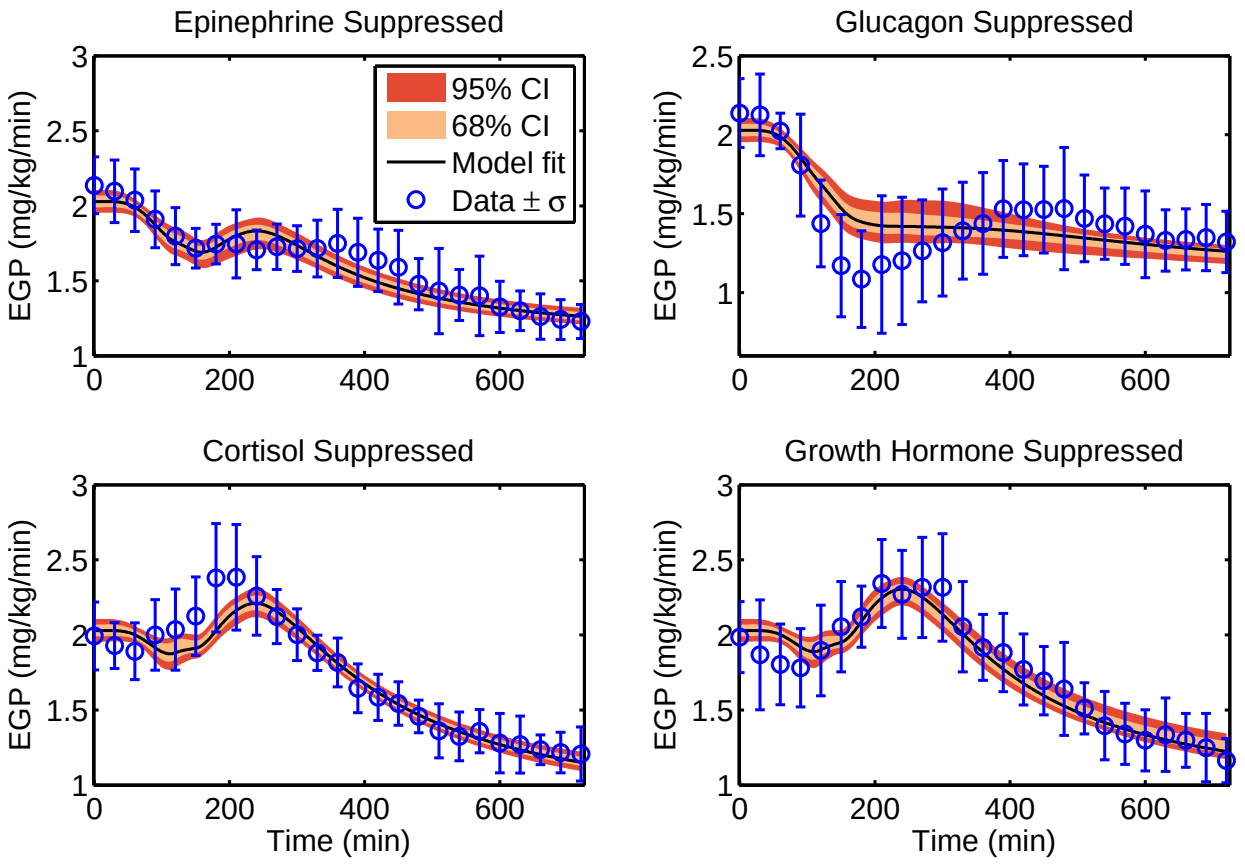

Figure 30: Final counterregulatory EGP model dynamics (black line) compared to data (blue, mean $\pm$ 1 standard deviation). Counterregulatory hormone data for epinpehrine [78], glucagon [79], cortisol [74], and growth hormone [82] during a continuous subcutaneous insulin infusion. The shaded region denotes 68% (beige) and 95% (red) confidence in dynamic response using accepted parameter sets found via MCMC.

4.0 MODELING SUBCUTANEOUS INSULIN DELIVERY

4.1 INTRODUCTION

Stress hyperglycemia and its accompanying deleterious effects are primarily treated via either continuous intravenous or intermittent subcutaneous insulin administration. Subcutaneously injected insulin is a less invasive form of delivery used preferentially when patients are deemed stable enough to transition from intravenous administration in the ICU. Therefore, a control-relevant model that can be tailored to match individual patient dynamics of subcutaneously administered insulin for multiple insulin types is the focus of this work. While several mathematical models have been proposed to describe subcutaneous insulin delivery [106, 107, 108], the present focus is:

- Low order state and parameter dimension model.
- Readily tailored to individual patients.
- Practically-identifiable parameters when applied to clinical data.
- Single structure for multiple insulin types.
- Single structure for insulin bolus and infusion.

Previously published models of subcutaneous insulin [106, 107, 108] use different mathematical structures for each type of infused insulin (*e.g.*, rapid-acting, regular, lente, etc.). The present work included regular and rapid-acting insulin types, and focused on constructing a single-structure model with parameters specific to insulin-type. To build a low-order, practically identifiable subcutaneous insulin model, a previously reduced model [109] starts from a literature review of subcutaneous insulin models [107], and is further analyzed using pub-

This material is submitted to Control Engineering Practice

lished human data [110, 111, 112, 113]. The model is fit using a Markov Chain Monte Carlo (MCMC) parameter search (described in Section 2.2.3.2) to provide posterior distributions of the model parameters. Finally, the reduced model of subcutaneous insulin delivery is validated with patient data from an intensive care clinical database to construct a virtual patient cohort for *in silico* analysis and potential use in control system design.

4.2 MATERIALS AND METHODS

4.2.1 Wilinska Model

Wilinska *et al.* [107] evaluates 11 different compartmental models for insulin dynamics, finding "model 10" to be the best for subcutaneous insulin administration (via either bolus injection or continuous infusion) of rapid-acting insulin analogues in insulin-dependent diabetics. This model is presented in Figure 31, and has two different pathways of insulin absorption. The transfer rates of the model are $ka1$, $ka2$ and ke $(1/min)$. LDa and LDb (mU/min) are Michaelis-Menten functions that capture local degradation at the insulin administration site. The Wilinska model is used as a starting point for building an ICU-relevant model that can capture the plasma insulin dynamics for a variety of insulin types, administration routes, and patients.

4.2.2 Clinical Insulin Data

Two different clinical studies are used to fit the plasma insulin data for regular insulin (highly purified porcine insulin; Actrapid MC, 40 U/mL, Novo Industries, Denmark). From ([110]), ten normal subjects were given an IV insulin infusion of 1 U/hr into the contralateral arm for 60 minutes to suppress endogenous insulin release from the pancreas. The study began (defined as time 0) when subjects were administered a 10 U subcutaneous "bolus" of insulin over 5 minutes (2 U/min). The plasma insulin level at time 0 of the study is used as the steady state plasma insulin for the model fit. In ([111]), nine insulin-dependent diabetics and three normal subjects were studied. In the bolus arm, insulin was delivered by a single

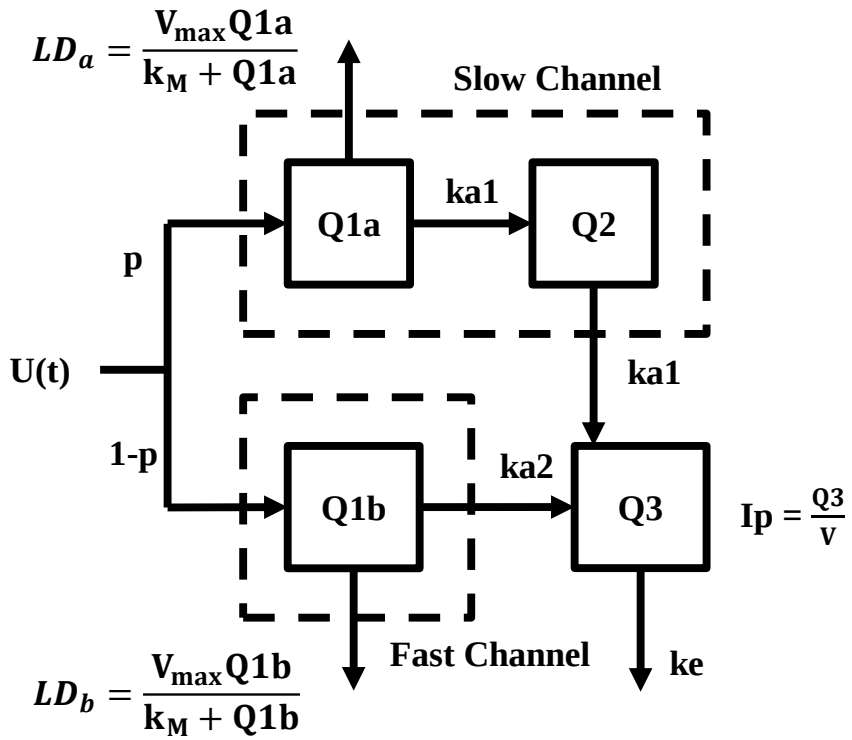

Figure 31: Wilinska model: Subcutaneous insulin absorption for bolus or continuous administration of rapid-acting insulin analogues for insulin-dependent diabetics [107]. Insulin injection is represented as U (mU) with the amount distributed between the two channels determined by a fraction, p. Compartments Q_{1a} and Q_{1b} (mU) are the insulin mass in each compartment with degradation (via LDa and LDb) and can also be absorbed into the plasma. Compartment Q_2 (mU) captures the slower dynamics associated with the fraction, p, of insulin administered. Ip (mU/L) represents insulin in the plasma compartment.

subcutaneous injection at a dose of 0.15 U/kg body weight. In the continuous infusion arm, six subjects were administered the same dose of insulin over 60 minutes.

Fast-acting insulin analogue data is used from two additional studies. A clinical study from [112] examined fourteen insulin-dependent diabetic subjects and compared two fast-acting analogues. Participants were injected subcutaneously with a 10 U bolus of insulin Lispro (Humalog, 100 U/mL, Eli Lilly, Indianapolis, IN) and (on a different day) a 10 U

bolus of insulin Aspart (NovoRapid, 100 U/mL, Novo-Nordisk, Bagsveard, Denmark). The parameter set fit to the Hedman [112] clinical study is validated using data from a clinical study of 24 insulin-dependent diabetic patients using the same insulin at a subcutaneous bolus dose of 7.1 ± 1.3 U ([113]).

4.2.3 Akaike Information Criterion

The Akaike Information Criterion [114, 115] (AIC) is computed for each of the models to establish a statistical comparison between the Wilinska model, the "extended" Wilinska model and our low-order model. The AIC is computed as follows:

$$AIC = N \ln\left(\frac{J(\underline{\theta})}{N}\right) + 2M \tag{4.1}$$

Here, $J(\underline{\theta})$ is the weighted sum of squared error as defined in Equation 2.14. N is the number of data points, and M is the number of model parameters. The criterion is minimized over choices of M to form a tradeoff between the quality of fit of the model to the data and the complexity of the model, as represented by its number of parameters, M. The model having the lower AIC score is preferred.

4.2.4 Wilinska Model Extension and Reduction

In our earlier work [109], a subcutaneous insulin absorption model from literature [107] is modified and reduced while fitting previously published data of regular [110, 111] and fast-acting [112, 113] insulin. Similar to the original review [107], Akaikes information criterion [115, 116] (AIC) is used to compare and select the model variation that best balances fitting error against over-parameterization. The original model, shown in Figure 32A is modified to replace the complementary fractions p and $1-p$, with a kinetically driven compartment ($Q_{sc}(t)$) and corresponding rate coefficients $k1$ and $k2$, respectively, governing the rate of material transfer into the two possible insulin transport channels to form the "Extended" model, as shown in Figure 32B. This structure was subsequently truncated by removing the second, single compartment (lower) as a result of the observation that, in the case of fitting each insulin type, the two compartment partition (top) is more utilized (total

fraction of insulin mass going through this channel is 99% for fast-acting insulin and 79% for regular insulin). The final model structure, the so-called "Reduced model", is shown in Figure 32C, where only one channel of insulin transport remains. Separate parameters are fit

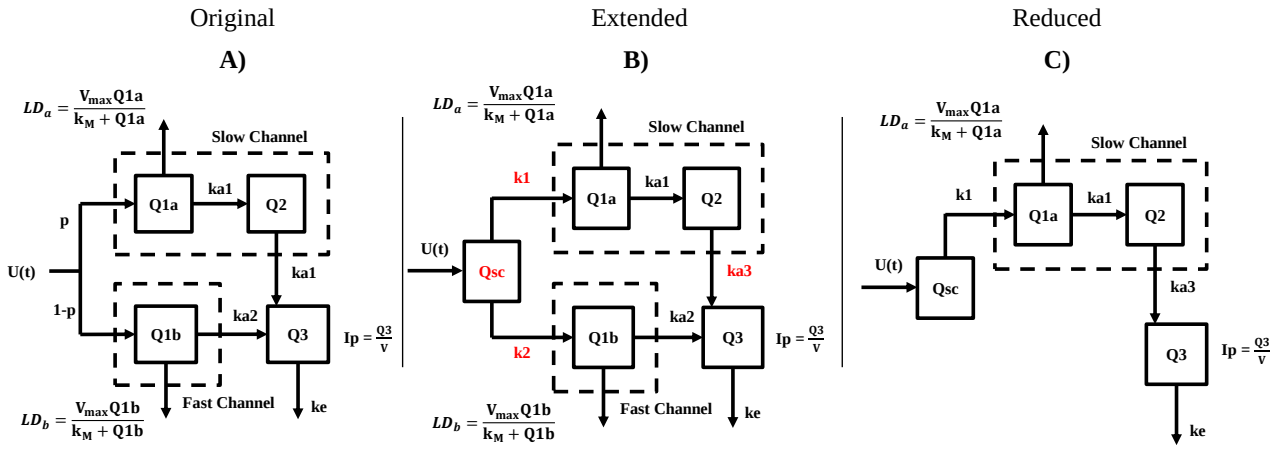

Figure 32: Reduction of the originally published model by Wilinska et al. [107] as described in [109].

for both fast-acting and regular insulin. Model selection is performed using AIC to establish the model having the best trade-off between complexity (as measured by the number of free parameters) and quality of fit (a weighted sum-of-squared error between model predictions and data). Table 5 shows the comparison between the three models investigated. The original model from [107] and the reduced model had the same number of fitted parameters, however, the structure of the reduced model, specifically the parameter k_{a3}, resulted in a better fit for both regular and fast-acting insulin, as shown in Table 5. The reduced model with low AIC scores for both regular and fast-acting insulin is considered a superior model to describe subcutaneous insulin dynamics for multiple insulin types.

Table 5: Number of parameters, sum of squared error, and AIC scores for the three models fit with separate parameter values for both fast-acting and regular insulin.

Model	Parameters	SSE		AIC	
		Regular	Fast	Regular	Fast
Wilinska et al.	7	368.2	336.2	101.7	104.7
Extended	9	351.4	158.7	106.9	79.5
Reduced	7	356.7	186.0	100.6	79.8

4.2.5 Composite Model

A previously published, clinically validated model of glucose and insulin dynamics [100] is combined with a version of the previously developed [109] reduced subcutaneous insulin model (chosen by Table 5), and is further simplified to possess fewer fitted parameters. Additionally, the original [107, 109] nonlinear degradation from state Q_{1a}, is replaced with a linear term.

The resulting composite model describes the dynamics of glucose and insulin, including exogenously administered glucose, insulin, and subcutaneous insulin. The mathematical description of the subcutaneous insulin model is as follows:

New subcutaneous insulin model:

$$\frac{dQ_{SC}(t)}{dt} = U_{SC}(t) - k_1 Q_{SC}(t) \tag{4.2}$$

$$\frac{dQ_{1a}(t)}{dt} = k_1 Q_{SC}(t) - k_v Q_{1a}(t) - k_{a1} Q_{1a}(t) \tag{4.3}$$

$$\frac{dQ_2(t)}{dt} = k_{a1} Q_{1a}(t) - k_{a1} Q_2(t) \tag{4.4}$$

This model feeds a circulating glucose and insulin model from [100]:

$$\frac{dI(t)}{dt} = -n_K I(t) - \frac{n_L I(t)}{1+\alpha_I I(t)} - n_I(I(t) - Q(t)) + \frac{U_{ex}(t) + k_{a1}Q_2(t)}{V_I} + (1-x_L)\frac{U_{en}(t)}{V_I} \tag{4.5}$$

$$\frac{dQ(t)}{dt} = n_I(I(t) - Q(t)) - n_C \frac{Q(t)}{1+\alpha_G Q(t)} \tag{4.6}$$

$$\frac{dG(t)}{dt} = -p_G G(t) - S_I(t)G(t)\frac{Q(t)}{1+\alpha_G Q(t)} + \frac{P(t) + EGP_b - CNS}{V_G} \tag{4.7}$$

$$U_{en}(t) = k_1 e^{-I(t)k_2/k_3} \tag{4.8}$$

Here, subcutaneous insulin input, $U_{SC}(t)$, enters the model through the $Q_{SC}(t)$ state. In the simplified model, insulin mass travels through the states $Q_{1a}(t)$ and $Q_2(t)$ and appears in the plasma compartment $I(t)$ with rate $k_{a1}Q_2(t)$. This is added to the exogenous (intravenous) insulin administration term from [100], as both serve to increase the amount of circulating insulin. Subcutaneous insulin is removed from the compartment $Q_{1a}(t)$ at a rate $k_v Q_{1a}(t)$. This is shown schematically in Chapter 2, Figure 5.

When the subcutaneous model is added to the insulin-glucose model, the state through which the two models are connected is the plasma insulin state, $I(t)$. In the previously described fitting and comparison of the isolated reduced subcutaneous model, the rate of insulin degradation is a first-order linear degradation from Equation (4.4). However, when concatenating the two models, the insulin state has nonlinear dynamics originating from the insulin-glucose model, described in Equation (4.5). To reconcile this difference, the same insulin data [110, 111, 112, 113] are refit using the dynamic equations from Equation 4.5 to model insulin concentration.

4.2.6 Parameter Identification

Parameter identification for the composite model described in Section 4.2.5 is done using the MCMC method detailed in Chapter 2.2.3.2. Prior parameter distributions for the composite model are obtained from MCMC and used to generate confidence intervals for the model.

Additionally, the Kullback-Liebler (KL) distance is used to compare the similarities resulting posterior parameter distributions between each insulin type. The KL distance is given by:

$$D(p||q) = \sum_x p(x) log_2 \frac{p(x)}{q(x)} \tag{4.9}$$

Here $D(p||q)$ is the Kullback-Leibler distance between probability mass functions $p(x)$ and $q(x)$.

4.3 RESULTS AND DISCUSSION

4.3.1 Parameter Space Reduction

MCMC is used to obtain separate posterior parameter distributions for both fast-acting and regular insulin. It is first run fitting three separate parameters (k_1, k_{a1}, and k_v) for each insulin type (six parameters total). The resulting distributions are then used to further reduce the model by comparing the similarities in distributions between type-specific parameters. The Kullback-Leibler (KL) distances for each parameter are calculated between insulin types as in Equation (4.9), and are summarized in Table 6.

Table 6: Final Kullback-Leibler distances between parameter distributions fitting regular (R) and fast-acting (F) insulin.

Distance	k_1	k_v	k_{a1}
$D(R\|\|F)$	2.71E-1	6.06E-1	5.77E-1
$D(F\|\|R)$	2.87E-1	1.74	8.51E-1
Total	5.58E-1	2.35	1.43

The parameter k_v is chosen to remain variable between insulin types due to having the largest KL distance between types. The parameter search space for the MCMC routine is decreased in the simplified model by fixing the parameters k_1 and k_{a1} to remain constant between insulin types. The resulting model is shown in Equation (4.2) to Equation (4.4), where only k_v varies between insulin type. The parameter k_v represents the effect of local degradation on subcutaneously delivered insulin before reaching the bloodstream.

MCMC is run again to obtain the final parameter distributions. Model development and simplification is done using plasma insulin concentrations without information about the unobserved compartments present in the model. Therefore Equations (4.2) to (4.4) have no physiological meaning, and the model may not capture any additional insulin types without modifications. Additional data of various other insulin types are necessary to extend the model utility beyond regular and fast-acting insulin.

4.3.2 Calibrating Model Parameters with MCMC Sampling

The MCMC algorithm is used a second time to compute the posterior parameter distributions after fitting the model (Equations (4.2) to (4.4)) to human glucose data. The resulting subcutaneous insulin model is prepended to an existing model of glucose and insulin dynamics from the literature [100]. The MCMC algorithm ran for 1,000,000 sampled parameter steps. The initial 500,000 steps are truncated to account for burn-in and the final 500,000 steps are used to generate the parameter distributions shown in Figure 33. Human data from [110, 111, 112, 113] were used to calibrate the model for fast-acting and regular insulin. To initialize Type 1 diabetic patients who had nonzero initial insulin concentrations from [112, 113], the model response to an insulin bolus of 5 units is simulated until the simulated insulin concentration (decreasing with time) matched that of the initial data point. The full state vector at this time point is used to initialize the model for parameter fitting purposes. This method attempts to capture the effect of insulin already on-board before the experiment is performed and data collected. Failure to address the nonzero unobservable insulin states led to a pronounced drop in insulin immediately following the start of the simulation, before the simulated experimental subcutaneous bolus had reached the bloodstream. The resulting

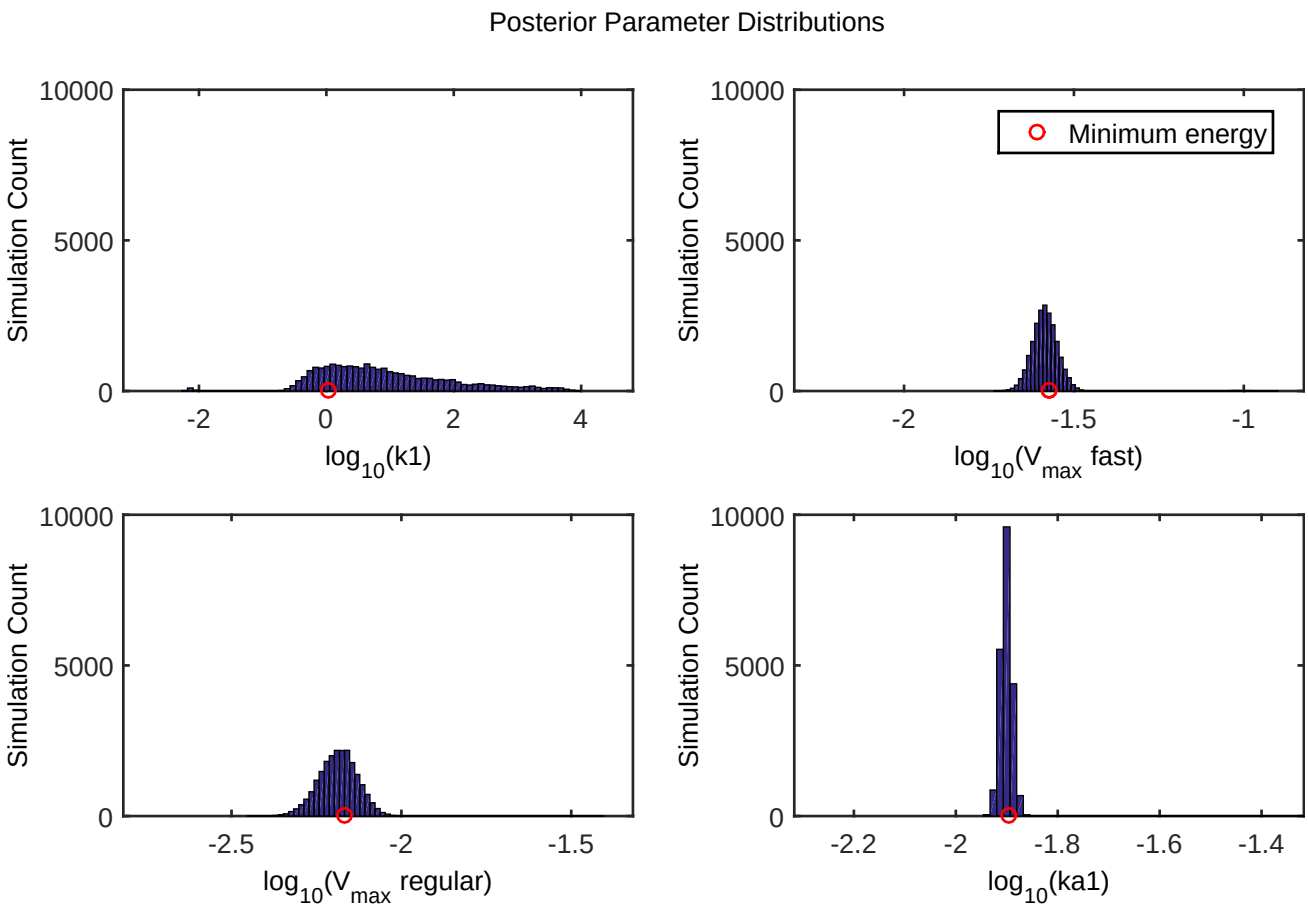

Figure 33: Subcutaneous insulin model parameter distributions for fast-acting and regular insulin found using MCMC optimization.

fits of the data using the minimum energy parameter sets found from MCMC are shown in Figures 34 and 35 for fast-acting and regular insulins, respectively. The final model parameters are shown in Table 7.

4.4 SUMMARY

Markov Chain Monte Carlo parameter optimization is used to consolidate from 4 parameters fit for each insulin type (8 total) to 3 parameters fit in total across insulin types for

Table 7: Final parameter values found using MCMC parameter optimization.

Parameter (units)	Regular	Fast
k_v (1/min)	2.68E-2	6.82E-3
k_1 (1/min)	1.08	1.08
k_{a1} (1/min)	1.27E-2	1.27E-2

the subcutaneous insulin infusion model. This parameter-efficient structure fits k_1 and k_{a1} across insulin types while V_{max} changes depending on the type of insulin administered. The composite model successfully simulates both regular and fast-acting subcutaneous insulin administration.

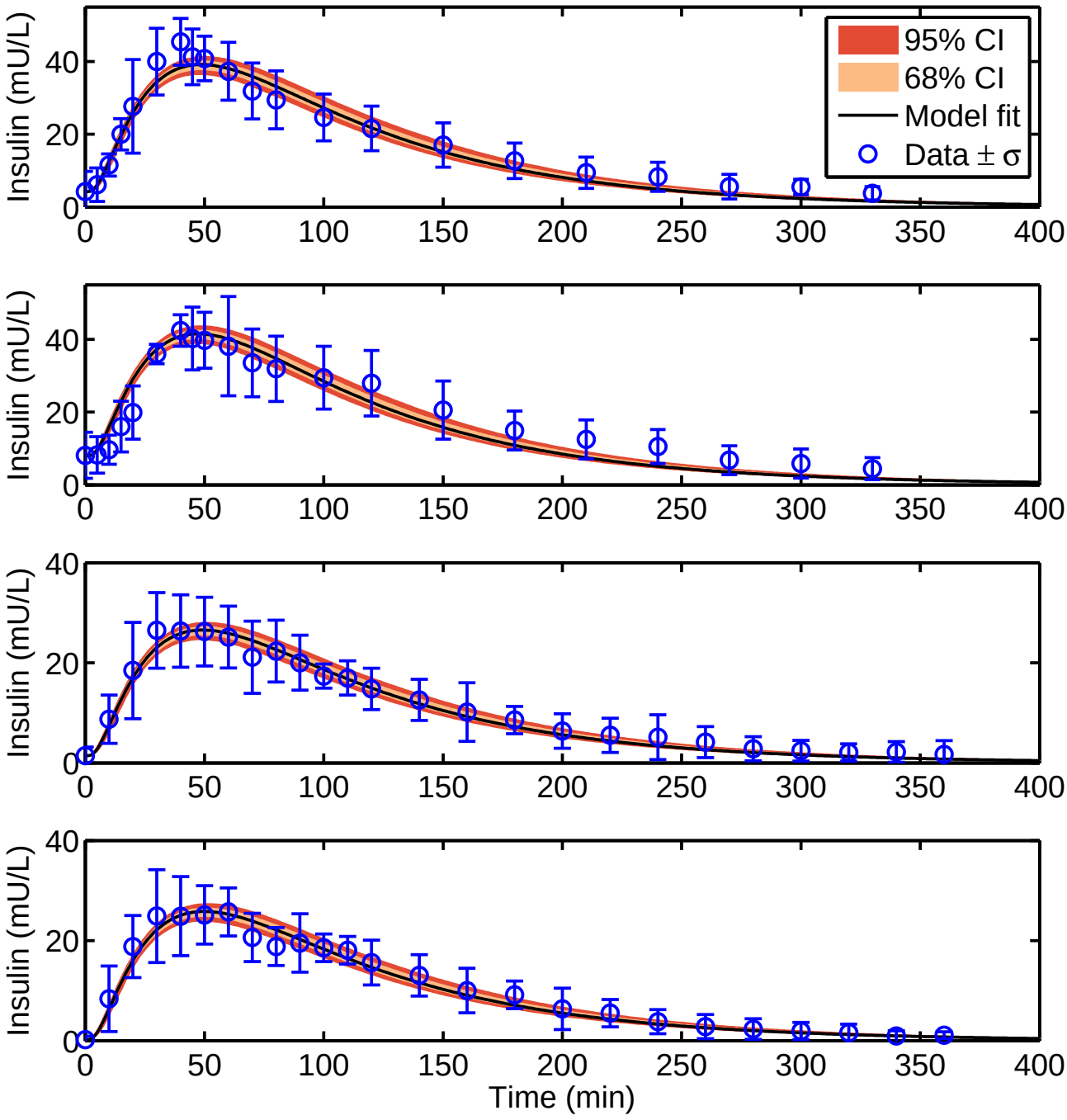

Figure 34: Model dynamics (black line) compared to data (mean: blue circles; error bars represent ± 1 standard error) for plasma insulin appearance following fast-acting subcutaneous insulin administration. The shaded region denotes 68% (beige) and 95% (red) confidence in dynamic response using accepted parameter sets found via MCMC. Top panel: 10 U insulin Lispro [112]. Second panel: 10 U insulin Aspart [112]. Third panel: 7.1 U insulin Lispro [113]. Bottom panel: 7.1 U insulin Aspart [113]. Note: y-axis changes between subfigures.

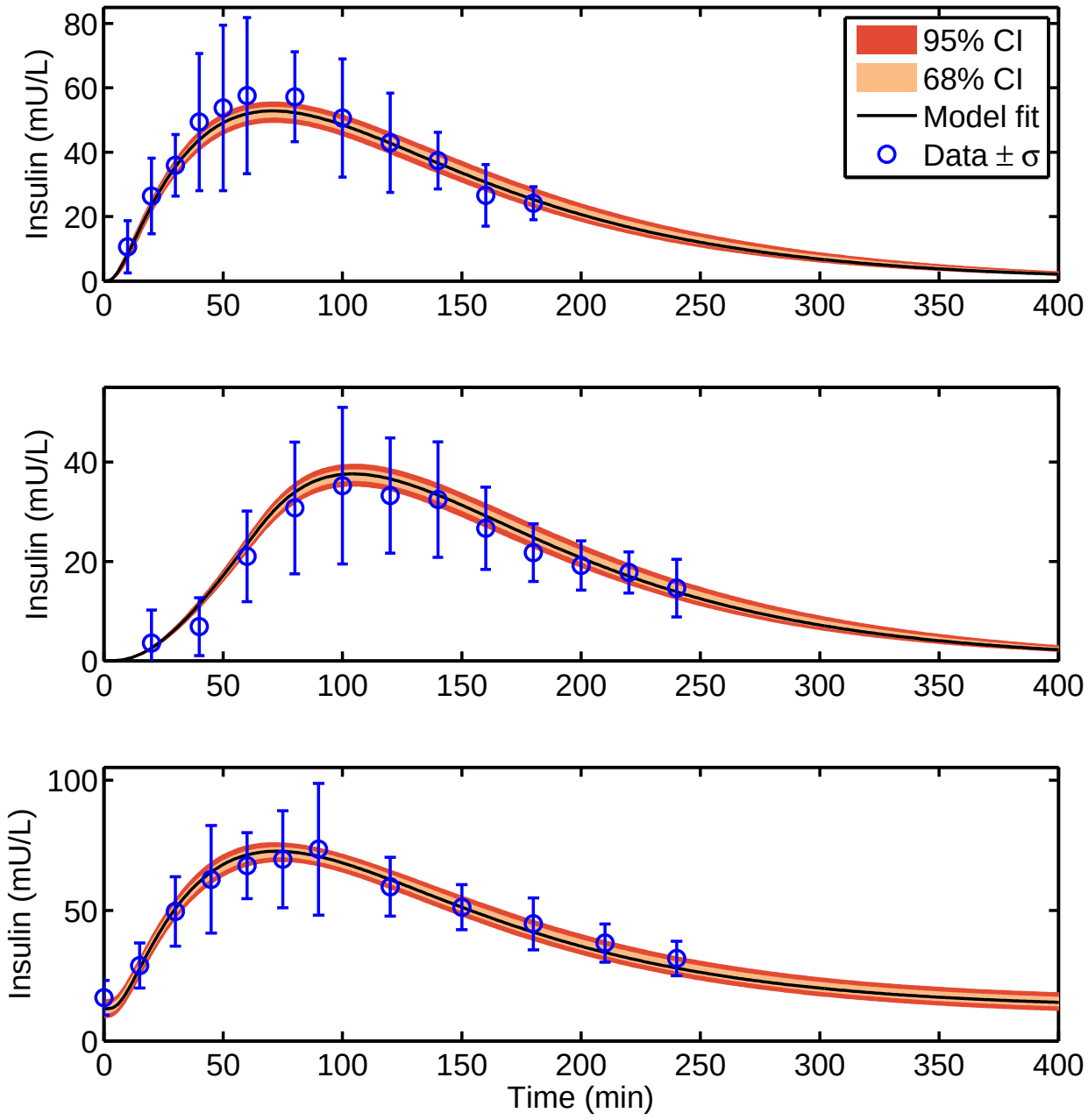

Figure 35: Model dynamics (black line) compared to data (mean: blue circles; error bars represent ± 1 standard error) for plasma insulin appearance following regular subcutaneous insulin administration. The shaded region denotes 68% (beige) and 95% (red) confidence in dynamic response using accepted parameter sets found via MCMC. Top panel: 9 U bolus [111]. Middle panel: 6.8 U continuous subcutaneous infusion over 60 minutes [111]. Bottom panel: 10 U bolus [110]. Note: y-axis changes between subfigures.

5.0 VIRTUAL PATIENTS: CONSTRUCTION AND ANALYSIS

5.1 INTRODUCTION

In this chapter clinical data is used to calibrate biologically relevant patient models, like those developed in the previous chapters. Figure 36 shows the iterative mechanism by which clinical data can be used to both: (i) develop patient models for better controller prediction, and (ii) tune controller behavior *in silico* by simulating patient response. The models are used to inform a model-based controller to predict and treat patients within a decision support system (DSS). The DSS allows for more patient-specific parameterization within the predictive model and can reduce the amount of time needed from medical personnel by automating the analysis of patient measurements and, potentially administering treatment.

Glucose and insulin data comes from the HIgh-DENsity Intensive Care (HIDENIC) data set containing ICU patient information from the University of Pittsburgh Medical Center (UPMC). The data is used to extract patient-specific parameter profiles as virtual patients and provide a testing platform for controller formulation. Controller performance is then evaluated based on overall ability to maintain normoglycemia despite fluctuations in the aforementioned individual parameter profiles and the delivery of nutritional support. The actions suggested by the controller can be presented, in a semi-closed-loop, to clinical personnel who will make the final treatment decision.

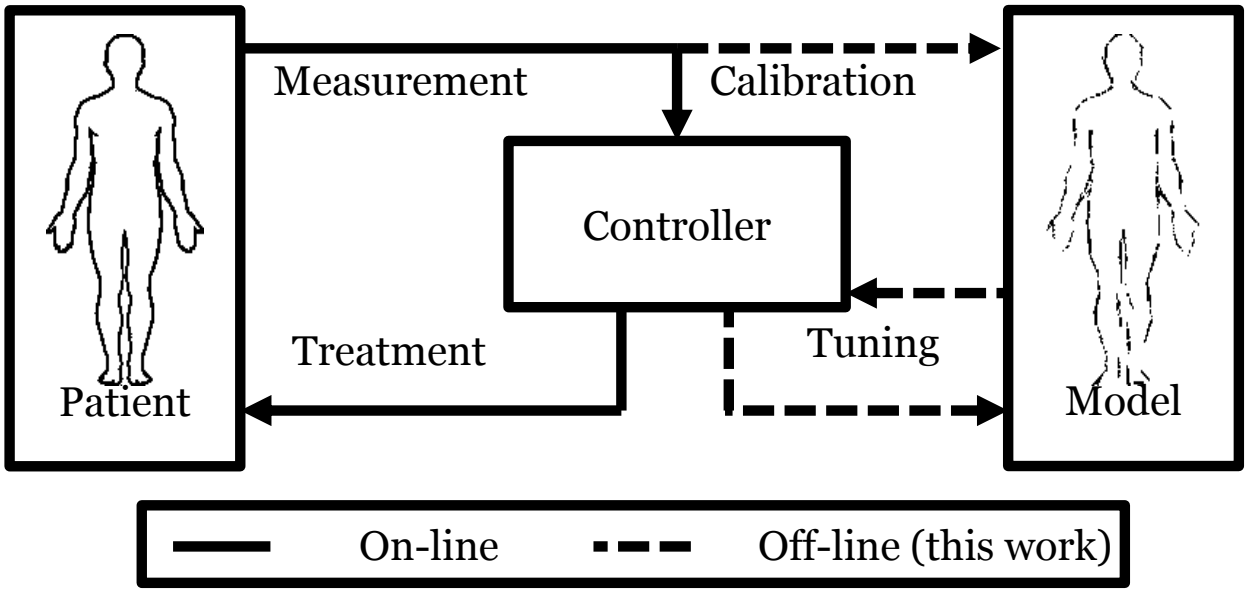

Figure 36: Cyclic process consisting of: gathering patient data (top left), model building and calibration with patient data (top right), iterative *in silico* controller tuning (bottom right), and controller driven treatment (bottom left).

5.2 CONSTRUCTING A VIRTUAL PATIENTS COHORT

5.2.1 Clinical Data Workflow

Patient data from the High-Density Intensive Care (HiDenIC) database at the University of Pittsburgh Medical Center (UPMC) are used to construct virtual patients. A series of Python scripts are used to query the SQL database and construct tables of patient data matching the criteria needed for model validation. Data is extracted for 48 non-diabetic patients, with a length of stay in the ICU between 1 to 14 days, and between the years 2003 and 2009. Selection of the 48 patients is based on the existence of a window of approximately 72 hours during which the following three conditions are met: frequent (approximately q3-q4

hour) finger stick glucose measurements [117], subcutaneous insulin administration, and no oral nutrition administration. These criteria allowed for the characterization of the delivered subcutaneous insulin effects on glucose levels in the absence of additional dynamic glucose processes such as gastric emptying or dynamics unique to diabetic patients. Intravenous glucose and insulin are also extracted over the interval of glucose measurements and modeled as direct inputs to Equations (4.7) and (4.5), respectively.

5.2.2 Virtual Patient Synthesis: Methods

For each extracted patient record, a metabolic profile is calculated in the form of a time-varying parameter, $S_I(t)$, the insulin sensitivity term from Equation (4.7), and a baseline constant EGP_b, similar to [118, 119]. The time-varying parameter $S_I(t)$ and constant EGP_b are fit for each patient so that the combined effects of any exogenous inputs resulted in the model output matching the glucose values recorded in the data to within the error of the fingerstick glucose measurement of 5% [117]. The parameter $S_I(t)$ is estimated every 5 minutes to approximate a continuous signal when compared to the hourly scale of glucose measurements in the database. A zero-order hold is applied to the $S_I(t)$ signal, thereby making it constant over each 5-minute interval. Regularization, with weight Γ, is used to smooth the $S_I(t)$ profile, due to the highly overparameterized problem of fitting $S_I(t)$ at 5-minute intervals to data that is sampled no more rapidly than hourly. The overall objective function fitting individualized $S_I(t)$ and EGP_b to each patient dataset is as follows:

$$\min_{S_I(t)} \frac{1}{N} J(S_I(t)) + \Gamma \sum_{i=1}^{N-1} \left(S_I(t_{i+1}) - S_I(t_i)\right)^2 \tag{5.1}$$

Here, the sum-of-squared error term is normalized by the number of points in the data record, and Γ is the regularization parameter that penalizes the variance of the time-varying, patient-specific insulin sensitivity parameter $S_I(t)$. The virtual patient fitting procedure is summarized in Figure 37. The regularization parameter Γ is determined by fitting 48 patient profiles across a span of Γ_i values and finding the value of Γ_i that results in a mean absolute percent error (MAPE) per point of 5% for a given patient, i. This value is chosen to match the coefficient of variation precision threshold set for the blood glucose sensor [117]. Figure 38

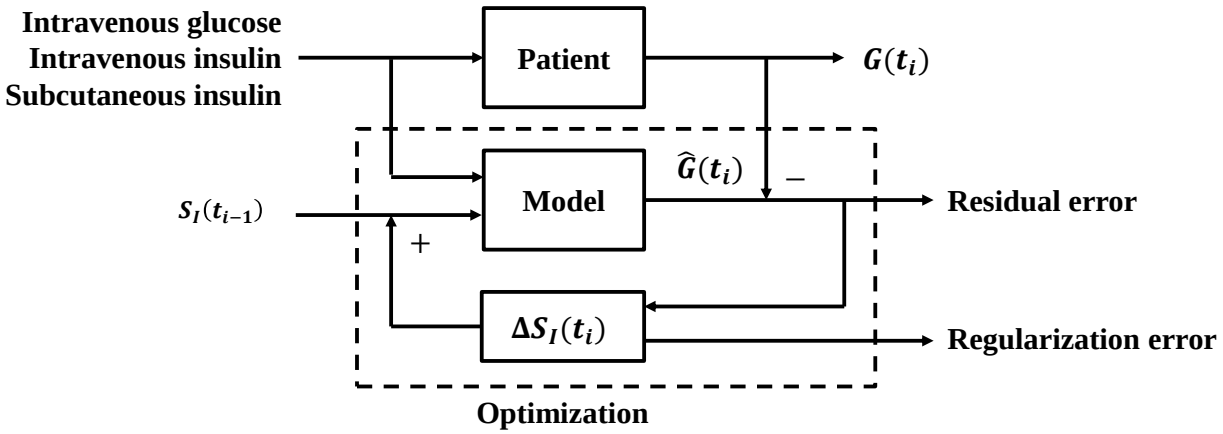

Figure 37: Block diagram for fitting metabolic profiles of patients by taking exogenous inputs and matching glucose output measurements through adjustment of insulin sensitivity, $S_I(t)$. Here, $G(t_i)$ is the glucose measurement from a patient at time t_i, which is fit by the model predicted glucose value $\hat{G}(t_i)$. The value $\Delta S_I(t_i)$ is the change in S_I from t_{i-1} to t_i.

shows the 48-patient distribution of Γ values that yielded a MAPE of 5%. The median Γ value of $7.34E7$ from the distribution in Figure 38 was used to fit the virtual patients in generating the patient cohort. Parameter estimation for $S_I(t)$ was performed using nonlinear least squares and solved using the interior point solver IPOPT [120] implemented in the Coopr/Pyomo package [121]. The model of ordinary differential equations was solved using orthogonal collocation on finite elements (5-minute duration for each element), with three Radau collocation points [122] per finite element.

5.2.3 Virtual Patient Synthesis: Results and Discussion

An example patient profile with modeled and measured glucose values, exogenous inputs, and $S_I(t)$ profile is shown in Figure 39. The results from fitting 48 patients from the HiDenIC database are summarized in Table 8. Overall, the time-varying parameter $S_I(t)$ and constant EGP_b are able to capture the blood glucose profiles for individual patients to within an

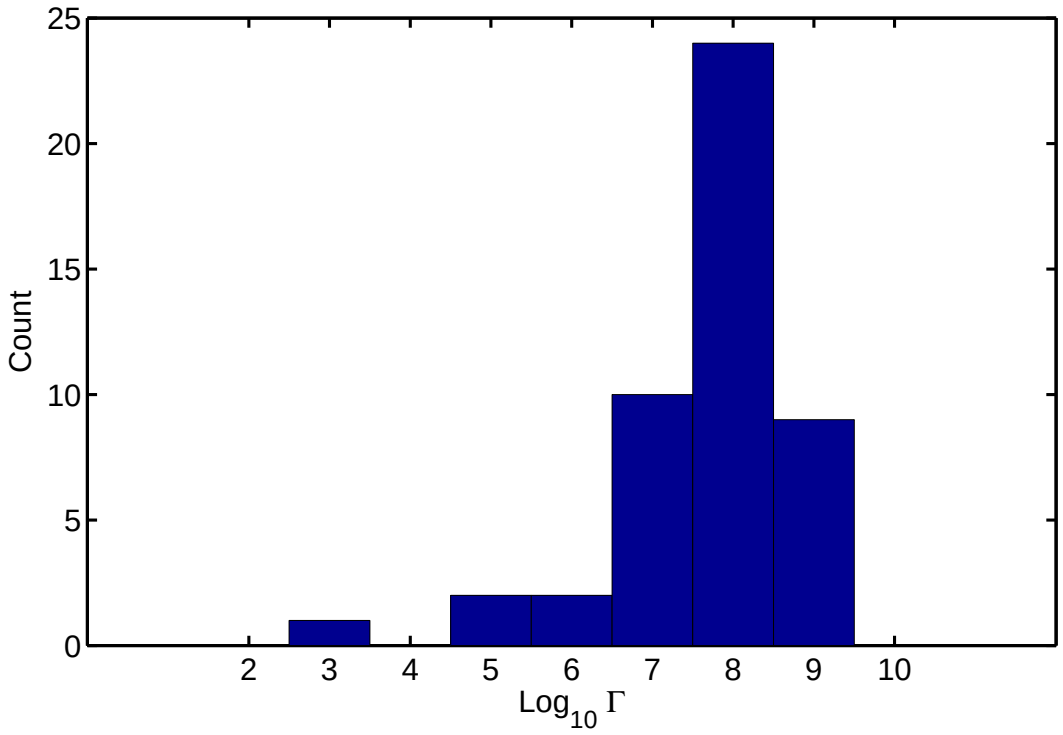

Figure 38: Distribution of 48 patient-specific Γ values where the mean absolute percent error per glucose measurement was 5%.

average absolute mean error:

$$\frac{1}{n}\sum_{i=1}^{n}\left[\frac{1}{m_i}\sum_{j=1}^{m}\left|[G_{i,j}]-[\hat{G_{i,j}}]\right|\right] \tag{5.2}$$

Here n is the total number of patients (48) and m_i is the number of glucose measurements per patient in the data. Patients were selected from the database if they have glucose measurements, intravenous and subcutaneous insulin infusions all present within a 72 hour window. Here $[\hat{G_{i,j}}]$ is the simulated glucose value, and the corresponding glucose measurement is $[G_{i,j}]$. The average absolute mean error is 3.7 mg/dL per patient per data point. This value is lower than the 5% blood glucose sensor error from [117] due to the choice of median Γ value. Model-based analysis indicates that patients fall outside of the desired targeted blood glucose range of 80 to 130 mg/dL on average 12 % of the time. Virtual patients are

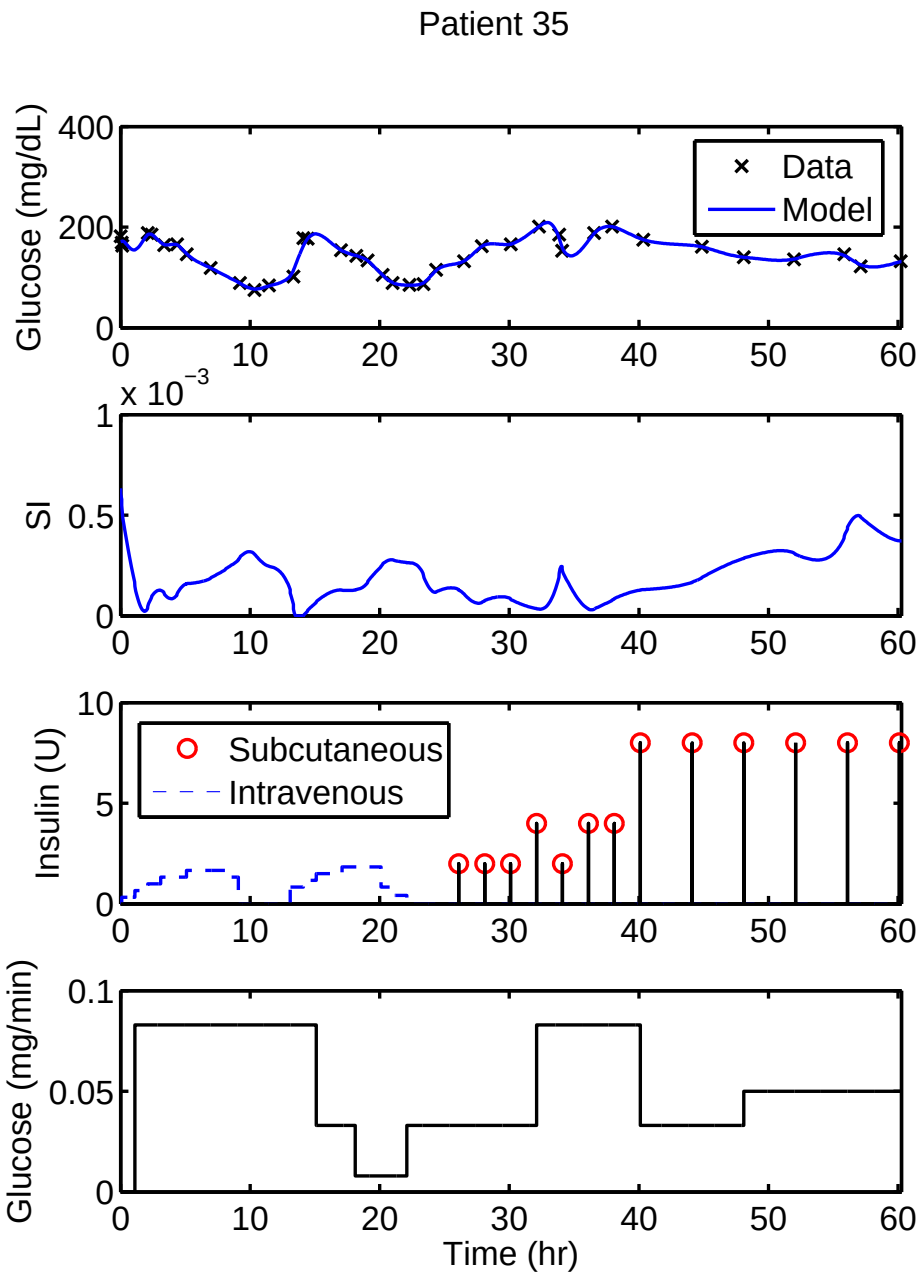

Figure 39: Representative patient fit by adjusting parameter $S_I(t)$. Top panel: Measured glucose values (x) and model-predicted glucose (line). Second panel: Time-varying parameter $S_I(t)$. Third panel: Exogenous subcutaneous (black line, red circle) and intravenous (blue dashed line) insulin. Bottom panel: Exogenous intravenous glucose.

Table 8: Results of fitting the $S_I(t)$ profile of 48 patients to match measured blood glucose. Note: (*) the parameter $S_I(t)$ is lower bounded by zero when the recorded exogenous glucose input does not sufficiently account for the observed increase in blood glucose.

Quantity (units)	Mean	SD	Minimum	Maximum
Mean absolute error (mg/dL)	3.7	3.0	0.4	14.3
Time in 80 to 130 mg/dL range (%)	88.2	13.5	45	100
$S_I(t)$ (L/mU/min)	3.3E-4	2.9E-4	0.0*	2.3E-3
EGP_b (mmol/L/min)	1.7	6.5E-1	1.0	4.9
Subcutaneous insulin given (U)	67	44	20	214
Patient data record length (hr)	66	7.9	37	72

constructed by fitting the composite model to intensive care unit data from patients who had received exogenous subcutaneous insulin in addition to intravenous glucose and insulin. One time-varying parameter, $S_I(t)$, and one constant parameter, EGP_b, are fit for each of 48 patients to form an individualized metabolic profile. Blood glucose measurements are captured using the recorded exogenous inputs as well as the fitted parameters, resulting in an average model error of 3.7 mg/dL per measurement per patient, to match blood glucose sensor error from [117], over an average time window of 66 hours.

One of the primary challenges in treating stress hyperglycemia in critical care is the intra- and inter-patient variations in glucose metabolism resulting from changes in insulin sensitivity. The fitted parameter profile, $S_I(t)$, calculated for each patient data set extracted from the critical care database forms a virtual patient cohort. Each unique, time-varying parameter profile can be used to simulate a realistic patient responding to exogenous inputs such as insulin and glucose administration in critical care. This forms a test platform for *in silico* controller design and optimization capable of utilizing subcutaneous insulin and expanding beyond strictly intravenous-based control.

5.3 CONTROLLING A VIRTUAL PATIENT COHORT

For zone glucose control (ZGC), we develop a DSS that runs closed-loop *in silico* to evaluate controller performance. Virtual patient simulations can be controlled by a model predictive controller (MPC) that uses zone control to minimize both hypoglycemic events and hyperglycemia through administration of insulin and glucose. Virtual patient simulations, originally fit to match clinical metabolic profiles, provide a platform to refine controller parameters. The results of performing virtual control on the clinically-derived virtual patients shows improved performance compared to the original patient data.

5.3.1 Virtual Patient Control: Methods

A preliminary nonlinear controller formulation is implemented to evaluate control performance on a virtual patient cohort. Model predictive control (MPC) is combined with moving horizon estimation (MHE), which allows the internal controller model to recalibrate based on newly received blood glucose measurements. Equations 5.3 through (5.5) describe the MPC/MHE formulation.

$$\min_{\mathbf{u_I},\mathbf{u_G}} \quad \sum_{i=k+1}^{k+P} \left(E_{pred}(i)\right)^2 + \Gamma_g u_g(i)^2 \tag{5.3}$$

$$s.t. \qquad BG_{pred}(i) = f\left(BG_{meas}(i-1), u(i), \theta(k)\right)) \tag{5.4}$$

$$E_{pred}(i) = \begin{cases} 0, & BG_{lb} \leq BG_{pred}(i) \leq BG_{ub} \\ BG_{pred}(i) - BG_{ub}, & BG_{pred}(i) \geq BG_{ub} \\ BG_{pred}(i) - BG_{lb}, & BG_{pred}(i) \leq BG_{lb} \end{cases} \tag{5.5}$$

Manipulated inputs $\mathbf{u_I}$ and $\mathbf{u_G}$ are exogenous insulin and glucose, respectively, over the interval $[k+1, P]$. The optimization penalizes predicted blood glucose values, $BG_{pred}(i)$, outside of the control zone. The zone is defined as the region between BG_{lb} and BG_{ub}. Regularization on absolute glucose infusion $u_G(K)$ is weighted by Γ_g to penalize unnecessary glucose infusion. Model predictions are generated by sampling a continuous-time nonlinear model $(f\left(BG_{meas}(i-1), u(k), p(k)\right)))$ at the measurement interval of 5 minutes over the

prediction horizon, P. The nonlinear model provides predicted glucose values $BG_{pred}(k)$ as a function of the current glucose measurement $BG_{meas}(k)$, input administration $u(k)$, and the model parameters $\theta(k)$. Inputs $u(k)$ for each time point k include glucose and insulin such that $u_I(k), u_G(k) \in u(k)$.

Equations (5.3) through (5.5) describe the formulation used for optimizing MHE.

$$\min_{\theta_{fit}(L)\in\theta} \quad \sum_{i=k-N}^{k} \left(BG_{est}(i) - BG_{meas}(i)\right)^2 \tag{5.6}$$

$$s.t. \qquad BG_{est}(k+1) = f\left(BG_{meas}(k), u(L), \theta(L)\right) \tag{5.7}$$

$$\theta_{lb} \leq \theta_{fit}(L) \leq \theta_{ub} \tag{5.8}$$

The past N discrete measurements are used to recalibrate the model parameters, $\theta_{fit}(L)$, over the interval $L \in [k-N, k]$ to match the model glucose concentration estimate, $BG_{est}(L)$ for each past measurement. A subset of parameters, $\theta_{fit}(L)$, belonging to the nonlinear model are adjusted to match model output with measurements. Examples of MPC/MHE and zone control are depicted in Figure 40. The overall DSS schematic displayed in Figure 41 shows the targeted implementation in the clinical setting that is simulated *in silico* to determine feasibility and controller confidence. Zone-MPC as shown in Figure 40 is evaluated *in silico* using a model of metabolic homeostasis (Appendix).

5.3.2 Virtual Patient Control: Results and Discussion

In a separate analysis, 99 patient records are extracted from the same HiDenIC database. The 99 patients were selected based on the density of glucose measurements available within the database. The results of implementing zone-MPC is a reduction in hypo- and hyperglycemia *in silico* for our 99 virtual patients. Glucose control metrics [124] are drastically improved as seen in Table 9 and overall population mean glucose is mostly maintained to within the desired control region as shown in Figure 42. To design a controller relevant to critical care patients, our detailed metabolic model captures and simulates 99 virtual patient's dynamics. The virtual patient test cohort is used to successfully simulate identical scenarios with and without glycemic control. We show, using the virtual patient test cohort, that glycemic variability is reduced and large hypo and hyperglycemic fluctuations are minimized using

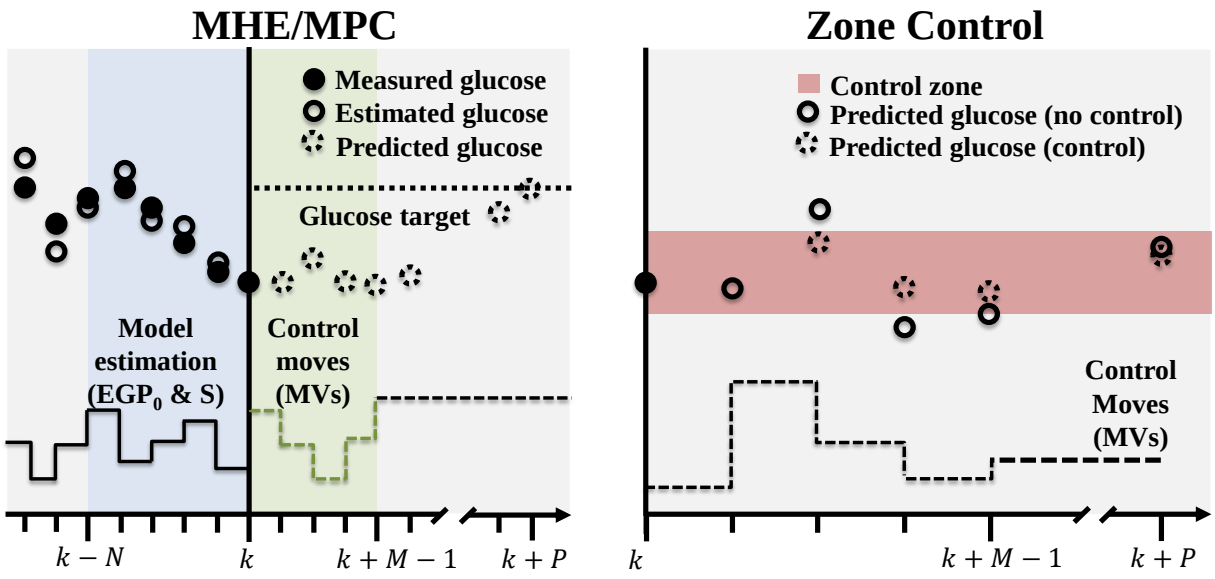

Figure 40: MPC/MHE schematic (left) showing prediction and estimation horizons along with optimal control actuation (adapted from [123]). MHE minimizes the error between past glucose measurements and model predictions by adjusting a subset of parameters, $\theta_{fit}(L)$. Zone control schematic (right) showing control moves only when predicted blood glucose leaves specified zone. Manipulated variables $u_I(K)$ and $u_G(K)$ are adjusted over prediction horizon with a penalty, Γ_g, for leaving $u_G(K)$ nonzero.

zone control. These results indicate a successful pilot study using virtual patients derived from a critical care population. This concept is extended through more detailed modeling and higher resolution measurements to form a robust simulation test platform for *in silico* critical care trials.

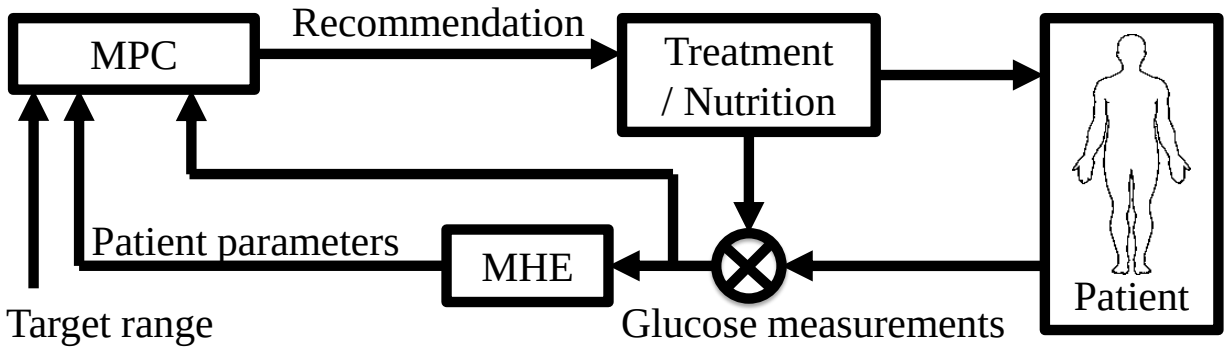

Figure 41: Patient specific time-varying parameters are estimated by the MHE algorithm using glucose measurements. Controller uses MPC to calculate optimal insulin and/or glucose infusion, the manipulated variables, to maintain blood glucose within target range.

Table 9: Summary of suggested statistics [124] for comparing glucose control protocols.

Glucose statistics	TGC	Original
Central tendency (median;IQR)	121; 12 (mg $dl^{-}1$)	128; 28 (mg $dl^{-}1$)
Dispersion (median;IQR)	17; 10 (mg $dl^{-}1$)	37; 24 (mg $dl^{-}1$)
Moderate hypoglycemia (41-70 mg $dl^{-}1$)	12%	47%
Severe hypoglycemia ($\leq$ 40 mg $dl^{-}1$)	0%	1%

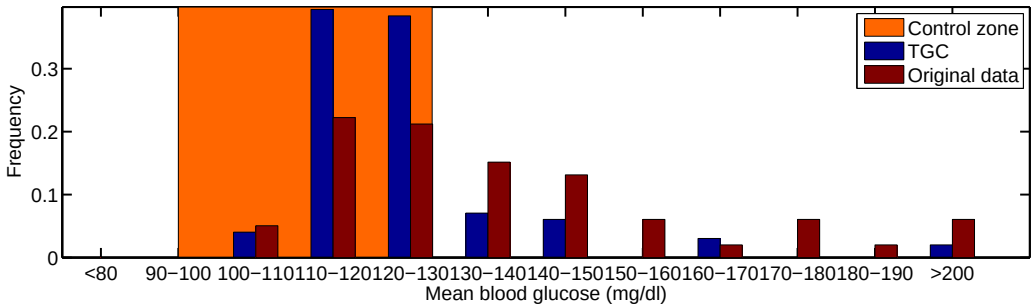

Figure 42: Per patient average blood glucose shows reduction in variance and mean glucose concentration, as well as an increased frequency of patients within the target zone, under Zone-MPC/MHE.

5.4 IMPROVING THE VIRTUAL PATIENT COHORT

Controller performance is limited by the accuracy of the model [32]. Model accuracy is also important for simulating a realistic patient response. Temporal resolution of the virtual patient simulator is improved by incorporating additional key dynamics. The modules listed in Table 10 are the core models used in developing the virtual patient cohort. It is our ultimate goal to incorporate additional modules such as the inflammatory challenge, counterregulation, and subcutaneous insulin models previously described. Additionally, a model of continuous glucose monitoring noise is added to the virtual patient to simulate realistic glucose measurement noise.

In addition to our simulator there have been a number of similar virtual patient platforms developed for glucose and insulin dynamics. The *in silico* control results presented earlier in this chapter (Section 5.3.2) use the core model of glucose and insulin dynamics from [125] (Appendix). However, a key state impacting glucose-insulin dynamics from [125] is free fatty acids (FFAs), which is unidentifiable without explicit measurements of plasma FFAs. As a result, the results below replace the core glucose-insulin model from [125] with a clinically validated model [100], resulting in the referenced core models in Table 10. Table 11 contains a list of other simulators with model structures that can be potentially be used in-

Table 10: Core components for a metabolic simulator that can accomodate multiple clinically available measurements

Module	Notes
Subcutaneous Insulin (Ch 4)	Capture subcutaneous insulin delivery
CGM (Ch 5)	Incorporate sensor measurements to infer blood glucose
Meal [125, 126]	Incorporate oral nutrition
Glucose [100]	Primary dynamics of plasma glucose
Insulin [100]	Lag and effect of insulin on plasma glucose
Cytokines (Ch 2 & 5)	Innate immune effects on glucose homeostasis
Stress hormones (Ch 2 & 3)	Hormonal modulation of glucose homeostasis

terchangeably with core insulin and glucose dynamic components from the virtual patient model. These published model structures could be used for increased versatility if additional data is available. The proposed core platform summarized by Table 10 forms a virtual pa-

Table 11: Published *in silico* simulator-algorithm pairs used for controller formulation and testing in critical care.

Principal Investigator	Model	Algorithm
Hovorka [127]	[119]	eMPC
Seborg [128]	[129]	MPC
Chase [100]	[129]	MPC
Van Den Berghe [130]	[21]	NL-MPC
Parker (this work)	[100]	MPC

tient to test implementation of control strategies and enables rapid algorithm prototyping and refinement *in silico*. Each patient undergoing ZGC has an individual plasma fingerprint, describing a personalized profile of how they will respond to insulin treatment based on $S_I(t)$ and EGP_b. The modules describing subcutaneous insulin dynamics were previously developed and added to the virtual patient platform from Chapter 4 in order to improve upon the model, and hence the quality of the control performance observed in Section 5.3.2.

The following sections describe the characterization and simulation of continuous glucose monitor (CGM) error and the application of the inflammatory model from Chapter 2 to human trauma data. These modules represent improvements to application-relevant components of the virtual patient simulator.

5.4.1 Continuouse Glucose Monitoring

Subcutaneous continuous glucose monitors (CGMs) provide dense measurements that can be mathematically reconstructed into the unmeasured plasma glucose levels for use in ZGC. We collect measurements of patient's glucose concentrations using a Dexcom G4 Platinum$^{\text{TM}}$(G4P) CGM with a frequency of 1/5 min^{-1}. A simple approach is used to build the module of the transport between plasma glucose and interstitial glucose. The dynamics are found to be well described using a first-order filter of the form:

$$\frac{dG_{SC}(t)}{dt} = \frac{1}{\tau}(G(t) - G_{SC}(t)) \tag{5.9}$$

$$G_{SCS}(t) = G_{SC}(t) + \sigma_{SC} \tag{5.10}$$

Here, $G(t)$, $G_{SC}(t)$, and $G_{SCS}(t)$ are the concentrations of blood glucose (BG), interstitial glucose (IG), and sensed interstitial glucose (IGs), respectively. The coefficient τ is the time constant associated with glucose transport from plasma to interstitial space and has been experimentally determined [131]. The parameter σ_{SC} is a noise term associated with the interstitial sensor measurement. Tables $1A$ and $4A$ from the G4P user's manual [117] containing experimental measurement error data are used to simulate the noise, statistically similar to the sensor, for a given range of glucose values. This module allows the overall

model to simulate a more realistic clinical environment where noisy, high frequency data is potentially available.

In addition to simulating noise for use in a virtual patient simulator, we also develop a technique to convert a noisy sensor measurement to a reconstructed blood glucose value. The slope is calculated between each blood glucose measurement which is then interpolated to shift the CGM measurement along the same line. This technique, described in Equation (5.11) and shown in Figure 43 can only be applied as a post-hoc analysis, rather than in real-time, and is useful for characterizing the noise observed from clinical samples. IG is estimated using blood glucose measurements to reconstruct sensed IG signal between the finger-stick blood glucose measurement time points. The IGs measurement is then projected along the angle of the two reference blood glucose measurements to recreate the real IG as shown in Equation (5.11). IG is then projected through the BG to IG first-order filter described in Equation (5.9).

$$IG(t_i) = IGs(t_i) + \frac{t_i - t_0}{t_n - t_0}\theta_{IG} + Z \tag{5.11}$$

Here, $IG(t_i)$ represents IG at time point t_i, n and 0 represent the time points of the first and second calibration glucose points, respectively. The parameters θ_{IG} and Z are the projection angle and vertical shift, respectively. Clinically measured θ and Z can be added to a virtual patient simulator to recreate the noise encountered when using a CGM. Controller performance *in silico* in response to CGM noise could then be used to evaluate the feasibility of ZGC using CGM measurements. Future work could include a comparison of control with or without blood glucose measurements and can begin to quantify the loss in controller performance as a result of the added CGM noise. Successful control with a CGM signal *in silico* could enables significant decrease in clinical manpower required for ZGC because CGM requires fewer human operating hours.

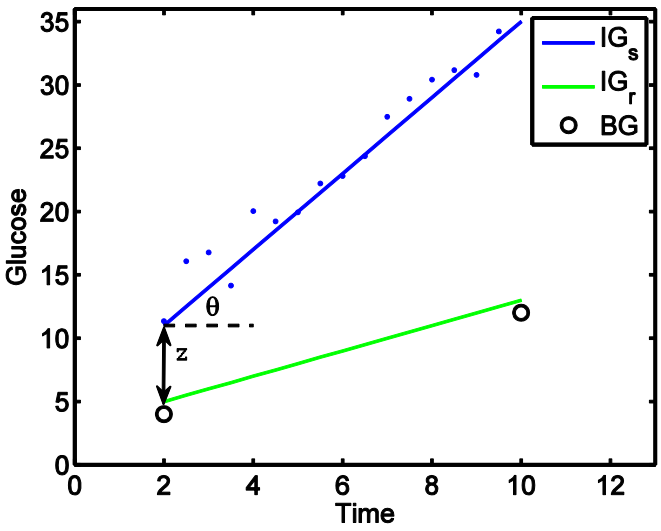

Figure 43: Schematic with synthetic data showing shift and projection of original sensed signal (blue) along blood glucose anchor points (black) to reconstruct blood glucose (green).

5.4.2 Simulating Plausible Mechanisms

The critical component of a patient-tailored DSS is a mathematical model that can resolve the dynamic changes resulting from an individuals unique metabolic state. The underlying mechanism of stress hyperglycemia is a complex network of biological signaling pathways that decrease sensitivity to insulin [132] and increase endogenous glucose production (EGP). In this section, the mathematical model described in Chapter 2 is used to identify and characterize the complex biological pathways leading to stress hyperglycemia. The modeled metabolic regulatory processes involved in dynamic modification of metabolism in the ICU include cytokines, such as TNF- and IL-6, and hormones, such as cortisol, which alter insulin-mediated glucose uptake (IMGU) in humans [73, 84]. As in Chapter 2, the metabolic regulatory pathway is coupled with a model of glucose and insulin homeostasis [100] from literature to resolve patient specific variations in metabolic state.

Patient data was used from the Cologne area participating in the German Trauma Registry effort. Blood glucose and IL-6 measurements were taken every 6 to 10 hours. Here,

IL-6 is used instead of TNF due to measurement availability and because they share a similar dynamic profile [13]. The dynamic differences between TNF and IL-6 compared to the frequency of measurements allows for this approximation. The inflammatory LPS state is allowed to vary with time along with the magnitude of IL-6 activation and cortisol inhibition of glucose uptake. These parameters are fit in order to match the measured glucose values from the dataset. The estimation process is shown schematically in Figure 44. The corre-

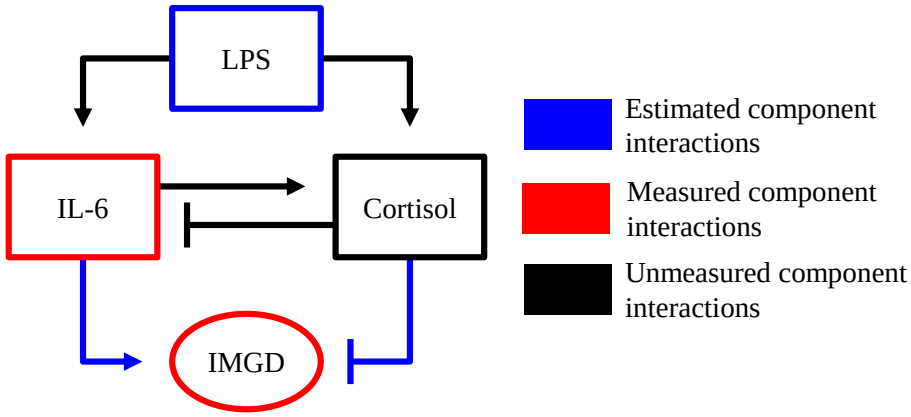

Figure 44: Diagram showing the acute inflammatory pathway governing insulin-mediated glucose dynamics (IMGD). LPS represents the inflammatory state and is fit over time to match the glucose dynamics and IL-6 measurements from human truama data.

sponding IL-6 measurements are compared to the IL-6/TNF state output from the model. The IL-6 data is classified as either an inlier or outlier using a random sample consensus (RANSAC) [133] algorithm. The RANSAC algorithm is an iterative process through which data is excluded from the objective function if it does not fit the model to within a given threshold. A random subset of data is iteratively selected and fit until a group of data points is selected as inliers, and the rest are excluded as outliers.

If the IL-6 data matches the model output to within a threshold value of 1 pg/ml then the data is classified as an inlier and added to the data being fit. The regions where the IL-6 data is classified as an inlier represents where the inflammatory model is a plausible

explanatory mechanism. Conversely, when outliers in the IL-6 data are detected, it represents a region where other dynamic processes are likely responsible for the changes observed in blood glucose. An example could be a sharp drop in glucose due to an unrecorded insulin infusion, as shown in Figure 46. This is a common occurrence and represents some of the limitations with the dataset used.

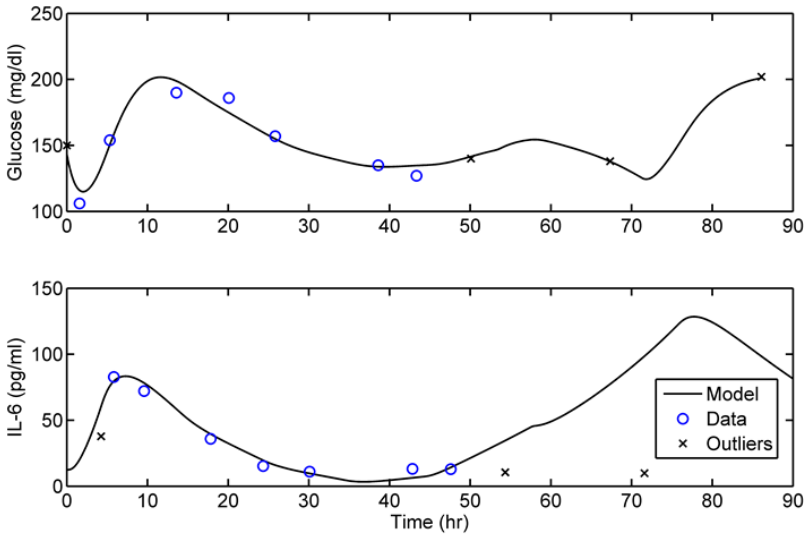

Figure 45: Example patient data fit using the outlier detection algorithm. Glucose data (top) is fit by adjusting the LPS state. Regions where IL-6 data (bottom) matches the model output is classified as an inlier (blue circles), otherwise they are considered outliers (black X).

5.5 DISCUSSION

A model of glucose and insulin is combined with mechanistic inflammatory dynamics (Equations (2.3) to (2.11)) to serve as a simulation platform to generate clinically-relevant critically

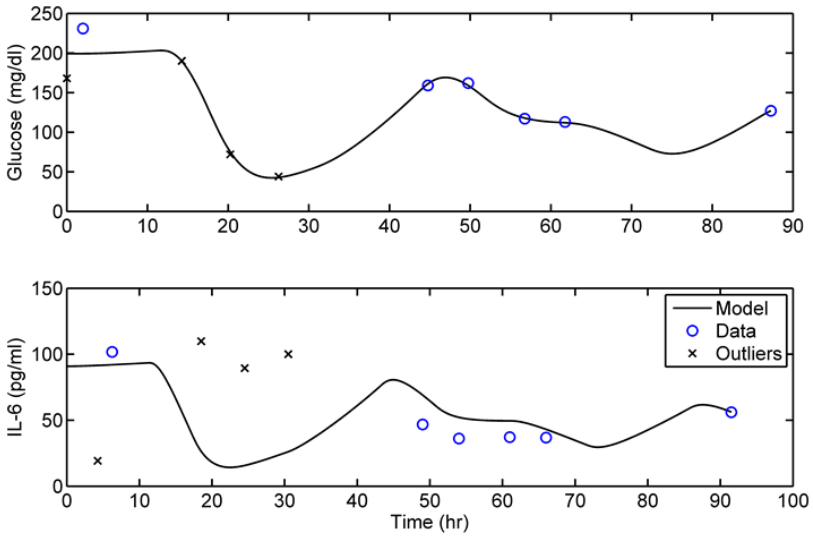

Figure 46: Example patient data fit using the outlier detection algorithm. Glucose data (top) is fit by adjusting the LPS state. Regions where IL-6 data (bottom) matches the model output is classified as an inlier (blue circles), otherwise they are considered outliers (black X). Early timepoints indicate a drop in glucose not explained by the IL-6 trajectory. This could be caused by an infusion of insulin that is unaccounted for in the data.

ill patient metabolic profiles. Two test patients from a data set of 215 trauma victims from two hospital centers in the Cologne area participating in the German Trauma Registry effort are chosen for analysis to provide virtual patient dynamics of clinical response that includes realistic inflammatory effects. The patient's measured IL-6 concentrations are used as a surrogate for the TNF model state. The model is able to estimate IL-6 concentrations falling around 100 pg/ml. This concentration falls within the $10 - 1,000$ pg/ml range of LPS concentration used to calibrate the original model.

With further resolved data, a library of these time-varying inflammatory profiles could be used to differentiate inflammation-driven metabolic effects. This database would then add to the virtual patient platform by providing mechanistic patient-to-patient variability. Such a virtual patient platform is useful for developing DSS control strategies, as well as to better

understand possible patient differentiation metrics for separating treatment cohorts (*e.g.*, driven by inflammation, counterregulation, or other exogenous factors) for which treatment strategies may differ as a result of their metabolic upset.

6.0 SUMMARY AND FUTURE WORK

6.1 MODELING MECHANISMS OF INSULIN RESISTANCE

There are many different mechanisms that cause changes to blood glucose in critical care patients. To treat patients with stress hyperglycemia we develop mathematical models to better understand the mechanistic interactions of both endogenous and exogenous processes. Elucidating these interactions provides the potential to guide patient-specific interventions that improve glucose control without aggravating stress hyperglycemia.

The previously developed model of acute inflammation as a driver of metabolic changes is a result of mechanisms found in literature corroborated or contrasted by human studies of stress hyperglycemia. The process of model refinement through available data and identifiable mechanisms is used to build the model described in section 2.2.1. Many different aspects of the disease of stress hyperglycemia were explored. These aspects include a deeper level of mechanism that were not ultimately included due to a shortage of human data. Thus, the "dead-ends described in sections 2.1.1 to 2.1.3 are avenues that warrant future investigation to elucidate the complex pathways and biomarkers involved in stress hyperglycemia. The scale and scope of the model may be further explored, looking at multiscale modeling implementations as found in [134, 135, 136] as well as differentiating between tissue-specific metabolic effects. Limited human experiments ultimately led to the necessary simplification, though increased resolution could allow for a more fundamental understanding.

The counterregulatory response is another important process governing changes to glucose metabolism. We constructed a model that quantifies the individual contributions of the four hormones: glucagon, epinephrine, cortisol, and growth hormone. The model provides insight into how the dynamics of counterregulatory hormone release influence glucose

metabolism. However, if additional rate data on glucose appearance and disposal is available, the model could be improved by allowing the glucose rate changes to feed back into the blood glucose balance.

6.1.1 Endogenous Insulin Release

Quantifying insulin release in critical care is challenging because it is often difficult to measure. Suppression of insulin released by the pancreas is a possible tissue-specific mechanism of stress hyperglycemia. There are many stress hormones that act to suppress endogenous release of insulin. Specifically, adrenergic signaling has a direct mechanism of suppressing insulin release by the pancreas. Thus, we construct a mechanistic model of adrenergic signaling in the pancreas by combining an adrenergic receptor model [137] with a mechanistic model of pancreatic β-cell signaling [138]. The model is calibrated using data from rat pancreatic islets exposed to epinephrine [139]. The model provides qualitatively accurate behavior when simulating the effects of glucose on pancreatic insulin release and subsequent suppression by epinephrine as shown in Figure 47.

However, due to the large number of parameters and relatively limited amount of data for model calibration, the model is ultimately not incorporated into the overall model of glucose and insulin dynamics. Furthermore, endogenous insulin release is rapidly suppressed by exogenous infusion of insulin, which occurs frequently in critical care. It is therefore unlikely that suppressed pancreatic insulin release plays a significant role when exogenous insulin has been given. Additional mechanistic modeling would be warranted for patients receiving or prescribed to receive sparse quantities of exogenous insulin (*e.g.*, during the final days of recovery).

6.2 SUBCUTANEOUS INSULIN

Subcutaneous insulin absorption into the plasma varies by insulin type. Regular insulin has a hexameric structure that cannot be readily absorbed into the plasma and must be

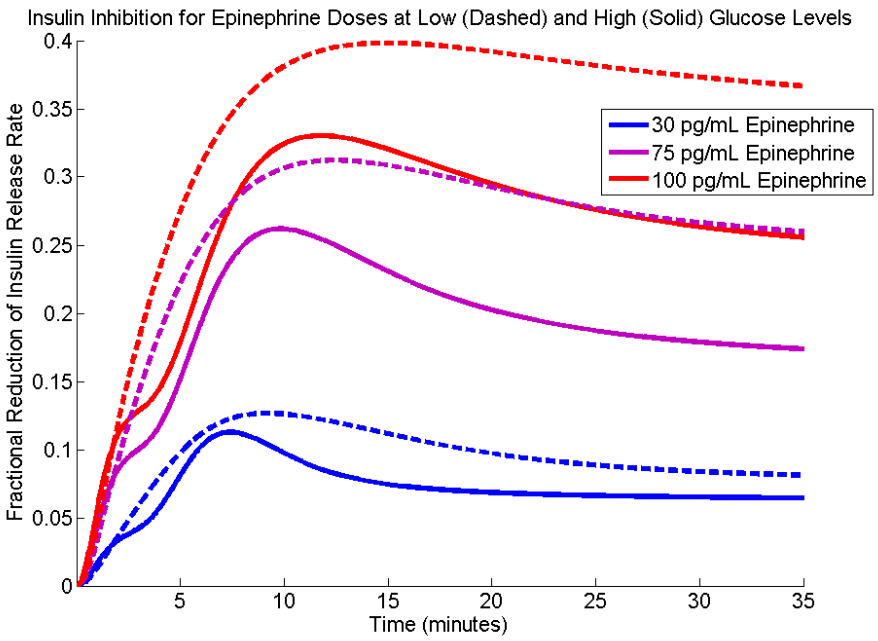

Figure 47: different inhibitory effects of a range of epinephrine on insulin release induced at low (4 mM) and high (10 mM) glucose exposure levels.

broken down (an equilibrium process) into its dimeric and monomeric forms prior to plasma absorption. Fast-acting insulin analogues, however, have only monomeric structure and are easily absorbed into the plasma.

Three subcutaneous insulin absorption models have been evaluated in order to capture the plasma insulin dynamics for regular and fast-acting insulin analogues, for healthy and type-1 diabetic patients, and CSII and bolus injections. Model selection begins with the best model (as measured by Akaike Information Criteria (AIC)[114]) from [107]. In [107] 11 different model formulations are evaluated using AIC to select the best model to use. Starting from this model, we use a combination of literature data sets to further tailor the model to our requirement: the ability to capture plasma insulin dynamics following subcutaneous administration of different types of insulin (*i.e.*, regular, fast-acting) using a single structure, but different parameter values.

As in [107], the AIC is used to balance model complexity with quality of fit, as quantified by sum of squared error between model predictions and literature data, for the studied types of insulin. The model with the lowest AIC score, representing the preferred trade-off of model complexity and accuracy, captures plasma insulin dynamics for different types of insulin and various patient conditions. The model can be used in the development of a control algorithm that will facilitate clinical decision-making for glucose control and insulin delivery in critical care.

6.3 VIRTUAL PATIENT DEVELOPMENT

6.3.1 Modularity

Mathematical models frequently fall into a the category of being too specific and therefore difficult to generalize. For a model to be easily extensible beyond the particular system or dataset for which it was created, it needs a particular structure to enable modularity. In the previous modeling sections, care was taken to build models that were extensible via modularity; they consist of (a) specific driver(s) of subsystem dynamics followed by an observed output, where the output becomes potential input to other modules. For subsystems with complex overlapping inputs or outputs, earlier modules are derived sequentially to reduce multiple inputs/outputs using their respective input-output module. From these modules we then form a hierarchical network that can integrate multiple inputs into a systems-level response.

Modularly designed models are capable of incorporating new data while not requiring full recalibration of model parameters, instead, specific modules can be refit as needed. In addition to data, incorporating new mechanistic insight is a fundamental characteristic of our modules achieved via Hill-type functions, as described below. A first order Hill-function (Michaelis-Menten) is shown in Equation (6.1) where non-competitive and competitive inhibition can be represented by redefining parameters as in Equations (6.2)) and (6.3)), respectively.

$$\frac{d[X]}{dt} = \frac{v_{app}[U]}{K_{app} + [U]} \tag{6.1}$$

$$v_{app} = \frac{v_{max}}{1 + \frac{[I_{nc}]}{K_{nc}}} \tag{6.2}$$

$$K_{app} = K(1 + \frac{[I_c]}{K_c}) \tag{6.3}$$

Here, $[X], [U], [I_{nc}]$, and $[I_c]$ are concentrations of output, input, non-competitive inhibitor, and inhibitor, respectively. Parameters v_{app} and k_{app} may have been fit originally to the input/output data set when no inhibition is taken into account. As new mechanistic information is discovered, for example with a different study, data from the new study can be used to refit the particular module shown in Equation 6.1 by replacing v_{app} and/or k_{app} with Equations (6.2) and/or (6.3) respectively. Equations (6.2) and (6.3) influence the efficacy and potency [140], respectively, of $[U]$ to drive $[X]$. Depending on the new component to be added, the additional parameters K_c or K_{nc} are added to the module and fit with the new data representing the inhibitor dynamics.

It is important to note that newly identified components may not need to be incorporated if they share linear, temporal dynamics with components already represented in the module. Such addition would merely break up a single, primary component, term into two additive terms which would have already been accounted for with a higher original parameter value. For example, $K_{app} = K(1 + \frac{[I_{nc}]}{K_{nc}})$ becomes $K_{app} = K(1 + \frac{[I_{nc,old}]}{K_{nc,old}} + \frac{[I_{nc,new}]}{K_{nc,new}})$ where, if $[I_{nc,new}] = a[I_{nc,old}]$ then $\frac{1}{K_{nc}} = \frac{1}{K_{nc,old}} + \frac{a}{K_{nc,new}}$. The importance of having two separate terms representing each inhibitory component occurs when components do not simultaneously or linearly influence the output of interest, or, when specific biomarkers are more clinically available. The approximation of linear, temporal synchronization allows us to model specific components as modules representing a larger pathway of interest. This is exemplified in Figure 12 where each major pathway is represented as a primary component: TNF for the innate immune response and cortisol for the stress response.

The virtual patient cohort provides a critical platform to rapidly test controller performance and better understand the dynamics associated with stress hyperglycemia. While some of the key modules listed in Table 10 were developed in this document, there may be

additional mechanisms to improve the biological accuracy of the virtual patient. With an emphasis on modularity, the virtual patient can be expanded to include additional components from Table 1.

APPENDIX

CORE MODEL OF GLUCOSE AND INSULIN DYNAMICS

The core model describing insulin and glucose dynamics from [125] is shown below. The model includes the effects of free fatty acids on glucose uptake.

$$\frac{dI(t)}{dt} = -n(I(t) - I_b) + p_5 u_1(t) \quad (.1)$$

$$\frac{dX(t)}{dt} = -p_2(X(t) - X_b) + p_3(I(t) - I_b) \quad (.2)$$

$$\frac{dG(t)}{dt} = p_1(G_b - G(t)) - p_4 X(t)G(t) + p_6(G(t)F(t) - G_b F_b) + \frac{u_2(t)}{Vol_G} \quad (.3)$$

$$\frac{dF(t)}{dt} = p_7(F_b - F(t)) - p_8 X(t)F(t) + p_9(G)(F(t)G(t) - F_b G_b) + \frac{u_3(t)}{Vol_F} \quad (.4)$$

$$p_9(G(t)) = 0.00021e^{-0.0055G(t)} \quad (.5)$$

Variables u_1, u_2, and u_3 are the appearance of insulin, glucose, and free fatty acids in the plasma, respectively.

Table 12: Model parameters

Parameter	Value	Unit
p_1	6.8E-2	min^{-1}
p_2	3.7E-2	min^{-1}
p_3	1.2E-5	min^{-1}
p_4	1.3	$mLmin^{-1}\mu mol^{-1}$
p_5	5.7E-4	mL^{-1}
p_6	6.0E-5	$min^{-1}\mu mol^{-1}$
p_7	3.0E-2	min^{-1}
p_8	4.5	$mLmin^{-1}\mu mol^{-1}$
k_1	2.0E-2	min^{-1}
k_2	3.0E-2	min^{-1}
p_{F2}	1.7E-1	min^{-1}
p_{F3}	1.0E-5	min^{-1}
n	1.4E-1	min^{-1}
G_b	98	$mgdL^{-1}$
F_b	380	$\mu molL^{-1}$
Vol_G	117	dL
Vol_F	11.7	L

BIBLIOGRAPHY

[1] T. M. Mahmoud, A. A. Abdelbaky, S. A. Hassan, M. A. Abdelrahman, A. M. Saeed, Admission Hyperglycemia: is it a Predictor of the Outcome of Postoperative Mechanically-ventilated ICU Patients?, Journal of American Science 8 (9).

[2] F. Farrokhi, D. Smiley, G. E. Umpierrez, Glycemic control in non-diabetic critically ill patients, Best Practice & Research Clinical Endocrinology & Metabolism 25 (5) (2011) 813–824. doi:10.1016/j.beem.2011.05.004.

[3] B. P. Kavanagh, K. C. McCowen, Glycemic Control in the ICU, New England Journal of Medicine 363 (26) (2010) 2540–2546. doi:10.1056/NEJMcp1001115.

[4] G. V. Bochicchio, M. Joshi, K. M. Bochicchio, A. Pyle, S. B. Johnson, W. Meyer, K. Lumpkins, T. M. Scalea, Early Hyperglycemic Control is Important in Critically Injured Trauma Patients:, The Journal of Trauma: Injury, Infection, and Critical Care 63 (6) (2007) 1353–1359. doi:10.1097/TA.0b013e31815b83c4.

[5] J. Hermanides, R. J. Bosman, T. M. Vriesendorp, R. Dotsch, F. R. Rosendaal, D. F. Zandstra, J. B. L. Hoekstra, J. H. DeVries, Hypoglycemia is associated with intensive care unit mortality*:, Critical Care Medicine 38 (6) (2010) 1430–1434. doi:10.1097/CCM.0b013e3181de562c.

[6] J. S. Krinsley, A. Grover, Severe hypoglycemia in critically ill patients: Risk factors and outcomes*:, Critical Care Medicine 35 (10) (2007) 2262–2267. doi:10.1097/01.CCM.0000282073.98414.4B.

[7] J. S. Krinsley, Glycemic variability: A strong independent predictor of mortality in critically ill patients*:, Critical Care Medicine 36 (11) (2008) 3008–3013. doi:10.1097/CCM.0b013e31818b38d2.

[8] M. Egi, R. Bellomo, E. Stachowski, C. J. French, G. Hart, Variability of blood glucose concentration and short-term mortality in critically ill patients, Anesthesiology 105 (2) (2006) 244–252.

[9] O. Badawi, M. D. Waite, S. A. Fuhrman, I. H. Zuckerman, Association between intensive care unit–acquired dysglycemia and in-hospital mortality*:, Critical Care Medicine 40 (12) (2012) 3180–3188. doi:10.1097/CCM.0b013e3182656ae5.

[10] J. S. Krinsley, Understanding glycemic control in the critically ill: three domains are better than one, Intensive Care Medicine 37 (3) (2011) 382–384. doi:10.1007/s00134-010-2110-3.

[11] S. M. Bagshaw, M. Egi, C. George, R. Bellomo, Early blood glucose control and mortality in critically ill patients in Australia*:, Critical Care Medicine 37 (2) (2009) 463–470. doi:10.1097/CCM.0b013e318194b097.

[12] A. Thorell, S. Efendic, M. Gutniak, T. Häggmark, O. Ljungqvist, Development of postoperative insulin resistance is associated with the magnitude of operation, The European Journal of Surgery = Acta Chirurgica 159 (11-12) (1993 Nov-Dec) 593–599.

[13] A. O. Agwunobi, C. Reid, P. Maycock, R. A. Little, G. L. Carlson, Insulin resistance and substrate utilization in human endotoxemia, The Journal of Clinical Endocrinology & Metabolism 85 (10) (2000) 3770–3778.

[14] H. Shamoon, R. Hendler, R. S. Sherwin, Synergistic interactions among antiinsulin hormones in the pathogenesis of stress hyperglycemia in humans, The Journal of Clinical Endocrinology and Metabolism 52 (6) (1981) 1235–1241. doi:10.1210/jcem-52-6-1235.

[15] M. Lehrke, U. C. Broedl, I. M. Biller-Friedmann, M. Vogeser, V. Henschel, K. Nassau, B. Göke, E. Kilger, K. G. Parhofer, Serum concentrations of cortisol, interleukin 6, leptin and adiponectin predict stress induced insulin resistance in acute inflammatory reactions, Critical Care 12 (6) (2008) R157.

[16] H. Kitano, K. Oda, T. Kimura, Y. Matsuoka, M. Csete, J. Doyle, M. Muramatsu, Metabolic syndrome and robustness tradeoffs, Diabetes 53 (suppl 3) (2004) S6–S15.

[17] G. Van den Berghe, P. Wouters, F. Weekers, C. Verwaest, F. Bruyninckx, M. Schetz, D. Vlasselaers, P. Ferdinande, P. Lauwers, R. Bouillon, Intensive insulin therapy in critically ill patients, New England journal of medicine 345 (19) (2001) 1359–1367.

[18] J.-C. Preiser, P. Devos, G. Van den Berghe, Tight control of glycaemia in critically ill patients, Current Opinion in Clinical Nutrition & Metabolic Care 5 (5) (2002) 533–537.

[19] J. S. Krinsley, Effect of an intensive glucose management protocol on the mortality of critically ill adult patients, in: Mayo Clinic Proceedings, Vol. 79, Elsevier, 2004, pp. 992–1000.

[20] G. E. Umpierrez, S. D. Isaacs, N. Bazargan, X. You, L. M. Thaler, A. E. Kitabchi, Hyperglycemia: an independent marker of in-hospital mortality in patients with undiagnosed diabetes, The Journal of Clinical Endocrinology & Metabolism 87 (3) (2002) 978–982.

[21] G. Van den Berghe, A. Wilmer, G. Hermans, W. Meersseman, P. J. Wouters, I. Milants, E. Van Wijngaerden, H. Bobbaers, R. Bouillon, Intensive insulin therapy in the medical ICU, New England Journal of Medicine 354 (5) (2006) 449.

[22] J.-C. Preiser, P. Devos, S. Ruiz-Santana, C. Mélot, D. Annane, J. Groeneveld, G. Iapichino, X. Leverve, G. Nitenberg, P. Singer, J. Wernerman, M. Joannidis, A. Stecher, R. Chioléro, A prospective randomised multi-centre controlled trial on tight glucose control by intensive insulin therapy in adult intensive care units: the Glucontrol study, Intensive Care Medicine 35 (10) (2009) 1738–1748. doi:10.1007/s00134-009-1585-2.

[23] S. R. Mehta, Effect of Glucose-Insulin-Potassium Infusion on Mortality in Patients With Acute ST-Segment Elevation Myocardial Infarction: The CREATE-ECLA Randomized Controlled Trial, JAMA 293 (4) (2005) 437. doi:10.1001/jama.293.4.437.

[24] S. Finfer, Intensive versus Conventional Glucose Control in Critically Ill Patients, New England Journal of Medicine 360 (13) (2009) 1283–1297. doi:10.1056/NEJMoa0810625.

[25] S. Finfer, Hypoglycemia and Risk of Death in Critically Ill Patients, New England Journal of Medicine 367 (12) (2012) 1108–1118. doi:10.1056/NEJMoa1204942.

[26] M. Wilson, J. Weinreb, G. W. S. Hoo, Intensive Insulin Therapy in Critical Care: A review of 12 protocols, Diabetes Care 30 (4) (2007) 1005–1011. doi:10.2337/dc06-1964.

[27] R. Tiruvoipati, B. Chiezey, D. Lewis, K. Ong, E. Villanueva, K. Haji, J. Botha, Stress hyperglycemia may not be harmful in critically ill patients with sepsis, Journal of Critical Care 27 (2) (2012) 153–158. doi:10.1016/j.jcrc.2011.06.011.

[28] H. Hirasawa, S. Oda, M. Nakamura, Blood glucose control in patients with severe sepsis and septic shock, World Journal of Gastroenterology 15 (33) (2009) 4132. doi:10.3748/wjg.15.4132.

[29] B. W. Whitcomb, E. K. Pradhan, A. G. Pittas, M.-C. Roghmann, E. N. Perencevich, Impact of admission hyperglycemia on hospital mortality in various intensive care unit populations*:, Critical Care Medicine 33 (12) (2005) 2772–2777. doi:10.1097/01.CCM.0000189741.44071.25.

[30] P. E. Marik, J.-C. Preiser, Toward understanding tight glycemic control in the ICU: a systematic review and metaanalysis, CHEST Journal 137 (3) (2010) 544–551.

[31] P. Parsons, P. Watkinson, Blood glucose control in critical care patients–a review of the literature, Nursing in critical care 12 (4) (2007) 202–210.

[32] M. Morari, Robust process control, Prentice Hall, Englewood Cliffs, N.J, 1989.

[33] M. E. Wilinska, R. Hovorka, Simulation Models for In-Silico Evaluation of Closed-Loop Insulin Delivery Systems in Type 1 Diabetes, in: V. Marmarelis, G. Mitsis (Eds.), Data-driven Modeling for Diabetes, Lecture Notes in Bioengineering, Springer Berlin Heidelberg, 2014, pp. 131–149.

[34] M. Breton, A. Farret, D. Bruttomesso, S. Anderson, L. Magni, S. Patek, C. D. Man, J. Place, S. Demartini, S. D. Favero, C. Toffanin, C. Hughes-Karvetski, E. Dassau, H. Zisser, F. J. Doyle, G. D. Nicolao, A. Avogaro, C. Cobelli, E. Renard, B. Kovatchev, o. b. o. T. I. A. P. i. S. Group, Fully Integrated Artificial Pancreas in Type 1 Diabetes Modular Closed-Loop Glucose Control Maintains Near Normoglycemia, Diabetes 61 (9) (2012) 2230–2237. doi:10.2337/db11-1445.

[35] S. J. Russell, F. H. El-Khatib, D. M. Nathan, K. L. Magyar, J. Jiang, E. R. Damiano, Blood Glucose Control in Type 1 Diabetes With a Bihormonal Bionic Endocrine Pancreas, Diabetes Care 35 (11) (2012) 2148–2155. doi:10.2337/dc12-0071.

[36] T. Battelino, J. Š. Omladič, M. Phillip, Closed loop insulin delivery in diabetes, Best Practice & Research Clinical Endocrinology & Metabolismdoi:10.1016/j.beem.2015.03.001.

[37] S. Eslami, A. Abu-Hanna, E. de Jonge, N. F. de Keizer, Tight glycemic control and computerized decision-support systems: a systematic review, Intensive Care Medicine 35 (9) (2009) 1505–1517. doi:10.1007/s00134-009-1542-0.

[38] L. Leelarathna, S. W. English, H. Thabit, K. Caldwell, J. M. Allen, K. Kumareswaran, M. E. Wilinska, M. Nodale, J. Mangat, M. L. Evans, others, Feasibility of fully automated closed-loop glucose control using continuous subcutaneous glucose measurements in critical illness: a randomized controlled trial, Crit Care 17 (2013) R159.

[39] G. Van den Berghe, How does blood glucose control with insulin save lives in intensive care?, Journal of Clinical Investigation 114 (9) (2004) 1187–1195. doi:10.1172/JCI200423506.

[40] L. Li, J. L. Messina, Acute insulin resistance following injury, Trends in Endocrinology & Metabolism 20 (9) (2009) 429–435. doi:10.1016/j.tem.2009.06.004.

[41] S. Van Cromphaut, Hyperglycaemia as part of the stress response: the underlying mechanisms, Best Practice & Research Clinical Anaesthesiology 23 (4) (2009) 375–386. doi:10.1016/j.bpa.2009.08.005.

[42] A. Thorell, A. Loftenius, B. Andersson, O. Ljungqvist, Postoperative insulin resistance and circulating concentrations of stress hormones and cytokines, Clinical Nutrition 15 (2) (1996) 75–79. doi:10.1016/S0261-5614(96)80023-9.

[43] K. C. McCowen, A. Malhotra, B. R. Bistrian, Stress-induced hyperglycemia, Critical care clinics 17 (1) (2001) 107–124.

[44] J.-M. Fernández-Real, W. Ricart, Insulin resistance and inflammation in an evolutionary perspective: the contribution of cytokine genotype/phenotype to thriftiness, Diabetologia 42 (11) (1999) 1367–1374.

[45] M. K. Piya, P. G. McTernan, S. Kumar, Adipokine inflammation and insulin resistance: the role of glucose, lipids and endotoxin, Journal of Endocrinology 216 (1) (2013) T1–T15. doi:10.1530/JOE-12-0498.

[46] S. Derde, I. Vanhorebeek, G. Van den Berghe, Insulin Treatment in Intensive Care Patients, Hormone Research 71 (1) (2009) 2–11. doi:10.1159/000173736.

[47] D. Voet, J. G. Voet, Biochemistry. Hoboken, John Wiley & Sons 1 (2004) 591.

[48] V. T. Samuel, G. I. Shulman, Mechanisms for Insulin Resistance: Common Threads and Missing Links, Cell 148 (5) (2012) 852–871. doi:10.1016/j.cell.2012.02.017.

[49] A. Herschkovitz, Y.-F. Liu, E. Ilan, D. Ronen, S. Boura-Halfon, Y. Zick, Common Inhibitory Serine Sites Phosphorylated by IRS-1 Kinases, Triggered by Insulin and Inducers of Insulin Resistance, Journal of Biological Chemistry 282 (25) (2007) 18018–18027. doi:10.1074/jbc.M610949200.

[50] J. L. Evans, B. A. Maddux, I. D. Goldfine, The molecular basis for oxidative stress-induced insulin resistance, Antioxidants & redox signaling 7 (7-8) (2005) 1040–1052.

[51] S. Jiang, J. L. Messina, Role of inhibitory B kinase and c-Jun NH2-terminal kinase in the development of hepatic insulin resistance in critical illness diabetes, AJP: Gastrointestinal and Liver Physiology 301 (3) (2011) G454–G463. doi:10.1152/ajpgi.00148.2011.

[52] K. D. Copps, M. F. White, Regulation of insulin sensitivity by serine/threonine phosphorylation of insulin receptor substrate proteins IRS1 and IRS2, Diabetologia 55 (10) (2012) 2565–2582. doi:10.1007/s00125-012-2644-8.

[53] R. Potashnik, A. Bloch-Damti, N. Bashan, A. Rudich, Irs1 degradation and increased serine phosphorylation cannot predict the degree of metabolic insulin resistance induced by oxidative stress, Diabetologia 46 (5) (2003) 639–648. doi:10.1007/s00125-003-1097-5.

[54] R. S. Parker, G. Clermont, Systems engineering medicine: engineering the inflammation response to infectious and traumatic challenges, Journal of The Royal Society Interface 7 (48) (2010) 989–1013. doi:10.1098/rsif.2009.0517.

[55] A. Witasp, L. Nordfors, M. Schalling, J. Nygren, O. Ljungqvist, A. Thorell, Expression of Inflammatory and Insulin Signaling Genes in Adipose Tissue in Response to Elective Surgery, The Journal of Clinical Endocrinology & Metabolism 95 (7) (2010) 3460–3469. doi:10.1210/jc.2009-2588.

[56] A. Witasp, L. Nordfors, M. Schalling, J. Nygren, O. Ljungqvist, A. Thorell, Increased expression of inflammatory pathway genes in skeletal muscle during surgery, Clinical Nutrition 28 (3) (2009) 291–298. doi:10.1016/j.clnu.2009.03.003.

[57] L. Rui, M. Yuan, D. Frantz, S. Shoelson, M. F. White, SOCS-1 and SOCS-3 Block Insulin Signaling by Ubiquitin-mediated Degradation of IRS1 and IRS2, Journal of Biological Chemistry 277 (44) (2002) 42394–42398. doi:10.1074/jbc.C200444200.

[58] X. Xu, A. Sarikas, D. C. Dias-Santagata, G. Dolios, P. J. Lafontant, S.-C. Tsai, W. Zhu, H. Nakajima, H. O. Nakajima, L. J. Field, R. Wang, Z.-Q. Pan, The CUL7 E3 Ubiquitin Ligase Targets Insulin Receptor Substrate 1 for Ubiquitin-Dependent Degradation, Molecular Cell 30 (4) (2008) 403–414. doi:10.1016/j.molcel.2008.03.009.

[59] G. Sabio, R. J. Davis, cJun NH2-terminal kinase 1 (JNK1): roles in metabolic regulation of insulin resistance, Trends in Biochemical Sciences 35 (9) (2010) 490–496. doi:10.1016/j.tibs.2010.04.004.

[60] R. A. DeFronzo, J. D. Tobin, R. Andres, Glucose clamp technique: a method for quantifying insulin secretion and resistance, American Journal of Physiology-Gastrointestinal and Liver Physiology 237 (3) (1979) G214–G223.

[61] E. F. du Toit, D. G., Myocardial Insulin Resistance: An Overview of Its Causes, Effects, and Potential Therapy, in: S. Arora (Ed.), Insulin Resistance, InTech, 2012.

[62] F. Andreelli, D. Jacquier, S. Troy, Molecular aspects of insulin therapy in critically ill patients, Current Opinion in Clinical Nutrition & Metabolic Care 9 (2) (2006) 124–130.

[63] S. Gray, J. K. Kim, New insights into insulin resistance in the diabetic heart, Trends in Endocrinology & Metabolism 22 (10) (2011) 394–403. doi:10.1016/j.tem.2011.05.001.

[64] C. M. Taniguchi, B. Emanuelli, C. R. Kahn, Critical nodes in signalling pathways: insights into insulin action, Nature Reviews Molecular Cell Biology 7 (2) (2006) 85–96. doi:10.1038/nrm1837.

[65] J. I. Mechanick, Metabolic Mechanisms of Stress Hyperglycemia, Journal of Parenteral and Enteral Nutrition 30 (2) (2006) 157–163. doi:10.1177/0148607106030002157.

[66] A. L. Carey, G. R. Steinberg, S. L. Macaulay, W. G. Thomas, A. G. Holmes, G. Ramm, O. Prelovsek, C. Hohnen-Behrens, M. J. Watt, D. E. James, B. E. Kemp, B. K. Pedersen, M. A. Febbraio, Interleukin-6 Increases Insulin-Stimulated Glucose Disposal in Humans and Glucose Uptake and Fatty Acid Oxidation In Vitro via AMP-Activated Protein Kinase, Diabetes 55 (10) (2006) 2688–2697. doi:10.2337/db05-1404.

[67] J. M. Stouthard, J. A. Romijn, T. Van der Poll, E. Endert, S. Klein, P. J. Bakker, C. H. Veenhof, H. P. Sauerwein, Endocrinologic and metabolic effects of interleukin-6

in humans, American Journal of Physiology-Endocrinology And Metabolism 268 (5) (1995) E813–E819.

[68] J. L Sarvas, The IL-6 Paradox: Context Dependent Interplay of SOCS3 and AMPK, Journal of Diabetes & Metabolism 01 (S13). doi:10.4172/2155-6156.S13-003.

[69] S. T. Nielsen, L. Lehrskov-Schmidt, R. Krogh-Madsen, T. P. J. Solomon, L. Lehrskov-Schmidt, J. J. Holst, K. Møller, Tumour necrosis factor-alpha infusion produced insulin resistance but no change in the incretin effect in healthy volunteers, Diabetes/Metabolism Research and Reviews 29 (8) (2013) 655–663. doi:10.1002/dmrr.2441.

[70] R. Krogh-Madsen, Influence of TNF- and IL-6 infusions on insulin sensitivity and expression of IL-18 in humans, AJP: Endocrinology and Metabolism 291 (1) (2006) E108–E114. doi:10.1152/ajpendo.00471.2005.

[71] E. Bach, R. R. Nielsen, M. H. Vendelbo, A. B. Møller, N. Jessen, M. Buhl, K. Thomas, L. Holm, S. B. Pedersen, H. Pilegaard, others, Direct Effects of TNF-α on Local Fuel Metabolism and Cytokine Levels in the Placebo-Controlled, Bilaterally Infused Human Leg Increased Insulin Sensitivity, Increased Net Protein Breakdown, and Increased IL-6 Release, Diabetes 62 (12) (2013) 4023–4029.

[72] H. Vedder, W. Schreiber, A. Yassouridis, S. Gudewill, C. Galanos, T. Pollmächer, Dose-dependence of bacterial lipopolysaccharide (LPS) effects on peak response and time course of the immune-endocrine host response in humans, Inflammation Research 48 (2) (1999) 67–74.

[73] R. A. Rizza, L. J. Mandarino, J. E. Gerich, Cortisol-Induced Insulin Resistance in Man: Impaired Suppression of Glucose Production and Stimulation of Glucose Utilization due to a Postreceptor Defect of Insulin Action*, The Journal of Clinical Endocrinology & Metabolism 54 (1) (1982) 131–138.

[74] P. De Feo, G. Perriello, E. Torlone, M. M. Ventura, C. Fanelli, F. Santeusanio, P. Brunetti, J. E. Gerich, G. B. Bolli, Contribution of cortisol to glucose counterregulation in humans, American Journal of Physiology-Endocrinology And Metabolism 257 (1) (1989) E35–E42.

[75] E. Bach, A. B. Møller, J. O. L. Jørgensen, M. H. Vendelbo, N. Jessen, J. F. Olesen, S. B. Pedersen, T. S. Nielsen, N. Møller, Intact Pituitary Function is Decisive for the Catabolic Response to TNF-α: Studies of Protein, Glucose and Fatty Acid Metabolism in Hypopituitary and Healthy Subjects, The Journal of Clinical Endocrinology & Metabolism 100 (2) (2014) 578–586. doi:10.1210/jc.2014-2489.

[76] A. Hillenbrand, M. Weiss, U. Knippschild, A. M. Wolf, M. Huber-Lang, Sepsis-Induced Adipokine Change with regard to Insulin Resistance, International Journal of Inflammation 2012 (2012) 1–7. doi:10.1155/2012/972368.

[77] M. Zarkovic, S. Ignjatovic, M. Dajak, J. Ciric, B. Beleslin, S. Savic, M. Stojkovic, P. Bulat, B. Trbojevic, Cortisol response to ACTH stimulation correlates with blood interleukin 6 concentration in healthy humans, European Journal of Endocrinology 159 (5) (2008) 649–652. doi:10.1530/EJE-08-0544.

[78] P. De Feo, G. Perriello, E. Torlone, C. Fanelli, M. M. Ventura, F. Santeusanio, P. Brunetti, J. E. Gerich, G. B. Bolli, Contribution of adrenergic mechanisms to glucose counterregulation in humans, American Journal of Physiology-Endocrinology And Metabolism 261 (6) (1991) E725–E736.

[79] P. De Feo, G. Perriello, E. Torlone, C. Fanelli, M. M. Ventura, F. Santeusanio, P. Brunetti, J. E. Gerich, G. B. Bolli, Evidence against important catecholamine compensation for absent glucagon counterregulation, American Journal of Physiology-Endocrinology and Metabolism 260 (2) (1991) E203–E212.

[80] N. D. Kruyt, D. J. van Westerloo, J. H. DeVries, Stress-Induced Hyperglycemia in Healthy Bungee Jumpers Without Diabetes Due to Decreased Pancreatic β-Cell Function and Increased Insulin Resistance, Diabetes Technology & Therapeutics 14 (4) (2012) 311–314. doi:10.1089/dia.2011.0171.

[81] G. Pagano, P. Cavallo-Perin, M. Cassader, A. Bruno, A. Ozzello, P. Masciola, A. M. Dall'Omo, B. Imbimbo, An in vivo and in vitro study of the mechanism of prednisone-induced insulin resistance in healthy subjects., Journal of Clinical Investigation 72 (5) (1983) 1814.

[82] P. De Feo, G. Perriello, E. Torlone, M. M. Ventura, F. Santeusanio, P. Brunetti, J. E. Gerich, G. B. Bolli, Demonstration of a role for growth hormone in glucose counterregulation, American Journal of Physiology-Endocrinology And Metabolism 256 (6) (1989) E835–E843.

[83] L. Leonidou, A. Mouzaki, M. Michalaki, A. L. DeLastic, V. Kyriazopoulou, H. P. Bassaris, C. A. Gogos, Cytokine production and hospital mortality in patients with sepsis-induced stress hyperglycemia, Journal of Infection 55 (4) (2007) 340–346. doi:10.1016/j.jinf.2007.05.177.

[84] P. Plomgaard, K. Bouzakri, R. Krogh-Madsen, B. Mittendorfer, J. R. Zierath, B. K. Pedersen, Tumor necrosis factor-α induces skeletal muscle insulin resistance in healthy human subjects via inhibition of Akt substrate 160 phosphorylation, Diabetes 54 (10) (2005) 2939–2945.

[85] D. Mesotten, P. J. D. Delhanty, F. Vanderhoydonc, K. V. Hardman, F. Weekers, R. C. Baxter, G. van den Berghe, Regulation of Insulin-Like Growth Factor Binding Protein-1 during Protracted Critical Illness, The Journal of Clinical Endocrinology & Metabolism 87 (12) (2002) 5516–5523. doi:10.1210/jc.2002-020664.

[86] E. Boonen, H. Vervenne, P. Meersseman, R. Andrew, L. Mortier, P. E. Declercq, Y.-M. Vanwijngaerden, I. Spriet, P. J. Wouters, S. Vander Perre, L. Langouche,

I. Vanhorebeek, B. R. Walker, G. Van den Berghe, Reduced Cortisol Metabolism during Critical Illness, New England Journal of Medicine 368 (16) (2013) 1477–1488. doi:10.1056/NEJMoa1214969.

[87] S. Khani, J. A. Tayek, Cortisol increases gluconeogenesis in humans: its role in the metabolic syndrome, Clinical Science 101 (6) (2001) 739–747.

[88] J. Fowelin, S. Attvall, H. Von Schenck, U. Smith, I. Lager, Combined effect of growth hormone and cortisol on late posthypoglycemic insulin resistance in humans, Diabetes 38 (11) (1989) 1357–1364.

[89] A. Steensberg, C. P. Fischer, C. Keller, K. Møller, B. K. Pedersen, IL-6 enhances plasma IL-1ra, IL-10, and cortisol in humans, American Journal of Physiology - Endocrinology and Metabolism 285 (2) (2003) E433–E437. doi:10.1152/ajpendo.00074.2003.

[90] C. Rask-Madsen, H. Domínguez, N. Ihlemann, T. Hermann, L. Køber, C. Torp-Pedersen, Tumor Necrosis Factor-α Inhibits Insulin's Stimulating Effect on Glucose Uptake and Endothelium-Dependent Vasodilation in Humans, Circulation 108 (15) (2003) 1815–1821. doi:10.1161/01.CIR.0000091406.72832.11.

[91] P. De Feo, G. Perriello, M. M. Ventura, P. Brunetti, F. Santeusanio, J. E. Gerich, G. B. Bolli, The pancreatic-adrenocortical-pituitary clamp technique for study of counter-regulation in humans, American Journal of Physiology-Endocrinology and Metabolism 252 (4) (1987) E565–E570.

[92] A. R. Sedaghat, A. Sherman, M. J. Quon, A mathematical model of metabolic insulin signaling pathways, American Journal of Physiology - Endocrinology And Metabolism 283 (5) (2002) E1084–E1101. doi:10.1152/ajpendo.00571.2001.

[93] A. Thorell, J. Nygren, O. Ljungqvist, Insulin resistance: a marker of surgical stress, Current Opinion in Clinical Nutrition & Metabolic Care 2 (1) (1999) 69–78.

[94] A. Chakraborty, W. Krzyzanski, W. J. Jusko, Mathematical modeling of circadian cortisol concentrations using indirect response models: comparison of several methods, Journal of pharmacokinetics and biopharmaceutics 27 (1) (1999) 23–43.

[95] S. Venkataraman, R. Munoz, C. Candido, S. F. Witchel, The hypothalamic–pituitary–adrenal axis in critical illness, Reviews in Endocrine and Metabolic Disorders 8 (4) (2007) 365–373. doi:10.1007/s11154-007-9058-9.

[96] M. N. SILVERMAN, B. D. PEARCE, C. A. BIRON, A. H. MILLER, Immune Modulation of the Hypothalamic-Pituitary-Adrenal (HPA) Axis during Viral Infection, Viral immunology 18 (1) (2005) 41–78. doi:10.1089/vim.2005.18.41.

[97] E. D. Weitzman, D. Fukushima, C. Nogeire, H. Roffwarg, T. F. Gallagher, L. Hellman, Twenty-four hour pattern of the episodic secretion of cortisol in normal subjects, The Journal of Clinical Endocrinology & Metabolism 33 (1) (1971) 14–22.

[98] B. K. Pedersen, M. A. Febbraio, R. A. Mooney, Interleukin-6 does/does not have a beneficial role in insulin sensitivity and glucose homeostasis, Journal of Applied Physiology 102 (2) (2006) 814–816. doi:10.1152/japplphysiol.01208.2006.

[99] S. J. van Deventer, H. R. Buller, J. W. ten Cate, L. A. Aarden, C. E. Hack, A. Sturk, Experimental endotoxemia in humans: analysis of cytokine release.

[100] J. Lin, N. N. Razak, C. G. Pretty, A. Le Compte, P. Docherty, J. D. Parente, G. M. Shaw, C. E. Hann, J. Geoffrey Chase, A physiological Intensive Control Insulin-Nutrition-Glucose (ICING) model validated in critically ill patients, Computer Methods and Programs in Biomedicine 102 (2) (2011) 192–205. doi:10.1016/j.cmpb.2010.12.008.

[101] Ankit Rohatgi, WebPlotDigitizer: Version 3.4, ZENODO, 2014.

[102] M. Lantz, S. Malik, M. L. Slevin, I. Olsson, Infusion of tumor necrosis factor (TNF) causes an increase in circulating TNF-binding protein in humans, Cytokine 2 (6) (1990) 402–406. doi:10.1016/1043-4666(90)90048-X.

[103] S. O. K. Song, J. Hogg, Z.-Y. Peng, R. Parker, J. A. Kellum, G. Clermont, Ensemble Models of Neutrophil Trafficking in Severe Sepsis, PLoS Comput Biol 8 (3) (2012) e1002422. doi:10.1371/journal.pcbi.1002422.

[104] A. Sokal, Monte Carlo Methods in Statistical Mechanics: Foundations and New Algorithms, in: C. DeWitt-Morette, P. Cartier, A. Folacci (Eds.), Functional Integration, Vol. 361, Springer US, Boston, MA, 1997, pp. 131–192.

[105] P. E. Cryer, Glucose counterregulation: prevention and correction of hypoglycemia in humans, American Journal of Physiology-Endocrinology And Metabolism 264 (2) (1993) E149–E155.

[106] G. Nucci, C. Cobelli, Models of subcutaneous insulin kinetics. A critical review, Computer Methods and Programs in Biomedicine 62 (3) (2000) 249–257. doi:10.1016/S0169-2607(00)00071-7.

[107] M. Wilinska, L. Chassin, H. Schaller, L. Schaupp, T. Pieber, R. Hovorka, Insulin Kinetics in Type-1 Diabetes: Continuous and Bolus Delivery of Rapid Acting Insulin, IEEE Transactions on Biomedical Engineering 52 (1) (2005) 3–12. doi:10.1109/TBME.2004.839639.

[108] J. Wong, J. G. Chase, C. E. Hann, G. M. Shaw, T. F. Lotz, J. Lin, A. J. Le Compte, A Subcutaneous Insulin Pharmacokinetic Model for Computer Simulation in a Dia-

betes Decision Support Role: Model Structure and Parameter Identification, Journal of diabetes science and technology (Online) 2 (4) (2008) 658–671.

[109] M. Vilkhovoy, A. Pritchard-Bell, G. Clermont, R. S. Parker, A Control-Relevant Model of Subcutaneous Insulin Absorption, 2014, pp. 10988–10993. doi:10.3182/20140824-6-ZA-1003.02360.

[110] E. W. Kraegen, D. J. Chisholm, Insulin responses to varying profiles of subcutaneous insulin infusion: kinetic modelling studies, Diabetologia 26 (3) (1984) 208–213.

[111] T. Kobayashi, S. Sawano, T. Itoh, K. Kosaka, H. Hirayama, Y. Kasuya, The pharmacokinetics of insulin after continuous subcutaneous infusion or bolus subcutaneous injection in diabetic patients, Diabetes 32 (4) (1983) 331–336.

[112] C. A. Hedman, T. Lindstrom, H. J. Arnqvist, Direct Comparison of Insulin Lispro and Aspart Shows Small Differences in Plasma Insulin Profiles After Subcutaneous Injection in Type 1 Diabetes, Diabetes Care 24 (6) (2001) 1120–1121. doi:10.2337/diacare.24.6.1120.

[113] J. Plank, A. Wutte, G. Brunner, A. Siebenhofer, B. Semlitsch, R. Sommer, S. Hirschberger, T. R. Pieber, A direct comparison of insulin aspart and insulin lispro in patients with type 1 diabetes, Diabetes care 25 (11) (2002) 2053–2057.

[114] H. Akaike, A Bayesian extension of the minimum AIC procedure of autoregressive model fitting, Biometrika 66 (2) (1979) 237–242. doi:10.1093/biomet/66.2.237.

[115] K. P. Burnham, Model selection and multimodel inference: a practical information-theoretic approach, 2nd Edition, Springer, New York, 2002.

[116] H. Akaike, A new look at the statistical model identification, Automatic Control, IEEE Transactions on 19 (6) (1974) 716–723.

[117] Roche Diagnostics Corporation, Evaluation Report: ACCU-CHEK(R) Inform II Test Strips (2012).

[118] J. G. Chase, G. M. Shaw, J. Lin, C. V. Doran, C. Hann, M. B. Robertson, P. M. Browne, T. Lotz, G. C. Wake, B. Broughton, Adaptive bolus-based targeted glucose regulation of hyperglycaemia in critical care, Medical Engineering & Physics 27 (1) (2005) 1–11. doi:10.1016/j.medengphy.2004.08.006.

[119] R. Hovorka, L. J. Chassin, M. Ellmerer, J. Plank, M. E. Wilinska, A simulation model of glucose regulation in the critically ill, Physiological Measurement 29 (8) (2008) 959–978. doi:10.1088/0967-3334/29/8/008.

[120] A. Wächter, L. T. Biegler, On the implementation of an interior-point filter line-search algorithm for large-scale nonlinear programming, Mathematical Programming 106 (1) (2006) 25–57. doi:10.1007/s10107-004-0559-y.

[121] W. E. Hart, J.-P. Watson, D. L. Woodruff, Pyomo: modeling and solving mathematical programs in Python, Mathematical Programming Computation 3 (3) (2011) 219–260. doi:10.1007/s12532-011-0026-8.

[122] U. M. Ascher, Computer methods for ordinary differential equations and differential-algebraic equations, Society for Industrial and Applied Mathematics, Philadelphia, 1998.

[123] D. E. Seborg, Process dynamics and control, 3rd Edition, John Wiley & Sons, Inc, Hoboken, N.J, 2011.

[124] S. Finfer, J. Wernerman, J.-C. Preiser, T. Cass, T. Desaive, R. Hovorka, J. I. Joseph, M. Kosiborod, J. Krinsley, I. Mackenzie, others, Clinical review: consensus recommendations on measurement of blood glucose and reporting glycemic control in critically ill adults, Crit Care 17 (3) (2013) 229.

[125] A. Roy, R. S. Parker, Dynamic modeling of free fatty acid, glucose, and insulin: An extended" minimal model", Diabetes technology & therapeutics 8 (6) (2006) 617–626.

[126] E. D. Lehmann, T. Deutsch, A physiological model of glucose-insulin interaction in type 1 diabetes mellitus, Journal of Biomedical Engineering 14 (3) (1992) 235–242.

[127] M. E. Wilinska, J. Blaha, L. J. Chassin, J. J. Cordingley, N. C. Dormand, M. Ellmerer, M. Haluzik, J. Plank, D. Vlasselaers, P. J. Wouters, R. Hovorka, Evaluating Glycemic Control Algorithms by Computer Simulations, Diabetes Technology & Therapeutics 13 (7) (2011) 713–722. doi:10.1089/dia.2011.0016.

[128] M. Ottavian, M. Barolo, H. Zisser, E. Dassau, D. E. Seborg, Adaptive blood glucose control for intensive care applications, Computer Methods and Programs in Biomedicine 109 (2) (2013) 144–156. doi:10.1016/j.cmpb.2012.01.011.

[129] U. Pielmeier, S. Andreassen, B. S. Nielsen, J. G. Chase, P. Haure, A simulation model of insulin saturation and glucose balance for glycemic control in ICU patients, Computer Methods and Programs in Biomedicine 97 (3) (2010) 211–222. doi:10.1016/j.cmpb.2009.06.004.

[130] N. Haverbeke, T. Van Herpe, M. Diehl, G. Van den Berghe, B. De Moor, Nonlinear model predictive control with moving horizon state and disturbance estimation-application to the normalization of blood glucose in the critically ill, in: in Proc. of the 17th IFAC World Congress (IFAC WC 2008), 2008.

[131] A. Basu, S. Dube, M. Slama, I. Errazuriz, J. C. Amezcua, Y. C. Kudva, T. Peyser, R. E. Carter, C. Cobelli, R. Basu, Time lag of glucose from intravascular to interstitial compartment in humans, Diabetes 62 (12) (2013) 4083–4087.

[132] D. Brealey, M. Singer, Hyperglycemia in Critical Illness: A Review, Journal of Diabetes Science and Technology 3 (6) (2009) 1250–1260. doi:10.1177/193229680900300604.

[133] M. A. Fischler, R. C. Bolles, Random sample consensus: a paradigm for model fitting with applications to image analysis and automated cartography, Communications of the ACM 24 (6) (1981) 381–395. doi:10.1145/358669.358692.

[134] J. Hetherington, T. Sumner, R. M. Seymour, L. Li, M. V. Rey, S. Yamaji, P. Saffrey, O. Margoninski, I. D. L. Bogle, A. Finkelstein, A. Warner, A composite computational model of liver glucose homeostasis. I. Building the composite model, Journal of The Royal Society Interface 9 (69) (2012) 689–700. doi:10.1098/rsif.2011.0141.

[135] T. Sumner, J. Hetherington, R. M. Seymour, L. Li, M. Varela Rey, S. Yamaji, P. Saffrey, O. Margoninski, I. D. L. Bogle, A. Finkelstein, A. Warner, A composite computational model of liver glucose homeostasis. II. Exploring system behaviour, Journal of The Royal Society Interface 9 (69) (2012) 701–706. doi:10.1098/rsif.2011.0783.

[136] E. Nyman, C. Brannmark, R. Palmer, J. Brugard, F. H. Nystrom, P. Stralfors, G. Cedersund, A Hierarchical Whole-body Modeling Approach Elucidates the Link between in Vitro Insulin Signaling and in Vivo Glucose Homeostasis, Journal of Biological Chemistry 286 (29) (2011) 26028–26041. doi:10.1074/jbc.M110.188987.

[137] W. J. Thomsen, R. R. Neubig, Rapid kinetics of. alpha. 2-adrenergic inhibition of adenylate cyclase. Evidence for a distal rate-limiting step, Biochemistry 28 (22) (1989) 8778–8786.

[138] L. E. Fridlyand, L. H. Philipson, Glucose sens ing in the pancreatic beta cell.

[139] W. S. Zawalich, K. C. Zawalich, H. Yamazaki, Divergent effects of epinephrine and prostaglandin E2 on glucose-induced insulin secretion from perifused rat islets, Metabolism 56 (1) (2007) 12–18. doi:10.1016/j.metabol.2006.08.016.

[140] D. M. Keenan, F. Roelfsema, J. D. Veldhuis, Dose-response downregulation within the span of single interpulse intervals, AJP: Regulatory, Integrative and Comparative Physiology 299 (1) (2010) R11–R18. doi:10.1152/ajpregu.00201.2010.